Organic Molecule Functionalized Nanoparticles and Redox Active Polymer: Synthesis, Characterization and Application

by

Samir Chandra Paul

A dissertation submitted to the Graduate Faculty of
Auburn University
in partial fulfillment of the
requirements for the Degree of
Doctor of Philosophy

Auburn, Alabama

December 10, 2016

Key Words: Nanoparticles, Silver, Gold, Naphthalene diimide, Coronene diimide, Electropolymerization

Approved by

Vince Cammarata, Chair, Associate Professor of Chemistry and Biochemistry
German Mills, Professor of Chemistry and Biochemistry
Rik Blumenthal, Associate Professor of Chemistry and Biochemistry
Christopher Easley, Associate Professor of Chemistry and Biochemistry
Minseo Park, Professor of Physics

Abstract

In the field of material chemistry, polymers and nanoparticles are most popular areas of current research and development. These two fields are quickly expanding and playing a vital role in a wide spectrum of areas ranging from electronics to photonics, conducting materials to sensors and medicine to biotechnology during the past decades. This dissertation mainly focuses on the synthesis and characterization of organic-inorganic hybrid nanostructure and redox active polymers. At the beginning of this dissertation, we have reviewed the recent literatures of functionalized nanoparticles and electroactive polymers. In Chapter Two, we report synthesis and characterization of redox active naphthalene diimide (NDI) functionalized metal nanoparticles. Silver and gold nanoparticles were synthesized from silver neodecanoate and gold(I) sodium thiosulfate, respectively, in presence of DPA-NDI-SH (where DPA= Diphenylamine) in a single reaction vessel. Dimethyl sulfoxide (DMSO) and dimethy formamide (DMF) were used as solvents for Ag and Au nanoparticles respectively. The synthesized nanoparticles were characterized by UV-Visible spectroscopy, TEM and X-ray diffraction. Incorporation of DPA-NDI-SH ligands on the surfaces of nanoparticles was confirmed by FT-IR.

In Chapter Three, synthesis of a new monomer containing coronene diimide with diphenylamine end group (DCTD) has been demonstrated. Polymer thin films of DCTD were grown onto gold, glassy carbon and ITO electrode surfaces via electropolymerization. Cyclic voltammetry of the resulting polymers show a reversible $2e^-$ oxidation of the diphenylbenzidine unit and reversible reductions of the aromatic diimide. The spectroelectrochemical and

electrochromic properties of these films were evaluated. Reversible switching between different colors corresponded to the redox states of diphenylbenzidine and imides were observed. The polymer film morphology was characterized by AFM.

Chapter Four discusses the electrochemical and solid state study of bilayer rectifying device. Polymers, poly(FD) and poly(DCTD) were sequentially electrodeposited on Au electrodes and their electrochemical study showed that electrons flow in only one direction in solution with supporting electrolyte. Also p-n junctions with these semiconductor polymers were fabricated and characterized by current-voltage responses and Shockley diode characteristics. We found that the device direction was switched upon changing the assembly order of bilayer.

In the final part of this work, we demonstrated that the naphthalene diimide functionalized semiconductor CdS nanoparticles can be synthesized and characterized. CdS nanoparticles were synthesized in DMSO from cadmium acetate and sodium sulfide in presence of naphthalene diimide (DPA-NDI-SH). The synthesized particles were characterized by UV-visible, fluorescence, XRD, TEM and FT-IR.

Acknowledgments

This dissertation was completed under the supervision of Professor Vince Cammarata. I would like to thank my advisor for his guidance, ideas, ingenuity, and direction. Also I am thankful to my committee members: Dr. German Mills, Dr. Rik Blumenthal, Dr. Christopher Easley and the University reader, Dr. Minseo Park for their valuable time to read my dissertation and helpful suggestions. Special thanks to Dr. German Mills and his student Mr. Sharif Hossain for their helpful discussion on nanoparticle project and also helping me to analyze particle size distribution by TEM. I am grateful to Professor Harold Zallen for a Malone-Zallen award. Also thanks to the graduate school for a graduate school dissertation award. I would like to express my gratitude to the department of Chemistry and Biochemistry for several teaching assistantships throughout my graduate study.

I would also like to thank Dr. David M. Stanbury, Dr. Anne E. V. Gorden, Dr. E. Duin, Dr. B. Merner and Dr. C. Shannon's group for allowing me to use their instruments. I am gratefull to Dr. Minseo Park and his student Vahid Mirkhani for their help to characterize the diodes. I am indebted to Dr. Victor from Materials Engineering, Auburn University and Md. Nuruddin and Manik Biswas from Materials Engineering, Tuskegee University for their help with XRD and TGA analysis. Also thanks to Mingming Wang for helping me to get AFM images of polymer samples. Last but not least, I appreciate the help from my previous group members. Dr. Lin Wang, Dr. Jie Liang, Dr. Yunfeng Li and Ms. Qingqing Wang, Mr. Ning Hao, I greatly benefited from their work. I would like say thanks to all of my friends and well wishers in Auburn and Bangladesh.

Finally I am grateful to my family, father, mother, brothers and sister, sister in law, brother in law and mother in law for their support and encouragement. Especially I would like to thank my wife and son for their unconditional love and patience.

Table of Contents

List of Tables

List of Schemes

List of Figures

Chapter One

INTRODUCTION AND BACKGROUND

1.1 Functionalization of metal nanoparticles

The applications of nanomaterials are diverse, ranging from catalysis to drug delivery and include surface chemistry, molecular sensing, optical and electronic devices.[1–4] Numerous scientists are effectively developing and proposing different nanoparticle synthetic procedures, theoretical models for their properties, characterization tools, and novel materials based on nanoparticles .[5–12] Over the years, different synthetic methods have been developed to obtain nanoparticles with proper size, shape and stability.[7–12] In nanoparticle synthesis, stability against agglomeration is an important issue. Nanoparticles are stabilized by capping or modifying the surfaces. Also surface modification makes nanoparticles phase compatible.[13] For example, long chain alkyl thiol functionalized Au nanoparticles are well-dispersed in organic solvents, such as chloroform or dichloromethane.[14] Other types of functionalization gives better stability in aqueous medium.[15] Synthetic procedures for nanoparticles are not limited to tuning just their shape, size and stability; functionalizing their surfaces with various important organic molecules provides additional possibilities in the research field of sensors, photovoltaics and biology.[16–18] Organic molecules present on the surface can enable particle self organization. Surface modification can also control the optical and electronic properties of the nanoparticles by interactions of surface molecules with surface electrons of the nanoparticles.[19–21]

1.2 Strategies for nanoparticles functionalization

Three different strategies are commonly applied for metal, metal oxide and semiconductor nanoparticle functionalization (Scheme 1.1).

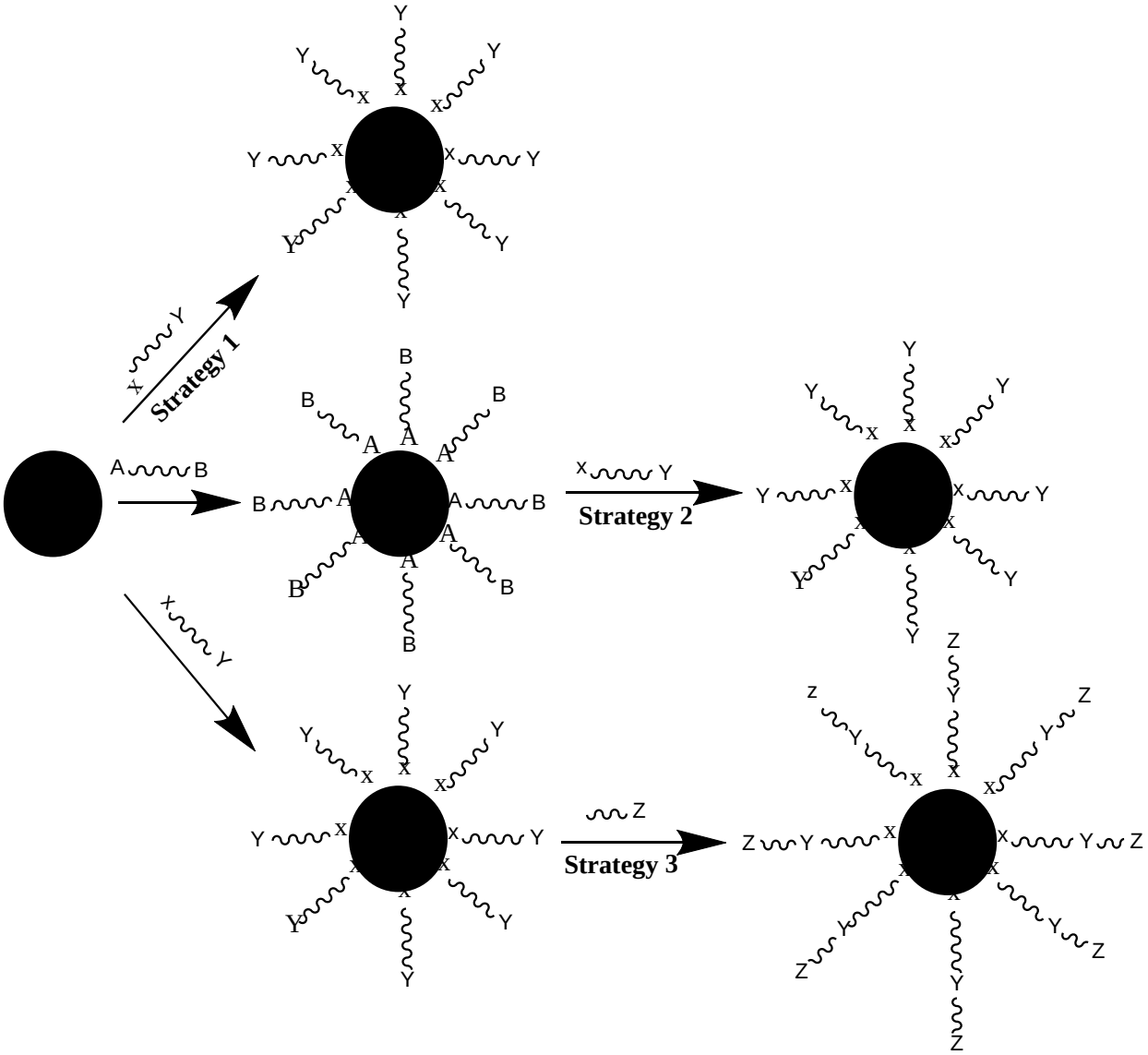

Scheme 1.1: Schematic diagram of three strategies to functionalize nanoparticles.[22]

(Adapted from ref. 22 Copyright 2008. Springer)

Strategy One:

The first strategy consists of the introduction of the whole functional molecule in a single step. In this process, the functional molecule needs to be synthesized first, containing a functional group which has strong affinity for the metal. It has been shown that a thiol (-SH) group should be attached to a functional molecule because of the strong binding affinity of sulfur to noble metal atoms.[23,24] Also other groups such as -COOH, -NH_2, -OH can often be introduced together with the thiol ligand on the surface of nanoparticles (Figure 1.1).[25] These functional groups can provide good solvent compatibility. For example, Carboxylate- terminate alkanethiol functionalized particles are stable in water although alkene thiol functionalized particles are only stable in an organic phase.[25] The single step method can be used for both aqueous and organic

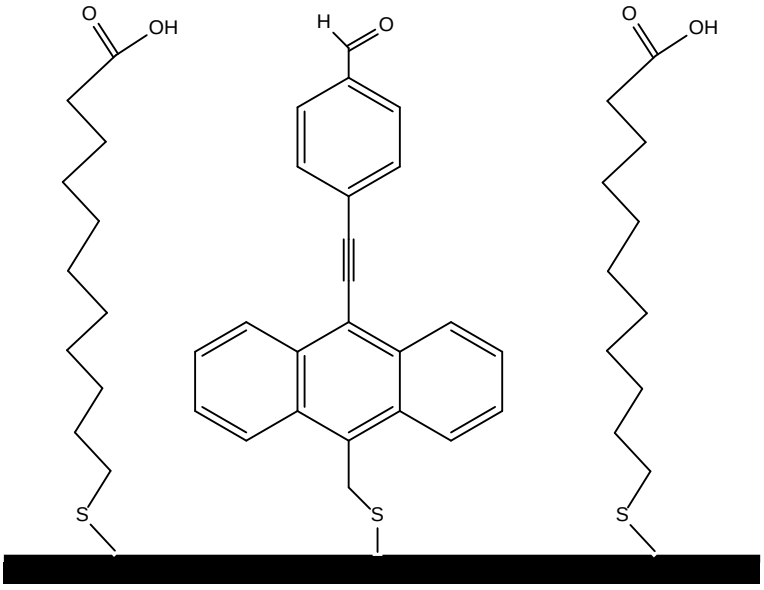

Figure 1.1 Functional molecule (containing both -SH and –COOH group) on nanoparticles surface.

(Reprinted with permission from ref. 25 Copyright 2006. American Chemical Society)

phase preparations.[26,27] Monodispersed Ni nanoparticles coated with oleic acid have been prepared in water in the presence of the surfactant dodecyl sulfate (SDS).[26] On the other hand, Co nanoparticles capped with oleic acid and triphenylphosphine were prepared in dichlorobenezene via thermal decomposition of $Co(CO)_8$.[27] Himatsu and Osterloh have developed a versatile method for the synthesis of silver and gold nanoparticles linked with oleylamine.[28] Oleylamine acts as both reductants for the starting materials chloroauric acid and silver acetate, as well as a capping agent. Different sized silver colloids were produced by controlling the temperature and solvent. They claimed that refluxing a lower boiling point solvent, such as hexane, yields smaller size nanoparticles.

Metal nanoparticles were studied using citrate as both stabilizing and reducing agent in aqueous media. This is the classical method, first reported in 1951 by Turkevich for gold nanoparticles.[7] Later many investigators extended the procedure for other metals such as Ag,[29,30] Pt,[31] Pd.[32] Kimling et al. revisited the Turkevich method and studied the kinetics of particle formation by changing different parameters (concentration, temperature and reaction time) and compared these methods quantitatively in terms of sizes and shapes of the particles using different analytical techniques: optical spectroscopy, X-ray scattering, and electron microscopy.[33] A Glutathione-Au nanocluster was made in a simple single step method by heating aqueous solution of chloroauric acid in presence of glutathione at 70^{o} C in water for 24 h.[34–37] Ethanol,[38] DMF,[39–41] DMSO[42–44] can play a dual role in the synthesis of nanoparticles since these solvents can act as reductants of the metal precursor. Moreover, Au nanoparticles can be stabilized by DMF as a capping agent.[45] In Chapter Two, we report single step synthesis for Au and Ag nanoparticles that involves heating of Au or Ag precursors in DMF and DMSO, respectively in presence of thiol containing naphthalene diimide (DPA-NDI-SH).

The well-known Brust-Schiffrin two phase method for preparing alkyl thiol capped nanoparticles at first was studied for Au nanoparticles.[14] Later other investigators have synthesized Ag,[46] Pt,[47]Pd,[48,49] Cu[50] CoPt alloy,[51] and PbS[52] nanoparticle using two phase method. According to the Brust method, $AuCl_4^-$ was transferred from aqueous to a nonaqueous phase (toluene) by a phase transfer reagent, tetraoctylammonium bromide (TOAB). Then the Au^{3+} was reduced by an aqueous solution of sodium borohydride in presence of dodecanethiol.

$$AuCl_{4\,(aq)}^- + N(C_8H_{17})_4^+{}_{(toluene)} \longrightarrow N(C_8H_{17})_4 + AuCl_{4\,(toluene)}^-$$

$$mAuCl_{4\,(toluene)}^- + nC_{12}H_{25}SH + 3me^-(\text{from aq. Reductant}) \longrightarrow 4mCl_{(aq)}^- + (Au_m)(SHC_{12}H_{25})_{n(toluene)}.$$

Murray and his research group studied Au nanoclusters coated with different thiol functionalized molecules using the twophase method.[53–59] Alkylthiol capped nanoparticles are well stable in different organic solvents such as CH_2Cl_2, $CHCl_3$, hexane and toluene. These nanoparticles have been used in studies on ligand exchange processes involving functionalized nanoparticles. This will be discussed in detail in the next section. Leff and others modified the two phase method using alkylamines to use alkylamine instead of thiols. They made dodecylamine and oleylamine stabilized Au nanoparticles.[60]

Strategy Two

The second common surface functionalization method is through a ligand exchange reaction.To tailor metal nanoparticles for different applications, it is necessary to control the particle surface with functional molecules. Sometimes there are some limitations to binding the functional molecule to the metal surface using the one step synthesis process. Limited solubility, steric hindrance of the functional molecule or incompatibility of functional ligand to the reaction

condition can result in poor control of size and shape of the particles generated via the single step reaction.[61] Therefore post synthetic modifications of the surface are widely used for better control of size, shape and solvent compatibility.[62] This method consists of two steps: (i) preparation of well defined nanoparticles with loosely bound ligands, followed by (ii) exchange of ligand by functional molecule (Scheme 1.1). The most studied ligand exchange reaction uses thiol capped nanoparticles as the starting material. If the thiol capped nanoparticle undergoes ligand exchange for another thiol containing functional molecule, it often produces nanoparticles containing mixed ligands on the surface. Hostetler et al., have elucidated the mechanism of thiol exchange and found that the reaction is Sn2 type associative.[63] Labande et al. has studied the ligand exchange of different ferrocenethiols with dodecanethiol capped Au nanoparticles.[64] Figure 1.2 clearly depicts the thiol to thiol exchange process that produces nanoparticles

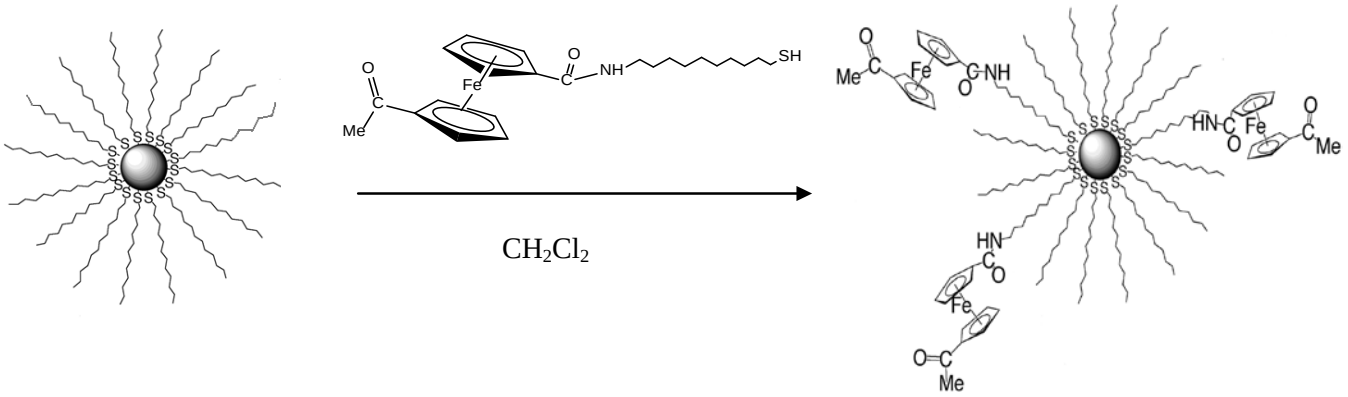

Figure1.2: Thiol to thiol exchange reaction on Au nanoparticles surface.

(Reprinted with permission from ref. 64. Copyright 2002.American Chemical Society)

capped with mixed ligands. However, using triphenylphosphine, (PPh_3) stabilized Au nanoparticles as the precursor results in a complete and fast exchange.[62,65] The product particles have higher stability against heat, aggregation and decomposition.[66,67] The kinetics and

mechanism of the exchange reaction was monitored by ^{1}H NMR spectroscopy.[62] The proposed mechanism in Figure 1.3 suggests that the reaction proceeds via three-stages rather than through a single step associative or dissociative mechanism. In the first stage, part of the phosphine ligand shell is rapidly replaced by a thiol containing ligand until no more particle-bound chlorides are available. In the second stage, removal of the remaining phosphine ligands producing either a free PPh_3 in solution (pathway I) or through direct transfer of PPh_3 to a closely associated $AuCl(PPh_3)$ (pathway II) occurs. During the final stage, the complete thiol ligand shell is reorganized into a more crystalline state. Ma and Chechik studied the mechanism of the ligand exchange for Au nanoparticles by EPR spectroscopy.[68,69] They found that the ligand exchange reaction with aged nanoparticles is less efficient because freshly prepared possess particles having the defect sites with high reactivity. Exchanges involving ligand other than thiol are also discussed in the literature, for example oleic acid capped Co, Fe_2O_3 nanoparticles;[70,71] octylamine capped Fe_2O_3;[72,73] oleic acid capped Ag.[71]

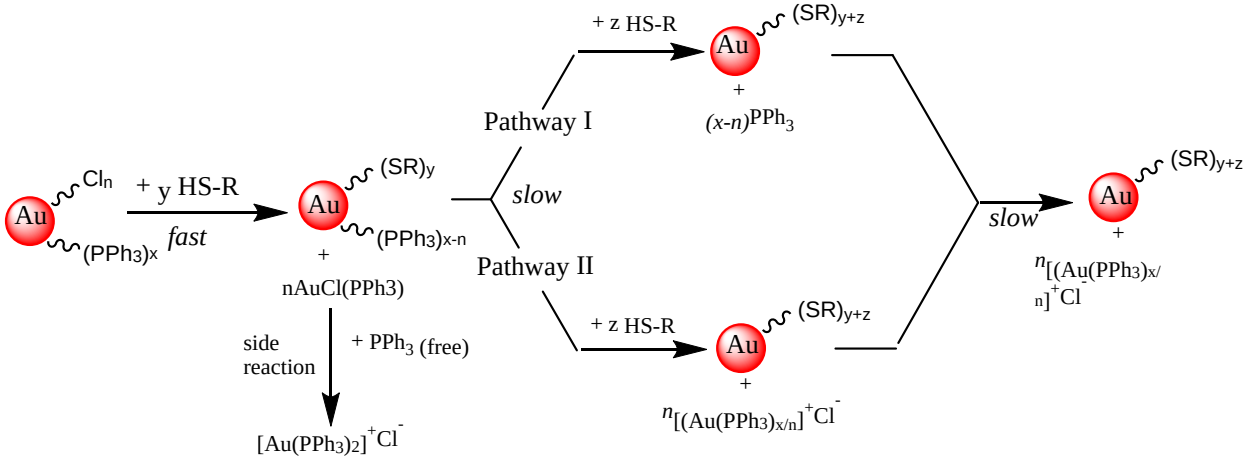

Figure 1.3: Proposed three-stage mechanism for the ligand exchange reaction between 1.5-nm Au_n-PPh_3 and thiols.

(Reprinted with permission from ref. 62. Copyright 2006.American Chemical Society)

To achieve the desire functionality, surface modification of semiconductor quantum dots has also been observed to occur via ligand exchange reaction for the following materials: CdSe;[74,75] CdSe/ZnS;[76] CuInS2/ZnS.[77]

Another versatile way to exchange ligand employs the phase transfer method. The particles are first synthesized in one phase (organic or aqueous) and then ligand exchange take place after by transferring to another phase to get the desired functional molecule on the surface. Lala et al. have made water-soluble, carboxylic acid stabilized Au nanoparticles and then exchanged cyclodextrin ligands for and octadecanethiol via phase transfer involving water and chloroform.[78] Recently, Alkilany et al. developed a simple and efficient method by the addition of methanol to citrate stabilized Au nanoparticles which transferred from water to CH_2Cl_2 containing thiolated poly(ethylene glycol).[79] Phase transfer of water soluble carboxymethyl celloluse (CMC) coated Pt nanoparticles to hexane with dodecanethiol narrows the size distribution and yield near hexagonal ligand packing.[80] The phase trsnsfer was performed by addition of concentrated HCl. The acid weakens the binding of CMC to the Pt nanoparticles and enabling dodecanethiol binding to the particles .[80]

Phase transfer from organic to aqueous phase also been demonstrated. Well dispersed nanoparticles in aqueous medium are required for biological and medical applications. Hong et al. prepared FePt magnetic nanoparticles functionalized with a mixed monolayer of poly(ethylene glycol)-terminated thiol and dopamine using a ligand exchange method.[81] Prior to the exchange reaction, particles were synthesized with different ligands such asoleic acid oleyl amine and 1,2-hexadeacnediol in a organic phase of phenyl ether.[82]

Strategy Three

This strategy consists of modification of existing surface ligands by reaction with another functional molecule (Scheme 1.1). McMahon and Emory described a covalent coupling strategy of amides to transfer nanoparticles from aqueous to organic phases maintaining high stability.[13] First they modified the Au surface with mercaptoacetic acid (MAA), and then they added dicyclohexylamine (DCHA) and dicyclohexylcarbodiimide (DCC) in DMSO. This method produces MAA-DCHA modified nanoparticles where DCC activates the carbonyl carbon and DCHA is coupled with the activated carbonyl. Another common type of ligand modification is accomplished by introducing a silicon-based ligand on the metal surface. Trialkyloxysilylpropane can be used to modify an existing functional group on the nanoparticle's surface. Roberts et al. made ferrocenated nanoparticles through this silicon-based reaction.[83] Reacting of a 10 fold excess of 3-aminopropyldimethylethoxysilane (APTMES) with oleic acid capped indium tin oxide (ITO) nanoparticles produces silane capped ITO nanoparticles. Ferrocene was coupled through the reaction of ferrocenoyl chloride and silane functionalized ITO nanoparticles.

1.3 Optical properties of nanoparticles

Noble metal and semiconductor nanoparticles show strong and broad absorption band in the UV-visible region. This band is called surface plasmon band.[19] The peak position, absorbance maxima, band width at half-maximum absorption are characteristics feature of the surface plasmon band.[84] Some particles of noble metals such as Au, Ag have the absorption band in the visible region, these particles show attractive colors in solution. The absorption band for spherical particles can be calculated from the Mie theory. This theory explained the surface plasmon resonance based on the Maxwell's equations for small spheres.[21,85]

The metal outer shell free electrons can travel through the materials. For nanoparticles, incident light interact with the surface as the mean free path of these electrons is larger than the particles size.[21] The surface electrons are a resonance in condition because the size of particles is much smaller than the wavelength of the incident light. As a results surface electrons oscillate upon exposure to specific photons, which enhances both the local and scattered fields around the nanoparticles.[86] So the incident light electric field induces a polarization of the free electrons. Therefore, a dipolar oscillation is created with period to time. This is called surface plasmon resonance. As this interaction is confined to the surface, changes in size and shape of the particles causes the alterations in the electric field density on the surface of the particles. As a result, surface plasmon resonance is also changed as the surface electrons are oscillating at different frequencies. Therefore, the nanoparticles with different size and shape exhibit different absorption bands. Moreover, the medium (solvent) and surface ligand or capping agents have an effect on the plasmon band as they alter the dielectric constant of the surrounding medium. The change in the dielectric constant affects the oscillation frequency because the electron density of the surface is altered. Ghosh et al. have shown that the absorption maxima varies between 520 and 550 nm for gold nanoparticles, depending on the refractive index of the solvent.[20] Their study also revealed that the absorption band gradually shifts to the red with increases in chain length of both the cationic and anionic surfactants indicating specific binding of the surfactant molecules around the gold particles. Wei and others have compared the absorption band of thiol and amine stabilized Ag nanoparticles absorption band. The absorption peak of thiol-stabilized nanoparticles is shifted to lower energies compared to that of amine-stabilized particles. Furthermore, with thiol-stabilized Ag nanoparticles, the position of the peak depends on the length of the alkyl chains of the thiol molecule.[87]

Ligands chemically bonded to the metal center behave like coordination compounds. Like coordination compounds, the metal atom electron density in the nanoparticles affected by both i) the ligand donating properties ii) the back donation from the metal center.[19] For example phosphinine stabilized Au nanoparticles exhibits an absorption band at a longer wavelength (~580nm) because the ligand exhibits a strong π-accepting properties.[88] Sometimes metal nanoparticles are partially reduced or oxidized by the ligand present on the surface.[89] Recently studies using time dependent density functional theory showed that a blue shift exists in the spectrum for positively charged clusters and a red shift is typical for negatively charged clusters.[90]

1.4 Electrochemistry of functional nanoparticles

Functionalized metal nanoparticles show size-dependent electrochemical properties. The electrochemistry of smaller (< 3-4 nm) nanoparticles shows quantized double layer (QDL) charging peak. QDL properties were investigated using different electroanalytical techniques such as cyclic voltammetry (CV), differential pulse voltammetry (DPV),[91,92] and chronoamperometry.[93] Quinn et al. found a fifteen single electron step charging process in the differential pulse voltammetry of hexanethiol-capped Au (C6S-Au_{147}) particles.[92] These particles show an average peak to peak spacing of about 0.25V and a double layer capacitance of about 0.64 aF(attoFarad). Deviation from this capacitance value has also been reported.[49,94,95] These deviations result from the irregular peak spacing in DPV. Moreover, the peak spacing depends on the nature of solvent[96–98]and electrolyte.[98,99]

In Figure 1.4, DPV response for C6S-Au_{147} (upper trace) is different than from the trace obtained in the case of C6S-Au_{38} (lower). Particles with a smaller Au core size exhibit an enlarged electrochemical potential spacing between the current peak for the first oxidation

$(MPC)^{0/+1}$ and the first reduction $(MPC)^{0/-1}$. This potential spacing is called the electrochemically calculated HOMO-LUMO energy gap. Ag and Au nanoparticles with sizes larger than 10 nm diameter undergo oxidation resulting in particle dissolving .[100,101] As

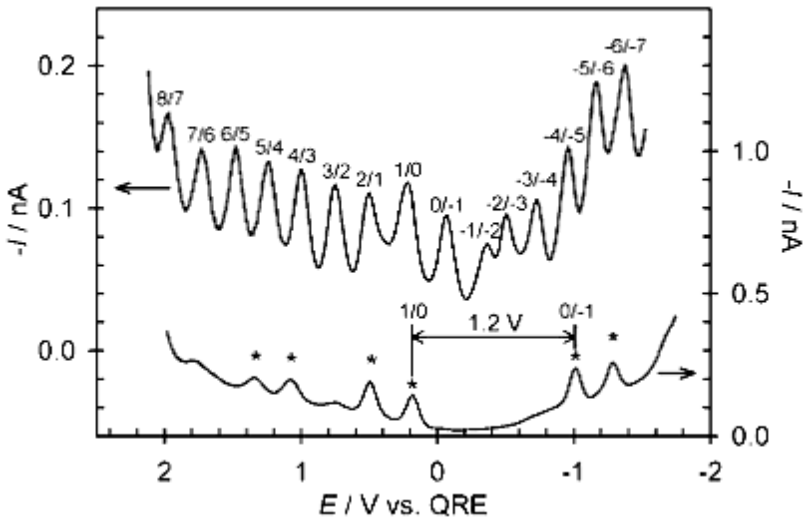

Figure 1.4: DPV responses for MPC solutions measured at a Pt microelectrode; as-prepared 177 μM C6S-Au_{147} (upper) showing 15 high-resolution QDL peaks and 170 μM C6S-Au_{38} (lower) showing a HOMO-LUMO gap.

(Reprinted with permission from ref. 92. Copyright 2003 American Chemical Society)

discussed earlier, molecules experiencing redox processes can be linked to the metal core with different synthetic methods. The electrochemistry of Au, Ag, and Pd nanoparticles coated with redox active molecules have been studied. The most studied redox molecule is ferrocene.[49,58,59,91,102–106] Other than ferrocene, the electrochemical reactions of antharaquinone,[107–110] viologen,[111] perylene diimide,[23,112] fullerene,[113–115] and phenothiazine,[53] incorporated onto the surface of nanoparticles have also been discussed. Electrochemical methods such as cyclic voltammetry (CV) and rotating disk electrode (RDE) voltammetry have been used to study the diffusion controlled current of soluble nanoparticles. Absorption or precipitation of nanoparticles on the electrode surfaces allows characterization using an

electrochemical quartz microbalance (EQCM) in conjunction with CV. The CV and DPV of viologen functionalized Pd nanoparticles has been accomplished.[116] The two pairs of quasi reversible peaks with formal potential at -0.47 and -0.85 V are observed close to the formal potential of free methyl viologen in solution. Peak potentials are linearly dependent on the square root of the scan rate, suggesting that the electrochemical process is diffusion controlled. To get more information about double-layer diffusion charging current and molecular capacitance RDE experiments were performed.[116] The study found molecular capacitance values of 7.7 and 37 aF at the prewave and postwave potentials, respectively. Others have reported different electrochemistry of viologen protected Au nanoclusters.[111] Only one pair of redox waves were observed with this Au cluster indicating that a different core metal might produce a different voltammetric response. In addition, *in situ* EQCM was used to explore the absorption/desorption on the electrode surface of the viologen capped Au nanocluster during the oxidation and reduction processes.[111]

1.5 Proposed application of functionalized nanoparticles based on photochemical properties

Highly organized organic-inorganic hybrid nanostructures can be achieved by assembling different functional molecules on the metal core structure. These nanostructured materials exhibit size-dependent optical, electronic and chemical properties with great potential in the field of biological nanosensor and optoelectronics.[117] In an attempt to extend the application of nanomaterials, different electro- and photo-active chromophoric functional molecules have been widely studied. For example, metal nanoparticles with Glutathione,[35–37] pyrene,[118,119] perylene diimide,[23,112] dansyl[120] fullerene,[113–115] stilbene,[121] porphyrin,[122,123] tiopronin,[111] and azobenzene,[124] were synthesized. Photophysical studies of chromophore-functionalized

nanoparticles show that quenching of the chromophore emission occurs, which makes it possible to form donor-acceptor system that mimics to natural photosynthesis system. The mechanisms of the deactivation of the excited singlet state can be used to understand charge transport processes.[122,124–126] According to Thomas and Kamat,[18] there are four different ways of deactivation: (a) energy transfer, (b) electron transfer, (c) intermolecular interaction and (d) emission from the chromophore bound to the metal nanoparticles. Energy transfer is the main deactivation pathway operating for fullerene functionalized Au cluster.[115] It has been shown that the emission of fullerene was quenched when this molecule binds to the Au nanoparticle surface. However a different scenario was observed with fullerene functionalized CdSe/ZnS quantum dots. The emission of CdSe/ZnS core was quenched when the fullerene is attached to its surface.[127]

Time-resolve spectroscopy of fullerene-Au structures show there are two UV-visible band at 360 and 700 nm and both decay viafirst-order kinetics with a lifetime of 16.7 and 14.3 μs, respectively.[115] The triplet excited species is the only long-lived transient formed following the excitation of fullerene. Also no electron transfer products such as radical cations or anions were found. It was concluded that the excited energy of the fullerene was dissipated through the energy-transfer mechanism. Energy transfer processes are also found with other nanostructures such as Au-fluorenyl[128] and Au-dansyl.[120] Transient absorption studies of the pyrene thiol-bound gold (Au-SR-Py) nanoassemblies provide exmples of excited-state quenching of the surface-bound fluorophores via electron transfer.[119] This study showed that the formation of pyrene cation radical took place. The kinetic study should that the decay of the pyrene cation radical leads to the recovery of the parent fluorophore via a back electron-transfer process.

1.6 Organic electroactive Polymer

Organic polymers have attracted substantial interest to the scientific community due to their promising electrical properties as active materials for organic electronics such as organic solar cells, organic light-emitting diodes, sensors and organic electrical charge-storage devices.[129–132] Therefore, in materials science, polymer synthesis and characterization became an important research field.[133,134]

Electrochemically active polymers are classified mainly as two types based on the mode of charge propagation. Charge propagation highly depends on the chemical structure of the polymer. The two main categories are electron-conducting polymers and proton (ion)-conducting polymers. There are two major categories of electron-conducting organic polymer based on the type of electron transport: redox polymer and conducting polymer. Chemical structures of some conducting polymers are shown in Figure 1.5.

In conducting polymers, electrons move from one end of the polymer to the other through delocalized π orbitals. These polymers typically are conductive after a redox process that experience a oxidation (p-doping) or reduction (n-doping). Redox polymers are characterized by the presence of specific electrochemically active sites which can be oxidized or reduced. These sites can be organic or inorganic in nature. Organic redox-active polymers can be highly-flexible, light-weight and environmentally friendly as compared to conventionally use inorganic metal centered polymers.[135,136] The electroactivity is highly localized and electrons move via sequential electron self-exchange steps between neighboring redox sites (electron hopping). In some examples, the macromolecules contain both redox centers together with electroactive or conductive polymer chain forming a copolymer.[137–139] These polymers can be synthesized both chemically and electrochemically. As redox polymers are electroactive, polymer thin films form an important class of chemically modified electrodes. There are different ways to modify

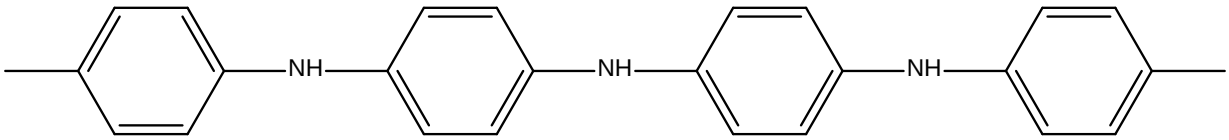

Polyaniline, PANI

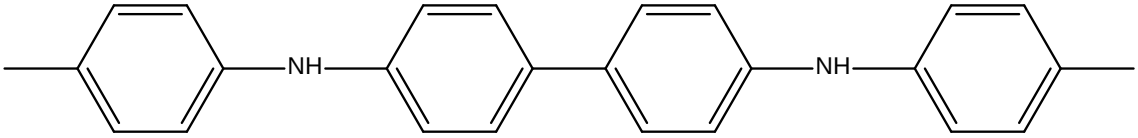

Polydiphenylamine, PDPA

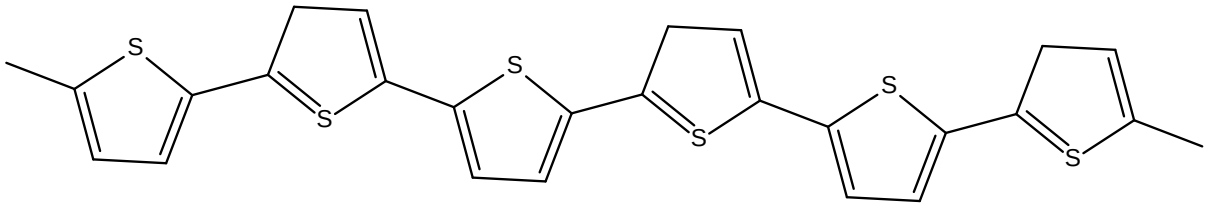

Polythiophene, PT

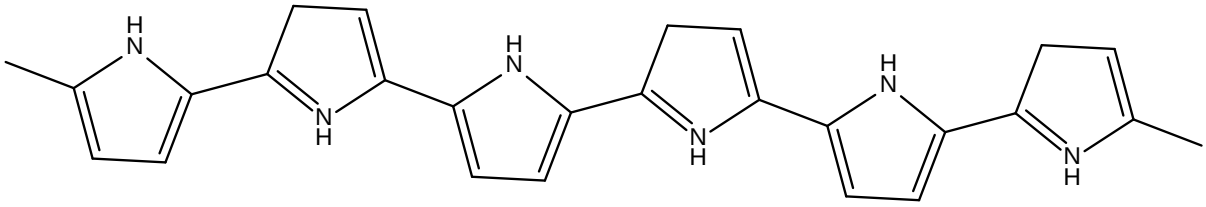

Polypyrrole, PPy

Figure 1.5: Chemical structure of common conducting polymers.

electrode surface, such as by dipping electrons in polymer solutions, evaporating droplets of a dilute polymer solution on the electrode, electrochemical precipitation, and electropolymerization. Here we will discuss only the electrochemical process.

1.7 Electropolymerization

Electropolymerization is a method by which a polymer is formed via oxidation or reduction of organic monomeric compounds. In this method, new covalent bonds form between the monomer precursors. It is a very powerful technique for development of modified electrodes. In the electropolymerization process, monomers are dissolved in a suitable solvent containing ionic electrolytes and an anodic or cathodic potential is applied to the working electrode. The selection of solvent and electrolyte are important because, in the range of oxidation potential of the monomer, both solvent and electrolyte should be stable. Organic solvents with very large potential windows and high relative permittivities are appropriate for good dissociation of the electrolyte and to establish a high ionic conductivity.[140] In the last couple of decades electropolymerization of different organic molecules have been studied extensively. The following are some advantages of making polymer films via electropolymerization:

1) Films can have good adhesion and electrical contact to the electrode surface;
2) This procesure provides a better control of film thickness and morphology;
3) Cleaner polymers are obtained as compared to chemical oxidation, i.e. less byproduct is present in the film.
4) Sometimes chemically synthesized polymers are insoluble in certain solvents, so it is hard to analyze the polymer properties and to fabricate devices. In electropolymerization, polymer growth occurs on the conducting surface, so analysis and device fabrication can be perform easily.

5) Comparable π-stacking of polymer film have reported with polymer film making via spin coating.[141]

In the early 1970's electropolymerization of aniline was first reported.[142] Later the procedure was extended to wide range of aromatic heterocyclic, benzenoid, or nonbenzenoid molecules such as: thiophene,[143] furan,[144] indole,[145] thianaphthene[146] and carbazole.[147] Different electrochemical techniques have been used for making polymer films: potentiostatic (constant-potential), galvanostatic (constant current) and potentiodynamic (potential scanning) methods. Among all of these methods the cyclic voltammetry (CV) method has been mostly studied. In the CV method one can easily evaluate the redox response of the polymer and regular increment of current intensity enables layer-by layer deposition of the polymer films.

The electropolymerization of aniline on ITO in 0.1M HCl solution is achieved by scanning from -0.2 to 1.0V vs Ag/AgCl.[148] The two oxidation and reduction peak currents increased upon increasing the number of scans and subsequently a polymer film grows on the ITO surfaces. Researchers have made complex functional conjugated architectures with electropolymerization. The polymers studied in the presenr work contain functional groups that can be polymerized only at the ends of the molecules. This means that the moiety at the molecular center is unable to undergo polymerization. By using this strategy a new class of conjugated materials with novel electronic and redox characteristics was attained by the conjugation of conducting polymer with different transition metal or redox organic center.[149] Our group has also synthesized different monomers of electropolymerizable diphenylamines containing different redox centers, including ferrocene, perylene, naphthalene etc.[150,151] The electropolymerization process of these compounds is discussed in detail later.

The characterization of the polymer films were films were performed using different analytical techniques. An electrochemical quartz crystal microbalance was used to study the growth of the polymer on the electrode surface.[152,153] *In situ* IR, UV-visible-NIR spectroscopy and fluorescence were also used to study the degree of polymerization and redox properties.[154] SEM and AFM tools are commonly used for analysis of film morphology.[155,156]

1.8 Spectroelectrochemistry

Spectroelectrochemistry is a powerful method to simultaneously analyze the electrochemical response and the optical characteristic of all redox states of the electroactive compounds. This method has been used for decades to study conducting polymer films. There are different optical methods that can be coupled to electrochemistry such as UV-visible and near-infrared absorption (UV-visible-NIR),[157] Raman spectroscopy,[158,159] infrared spectroscopy (IR),[154] X-ray absorption or scattering[160,161] and fluorescence.[154] This coupled technique requires a specific cell design for each different optical method. One side of the cell needs to be conducting in order to enable electrochemical reactions occur. Usually optically transparent electrodes (OTEs) are used as the conducting surface. ITO or very thin films of gold or platinum on substrates normally constitute the conducting surface in the spectroelectrochemical cell.

In our lab, electrochemistry coupled with UV-visible-NIR characterization was performed for different polymers.[162–165] A special type of spectroelectrochemical cell was designed to meet this purpose (Figure 1.6). The cell body was made of Teflon. There were two windows (front and rear) to pass the light beam. On the top of cell there are three apertures, two holes for electrodes (reference and counter) and the other is for degassing. The rear window consist of a glass slide and the front window consist of ITO coated glass slide which acts as a

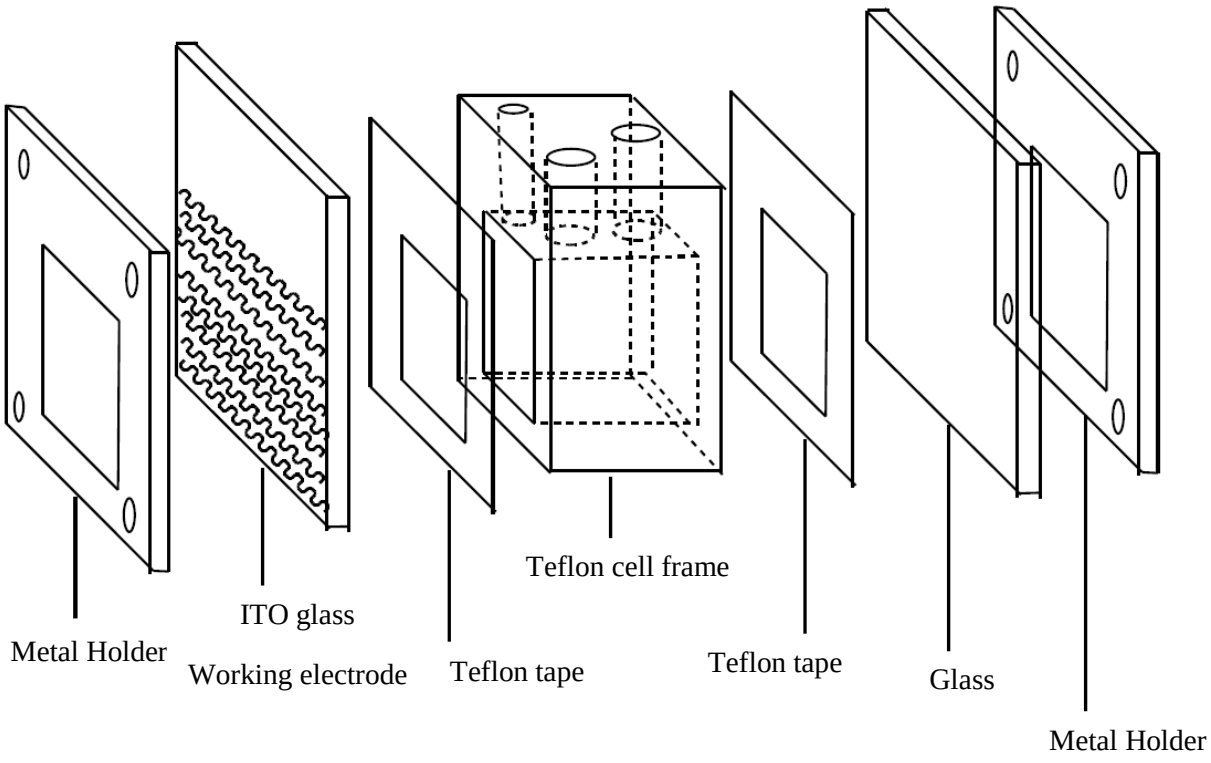

A: Separated cell view

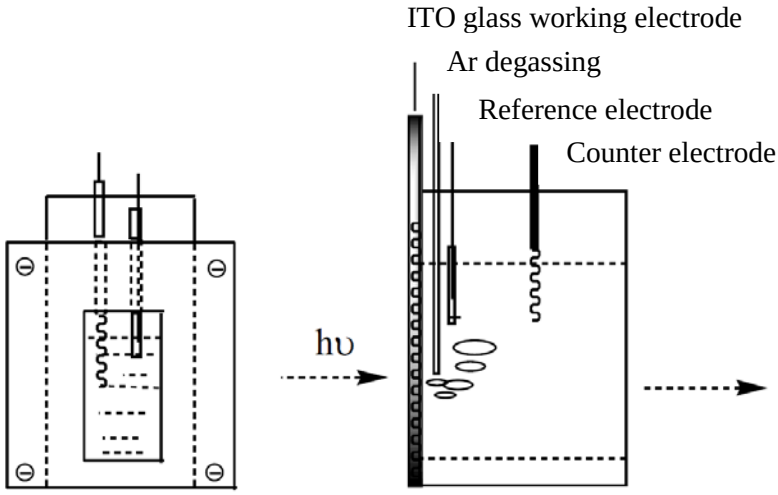

B: Assembled cell view

Figure: 1.6: Diagram of the spectroelectrochemical cell.

working electrode. The cell can be set up in the sample compartment of a UV-visible spectrophotometer and can be connected to the potentiostat.

1.9 Application of electroactive polymer

Energy storage materials:

Development of organic energy storage materials are increasing due to potential low production costs and low processing energy as well as environmental friendliness.[166] Conducting polymers are attractive for both batteries and supercapacitors. Polyaniline (PANI) has been used as an electrode material in a redox supercapacitor because of the material stability,controllable electrical conductivity and easy processibility.[167] de Oliveira synthesized nanocomposites of polypyrrole/graphene via oxidative polymerization and use them a supercapacitors.[168] In the lithium ion batteries, cathode materials need to be improved to achieve high-rate cycling capabilities needed to meet power and energy requirements. Poly(anthraquinonyl sulfide) has been shown to possess excellent reversibility and cyclabilty useful as a novel organic cathode material for rechargeable lithium batteries.[169] Recently conducting polymer-based flexible supercapacitors have also been reported.[170]

***Electrochromic Materials*:**

Electrochromic materials display different colors reversibly upon change of potential. The color change depends on the redox state of the material. Since compounds with multiple redox states may exhibit various colors.[151] The absorption band of electrochromic materialschanges in the UV-visible range.[171] Electrochromic materials are used in smart-windows, electrochromic mirrors or other display devices. Different compounds show electrochromic properties ranging from various inorganic metal oxides WO_3,[172] V_2O_5,[173] Co_3O_4,[174] MoO_3[175] to organic conducting polymers.[171,176] According to Mortimer and co-authors,

all conducting polymers show redox switching with a new optical band, so that transport of electronic charge and counter ions occur in the polymer matrix.[171] Oxidation of the polymer often shifts the absorption band to longer wavelengths. The color change between the p-doped and undoped polymer depends on the band gap. For example, for polypyrrole thin films color can change to blue-violet from yellow-green upon oxidation (Figure 1.7). The electrochromic properties a polymeric thiophene derivative, poly(3,4-(ethylenedioxy)thiophene(PEDOT) was studied extensively because the material exhibits it has a lower band gap than the parent polythiophene.[176] This low band gap makes such a polymer a better candidate as an electrochromic material including color changes from blue back (neutral) to a sky-blue tint

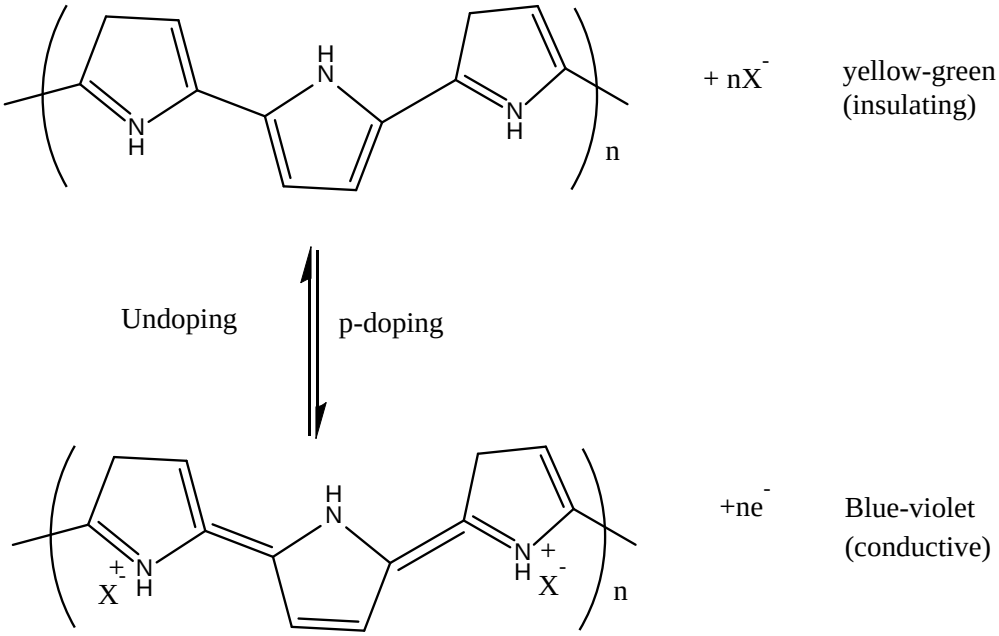

Figure 1.7: Electrochromism in polypyrrole thin films. The yellow-green (undoped) form undergoes reversible oxidation to the blue-violet (conductive).[171]

(doped). Polyelectrochromism (involving yellow–green todark blue–black) in PANI was observed for multiple protonation/de-protonation processes.[177]

***Electronic Device*:**

Conducting polymers are promising materials as the basis of low-cost microelectronic technology. It shows they are candidates for potential applications in electrical and electronic devices such as transistors, photodiodes, light-emitting diodes (LEDs) and solar cells.[132] Organic molecules were first used for field effect transistors (FET) in 1983.[178] For fabrication of organic devices researchers have been using many techniques such as solution process deposition, spin coating, vacuum evaporation and self assembled thin films, Langmuir-Blodgett film, and electropolymerization.[132] Thin film of poly(3-alkyl thiophene)(P3AT) exhibit high carrier mobility because of π-π stacking between adjacent polymer chains.[179] Two dimensional conjugated sheets of poly (3-hexylthiophene) (P3HP) with carrier mobilities of up to $0.1 cm^2V^{-1}s^{-1}$ have been reported.[180] Park and others demonstrated the effect of chain length of thiophene polymers on the performance of EFT.[181] Their study showed that short side chain in thiophene polymers form highly dense π-stacked structure exhibiting high field effect mobilities.

Molecular diodes can be used for current rectification where charge flow in only direction is achieved. Most diodes are made of inorganic semiconducting materials: silicon, germanium and selenium. Murray's research group first reported rectifiers with modified electrode surfaces containing electroactive polymeric bilayers of Ru, Fe and Os complexes derivatives, such as poly($(bpy)_2Os(vpy)_2$) and poly-$Ru(VB)_3$, where bpy = 2,2-bipyridine, vpy = 4-vinylpyridine and VB = 4-methyl-4'- vinyl-2,2'-bipyridine.[182–184] Synthesis of P-N junctions based on conducting polymer bilayers is a big challenge because of the bipolar nature of conducting polymers. Most bilayer rectification devices are fabricated by doping cations and

anions into the polymer matrix. Electropolymerization is a frequently used method for fabrication of bilayer p-n diodes. Aizama and Shinohara electrochemically synthesized bilayers of polypyrrole and polythiophene on Pt electrodes where the bilayer works as a p-n junction diode . In this junction, polypyrrole and polythiophene were anion and cation doped respectively.[185] Recently, polyacetylene based bilayer P-N junctions were developed where the dopant concentration was varied in the n-type layer.[186] Other than the chemical doping method, this P-N junction could also be made by a photochemical doping method.[187] Hoven et al. constructed heterojunctions with conjugated polymeric bilayers where they changed the polymer chains using cationic conjugated containing fluoride polyelectrolytes counteranions (p-type) and neutral conjugated polymers bearing anion-trapping (n-type) sites, producing devices exhibiting excellent current rectification.[188]

1.10 Background and Motivation of this work

Our research group is always interested in synthesizing new materials that have promising optical and electronic properties. Different monomers with a structural motif R-X-R have been synthesized in our lab (R is the diphenylamine (DPA) end group and X is an electroactive functional unit).[150,151,164,189,190] Monomer structures are shown in the Figure 1.8. The electrochemical technique was used to make the polymer of these monomers on different conducting surfaces: Au, ITO, GC and Pt[150] Wang L. et al. have synthesized monomers with X= naphthalene diimide group, N,N'- Di[p-phenylamino(phenyl)]-1,4,5,8-naphthalene tetracarboxylic diimide(DNTD) and ferrocenedicarboxamido group ,1,1'-bis[[p- phenylamino-(phenyl)]amido]-ferrocene(FD).[150] These are well soluble in dichloromethane and can be polymerized by the electrooxidation method. The Polymer growth mechanism was explored

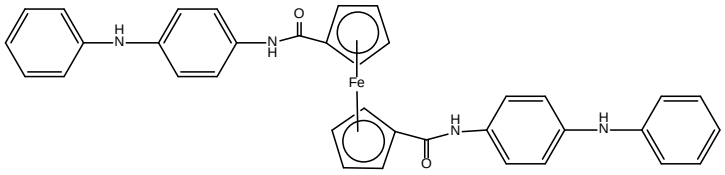

FD

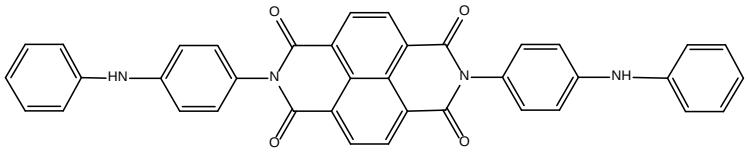

DNTD

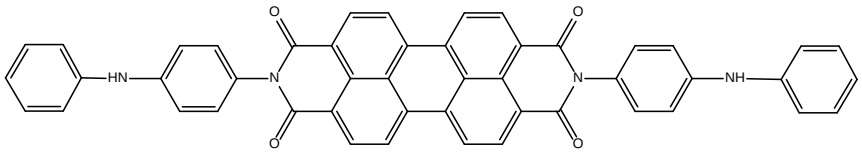

DPTD

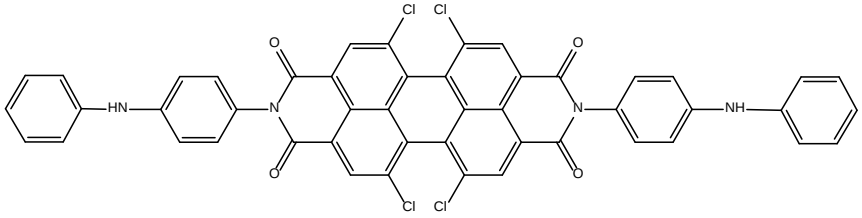

Cl_4DPTD

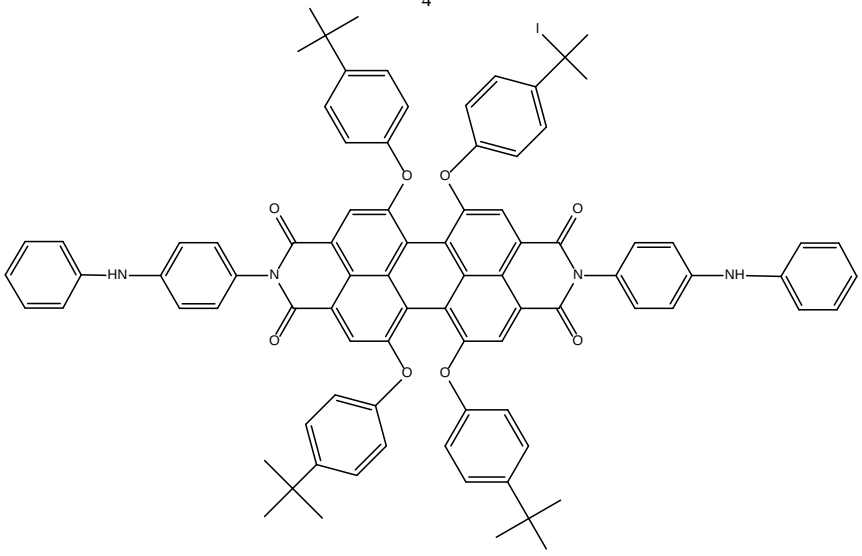

$(tBuPhO)_4$DPTD

Figure 1.8: Chemical structure of monomers synthesized in our lab with structure motif of R-X-R, R=diphenylamine (DPA) group and electroactive unit X.

using the electrochemical quartz crystal nanobalance (EQCN) in conjugation with standard cyclic voltammetry.[151,189] Spectroelectrochemistry was used to study the intermediate forms of the polymers generated via changes of potential. Wang Q. Q. studied the SAM formation on gold surfaces with asymmetric monomers (DPA-NDI-SH) where naphthalene diimide flanked by diphenylamine and benzene thiol.[162] On the other hand, similar types of symmetric monomers containing perylene diimide (DPTD) exhibit low solubility in dichloromethane. When about 5% (V/V) trifluoroacetic acid is added to dichloromethane, the compounds are shown to be more soluble and could be polymerized. Liang J. has synthesized different derivatives of DPTD by changing the diphenylamine group as well as via adding new groups in the parent structure of the perylene in the bay position.[151] These derivatives, (^{t}BuPhO)$_4$DPTD, Cl$_4$DPTD showed better solubility in dichloromethane than the parent compound.

Recently our group has fabricated molecular organic electronic devices, such as photovoltaic and diode systems based on the above mentioned polymers.[165] Bilayer polymers film diodes showed current rectification in both solution with supporting electrolyte and in the solid state. Also photovoltaic studies were performed on n-type perylene diimide polymers with p-type Cu phthalocyanine (CuPc). The objective of this study was to prepare of organic-inorganic hybrid nanostructures and electropolymerize of monomers with new electroactive centers and diode fabrication with such polymers. The specific objectives are

- Preaparation of naphthalene diimide linked to Ag and Au nanoparticles and their characterization
- Synthesis and electropolymerization of new monomers containing an electroactive coronene center flanked by a diphenylamine group (DCTD). The redox behavior, electrochromism and film morphology were studied.

- Rectification study of a bilayer of poly(DCTD) and poly(FD) in solution via electrochemical methods and solid state diode fabrication and characterization.

1.11 References

1. Shenhar, R.; Rotello, V. M. Nanoparticles: Scaffolds and Building Blocks. *Acc. Chem. Res.* **2003**, *36*, 549–561.

2. Roucoux, A.; Schulz, J.; Patin, H. Reduced Transition Metal Colloids: A Novel Family of Reusable Catalysts? *Chem. Rev.* **2002**, *102*, 3757–3778.

3. Elghanian, R.; Storhoff, J. J.; Mucic, R. C.; Letsinger, R. L.; Mirkin, C. a. Selective Colorimetric Detection of Polynucleotides Based on the Distance-Dependent Optical Properties of Gold Nanoparticles. *Science* **1997**, *277*, 1078–1081.

4. Dreaden, E. C.; Austin, L. a; Mackey, M. A; El-Sayed, Size Matters: Gold Nanoparticles in Targeted Cancer Drug Delivery. *Ther. Deliv.* **2012**, *3*, 457–478.

5. Amendola, V.; Bakr, O. M.; Stellacci, F. A Study of the Surface Plasmon Resonance of Silver Nanoparticles by the Discrete Dipole Approximation Method: Effect of Shape, Size, Structure, and Assembly. *Plasmonics* **2010**, *5*, 85–97.

6. Cho, E. J.; Holback, H. Nanoparticle Characterization: State of the Art, Challenges, and Emerging Technologies. *Mol. Pharm.* **2013**, *10*, 2093–2110.

7. Turkevich, J.; Stevenson, P. C.; J. Hillier, J. A study of the nucleation and growth processes in the synthesis of colloidal gold. *Disc. Farad. Soc.* **1951**, *11*, 55–75.

8. Frens, G. Particle Size and Sol Stability in Metal Colloids. *Colloid Polym Sci.* **1972**, *250*, 736–741.

9. Baigent, C.L.; Müller, G. A Colloidal Gold Prepared Using Ultrasonics. *Experientia* **1980**, *36*, 472–473.

10. Kalishwaralal, K.; Deepak, V.; Pandian, S. R. K; Gurunathan, S. Biological Synthesis of Gold Nanocubes from Bacillus licheniformis. *Bioresour. Technol.* **2009**, *100*, 5356–5358.

11. Carroll, K. J.;Reveles, J. U. Shultz, M. D.; Khanna, S. N.; Carpenter, E. E. Preparation of Elemental Cu and Ni Nanoparticles by the Polyol Method: An Experimental and Theoretical Approach. *J. Phys. Chem. C* **2011**, *115*, 2656–2664.

12. Wu, L.; Li, Q.; Wu, C. H.; Zhu, H.; Mendoza-Garcia, A.; Shen, B.; Guo, J.; Sun, S. Stable Cobalt Nanoparticles and Their Monolayer Array as an Efficient Electrocatalyst for Oxygen Evolution Reaction. *J. Am. Chem. Soc.* **2015**, 137, 7071–7074.

13. McMahon, J. M.; Emory, S. R. Phase Transfer of Large Gold Nanoparticles to Organic Solvents with Increased Stability. *Langmuir* **2007**, *23*, 1414–1418.

14. Brust, M.; Walker, M.; Bethell, D.; Schiffrin, D. J.; Whyman, R.Synthesis of Thiol-derivatised Gold Nanoparticles in a Two-PhaseLiquid-Liquid System. *J. Chem. Soc., Chem. Commun.* **1994**, 801-802.

15. Gittins, D. I.; Caruso, F. Spontaneous Phase Transfer of Nanoparticulate Metals from Organic to Aqueous Media. *Angrew Chem. Int. ed.* **2001**, *40*, 3001-3004.

16. Tan, E.; Yin, P. Lang, X. Wang, X., Youa T.; Guo, L. Functionalized Gold nanoparticles as Nanosensor for Sensitive and Selective detection of Silver ions and Silver Nanoparticles by Surface-Enhanced Raman Scattering. *Analyst* **2012**, ***137***, 3925-3928.

17. Jain, S.; Hirst, D. G.; O'Sullivan, J. M. Gold nanoparticles as Novel Agents for Cancer Therapy. *Br. J. Radiol.* **2012**, *85*, 101–113.

18. Thomas, K. G.; Kamat, P. V. Chromophore-Functionalized Gold Nanoparticles. *Acc. Chem. Res*. **2003**, *36*, 888–898.

19. Moores, A.; Goettmann, F. The Plasmon Band in Noble Metal Nanoparticles: An Introduction to Theory and Applications. *New J. Chem.* **2006**, *30*, 1121–1132.

20. Ghosh, S. K.; Nath, S.; Kundu, S.; Esumi, K.; Pal, T. Solvent and Ligand Effects on the Localized Surface Plasmon Resonance (LSPR) of Gold Colloids. *J. Phys. Chem. B* **2004**, *108*, 13963–13971.

21. Eustis, S.; El-Sayed, M. A. Why Gold Nanoparticles Are More Precious than Pretty Gold: Noble Metal Surface Plasmon Resonance and Its Enhancement of the Radiative and Nonradiative Properties of Nanocrystals of Different Shapes. *Chem. Soc. Rev.* **2006**, *35*, 209-217.

22. Neouze, M.-A.; Schubert, U. Surface Modification and Functionalization of Metal and Metal Oxide Nanoparticles by Organic Ligands. *Monatshefte für Chemie - Chem. Mon.* **2008**, *139*, 183–195.

23. Santosh, G.; Shirman, E.; Weissman, H.; Shimoni, E.; Pinkas, I.; Rudich, Y.; Rybtchinski, B. Photofunctional Self-Assembled Nanostructures Formed by Perylene Diimide−Gold Nanoparticle Hybrids. *J. Phys. Chem. B* **2010**, 114, 14389–14396.

24. Ipe, B. I.; Thomas, K. G. Photoinduced Charge Separation in a Fluorophore−Gold Nanoassembly. *J. Phys. Chem. B* **2002**, *106*, 18–21.

25. Zin, M. T.; Yip, H-L.; Ma, W. H.; Jen, A. K.-Y. Arrays of Covalently Bonded Single Gold Nanoparticles on Thiolated Molecular Assemblies. *Langmuir* **2006**, *22*, 6346-6351.

26. Sidhaye, D. S.; Bala, T.; Srinath, S.; Srikanth, H.; Poddar, P.; Sastry, M.; Prasad, B. L. V. Preparation of Nearly Monodisperse Nickel Nanoparticles by a Facile Solution Based Methodology and Their Ordered Assemblies. *J. Phys. Chem. C* **2009**, *113*, 3426–3429.

27. Yang, H. T.; Shen,C. M.; Wang, Y. G.; Su, Y. K. Yang, T. Z.; Gao, H. J. .Stable cobalt nanoparticles passivated with oleic acid and triphenylphosphine. *Nanotechnology*, **2004**, *15*, 70–74.

28. Hiramatsu, H.; Osterloh, F. E. A Simple Large-Scale Synthesis of Nearly Monodisperse Gold and Silver Nanoparticles with Adjustable Sizes and with Exchangeable Surfactants. *Chem. Mater.* **2004**, 16, 2509–2511.

29. Bastús, N. G.;Merkoçi, F.; Piella, J.; Puntes, V. Synthesis of Highly Monodisperse Citrate-Stabilized Silver Nanoparticles of up to 200 nm: Kinetic Control and Catalytic Properties. *Chem. Mater.* **2014**, *26*, 2836–2846.

30. Pillai, Z. S.; Kamat, P. V. What Factors Control the Size and Shape of Silver Nanoparticles in the Citrate Ion Reduction Method? *J. Phys. Chem. B* **2004**, *108*, 945–951.

31. Lin, C-S.; Khan, M. R.; Lin, S. D. The Preparation of Pt Nanoparticles by Methanol and Citrate. *J. Colloid Interface Sci.* **2006**, *299*, 678-85.

32. Henglein, A. Colloidal Palladium Nanoparticles: Reduction of Pd(II) by H_2; $Pd_{Core}Au_{Shell}Ag_{Shell}$ Particles. *J. Phys. Chem. B* **2000**, *104*, 6683–6685.

33. Kimling, J.; Maier, M.; Okenve, B.; Kotaidis, V.; Ballot, H.; Plech, A. Turkevich Method for Gold Nanoparticle Synthesis Revisited. *J. Phys. Chem. B* **2006**, *110*, 15700−15707.

34. Chen, Y-S.; Choi, H.; Kamat, P. V. Metal-Cluster-Sensitized Solar Cells. A New Class of Thiolated Gold Sensitizers Delivering Efficiency Greater Than 2%. *J. Am. Chem. Soc.* **2013**, *135*, 8822–8825.

35. Luo, Z.; Yuan, X.; Yu, Y.; Zhang, Q., Leong, D. T. Lee, J. Y.; Xie, J. From Aggregation-Induced Emission of Au(I)–Thiolate Complexes to Ultrabright Au(0)@Au(I)–Thiolate Core–Shell Nanoclusters. *J. Am. Chem. Soc.* **2012**, 134, 16662–16670

36. Stamplecoskie, K. G.; Kamat, P. V. Size-Dependent Excited State Behavior of Glutathione-Capped Gold Clusters and Their Light-Harvesting Capacity. *J. Am. Chem. Soc.* **2014**, *136*, 11093–11099.

37. Stamplecoskie, K. G.; Chen, Y-S.; Kamat, P. V. Excited-State Behavior of Luminescent Glutathione-Protected Gold Clusters. *J. Phys. Chem. C* **2014**, *118*, 1370–1376.

38. Liz-Marzán, L. M.; Lado-Touriño, I. Reduction and Stabilization of Silver Nanoparticles in Ethanol by Nonionic Surfactants. *Langmuir* **1996**, *12*, 3585–3589.

39. Chen, Y.; Gu, X.; Nie, C-G.; Jiang, Z-Y.; Xie, Z-X.; Lin, C-J. Shape Controlled Growth of Gold Nanoparticles by a Solution Synthesis. *Chem. Commun.* **2005**, 4181-4183.

40. Esumi, K.; Kameo, A.; Suzuki, A.; Torigoe, A. Preparation of Gold Nanoparticles in Formamide and N,N-dimethylformamide in the Presence of Poly(amidoamine) Dendrimers with Surface Methyl Ester Groups. *Colloid Surface A* **2001,** *189*, 155–161.

41. Pastoriza-Santos, I.; Liz-Marzán, L. M. Formation and Stabilization of Silver Nanoparticles through Reduction by N,N-Dimethylformamide. *Langmuir* **1999**, *15*, 948–951.

42. Duggan, J. N.; Roberts, C. B. Aggregation and Precipitation of Gold Nanoparticle Clusters in Carbon Dioxide-Gas-Expanded Liquid Dimethyl Sulfoxide. *J. Phys. Chem. C* **2014**, *118*, 14595−14605.

43. Patakfalvi, R.; Diaz, D.; Velasco-Arias, D.; Rodriguez-Gattorno, G.; Santiago-Jacinto, P. Synthesis and Direct Interactions of Silver Colloidal Nanoparticles with Pollutant Gases. *Colloid Polym. Sci.* **2008**, *286*, 67-77.

44. Rodríguez-Gattorno, G.; Díaz, D.; Rendón, L.; Hernández-Segura, G.O. Metallic Nanoparticles from Spontaneous Reduction of Silver(I) in DMSO. Interaction between Nitric Oxide and Silver Nanoparticles. *J. Phys. Chem. B* **2002**, *106*, 2482–2487.

45. Kawasaki, H.; Yamamoto, H.; Fujimori, H.; Arakawa, R.; Iwasaki, Y.; Inada, M. Stability of the DMF-Protected Au Nanoclusters: Photochemical, Dispersion, and Thermal Properties. *Langmuir* **2010**, 26, 5926–5933.

46. Kang, S. Y.; Kim, K. .Comparative Study of Dodecanethiol-Derivatized Silver Nanoparticles Prepared in One-Phase and Two-Phase Systems. *Langmuir* **1998**, *14*, 226–230.

47. Gracea, N. A.; Pandian, K. Synthesis of gold and Platinum nanoparticles using Tetraaniline as Reducing and Phase Transfer Agent—A Brief Study and Their Role in the Electrocatalytic Oxidation of Glucose. *J. Phys. Chem. Solids* **2007**, *68*, 2278–2285.

48. Chen, S.; Huang, K.; Stearns, J. A. Alkanethiolate-Protected Palladium Nanoparticles. *Chem. Mater.* **2000**, *12*, 540–547.

49. Zamborini, F. P.; Gross, S. M.; Murray, R. W. Synthesis, Characterization, Reactivity, and Electrochemistry of Palladium Monolayer Protected Clusters. *Langmuir* **2001**, *17*, 481–488.

50. Song, X.; Sun, S.; Zhang, W.; Yin, Z. A Method for the Synthesis of Spherical Copper Nanoparticles in the Organic Phase. *J. Colloid Interface Sci.* **2004**, *273*, 463–469.

51. Demortiere, A.; Petit, C. First Synthesis by Liquid−Liquid Phase Transfer of Magnetic Co_xPt_{100-x} Nanoalloys. *Langmuir* **2007**, *23*, 8575–8584.

52. Song, W.; Wu, C.; Yin, H.; Liu, X.; Sa, P.; Hu, J. Preparation of PbS Nanoparticles by Phase-Transfer Method and Application to Pb^{2+}-Selective Electrode Based on PVC Membrane. *Anal. Lett.* **2008**, *41*, 2844–2859.

53. Templeton, A. C.; Hostetler, M. J.; Warmoth, E. K.; Chen, S.; Hartshorn, C. M.; Krishnamurthy, V. M.; Forbes, M. D. E.; Murray, R. W. Gateway Reactions to Diverse, Polyfunctional Monolayer Protected Gold Clusters. *J. Am. Chem. Soc.* **1998**, *120*, 4845-4849.

54. Lee, W.-J.; Hostetler, M. J.; Murray, R. W.; Majda, M. Electron Hopping and Electronic Conductivity in Monolayers of Alkanethiol-Stabilized Gold Nano-Clusters at the Air/Water Interface. *Isr. J. Chem.* **1997**, *37*, 213-223.

55. Dongil Lee, Robert L. Donkers, Gangli Wang, Amanda S. Harper, and Royce W. Murray,Electrochemical and Optical Absorbance and Luminescence of Molecule-like Au_{38} Nanoparticles. *J. Am. Chem. Soc.* **2004**, 126, 6193-6199.

56. Hostetler, M. J.; Wingate, J. E.; Zhong, C.-Z.; Harris, J. E.; Vachet, R. W.; Clark, M. R.; Londono, J. D.; Green, S. J.; Stokes, J. J.; Wignall, G. D.; Glish, G. L.; Porter, M. D.; Evans, N. D.; Murray, R. W. Alkanethiolate Gold Cluster Molecules with Core Diametersfrom 1.5 to 5.2 nm: Core and Monolayer Properties as a Functionof Core Size. *Langmuir* **1998**, *14*, 17-30.

57. Hostetler, M. J.; Zhong, C.-J.; Yen, B. K. H.; Anderegg, J.;Gross, S. M.; Evans, N. D.; Porter, M.; Murray, R. W. Stable, Monolayer-Protected Metal Alloy Clusters. *J. Am. Chem. Soc.* **1998**, *120*, 9396-9397.

58. Green, S. J.; Stokes, J. J.; Hostetler, M. J.; Pietron, J. J.; Murray, R. W. Three-Dimensional Monolayers: Nanometer-sized Electrodes of Alkanthiolate-Stabilized Gold Cluster Molecules. *J. Phys.Chem. B* **1997**, *101*, 2663-2668.

59. Green, S. J.; Pietron, J. J.;Stokes, J. J.; Hostetler, M. J.; Vu, H.; Wuelfing, W. P.; Murray, R.W. Three-Dimensional Monolayers: Voltammetry of Alkanethiolate-Stabilized Gold Cluster Molecules. *Langmuir* **1998**, *14*, 5612-5619.

60. Leff, D. V.; Brandt, L.; Heath, J. R. Synthesis and Characterization of Hydrophobic, Organically-Soluble Gold Nanocrystals Functionalized with Primary Amines. *Langmuir* **1996**, *12*, 4723–4730.

61. Rucareanu, S.; Maccarini, M.; Shepherd, J. L.; Lennox, R. B. Polymer-Capped Gold Nanoparticles by Ligand-Exchange Reactions. *J. Mater. Chem.* **2008**, *18*, 5830–5834.

62. Woehrle, G. H.; Brown, L. O.; Hutchison, J. E. Thiol-Functionalized, 1.5-nm Gold Nanoparticles through Ligand Exchange Reactions: Scope and Mechanism of Ligand Exchange. *J. Am. Chem. Soc.* **2005**, *127*, 2172–2183.

63. Hostetler, M. J.; Templeton, A. C.; Murray, R. W. Dynamics of Place-Exchange Reactions on Monolayer-Protected Gold Cluster Molecules. *Langmuir* **1999**, *15*, 3782–3789.

64. Labande, A.; Ruiz, Astruc, D. Supramolecular Gold Nanoparticles for the Redox Recognition of Oxoanions: Syntheses, Titrations, Stereoelectronic Effects, and Selectivity. *J. Am. Chem. Soc.* **2002**, *124*, 1782–1789.

65. Petroski, J.; Chou, M. H.; Creutz, C. Rapid Phosphine Exchange on 1.5-nm Gold Nanoparticles. *Inorg. Chem.* **2004**, *43*, 1597–1599.

66. Brown, L. O.; Hutchison, J. E. Convenient Preparation of Stable, Narrow-Dispersit, Gold Nanocrystals by Ligand Exchange Reactions. *J. Am. Chem. Soc.* **1997**, *119*, 12384–12385.

67. Warner, M. G.; Reed, S. M.; Hutchison, J. E. Small, Water-Soluble, Ligand-Stabilized Gold Nanoparticles Synthesized by Interfacial Ligand Exchange Reactions. *Chem. Mater.* **2000**, *12*, 3316–3320.

68. Chechik, V. Reduced Reactivity of Aged Au Nanoparticles in Ligand Exchange Reactions. *J. Am. Chem. Soc.* **2004**, *126*, 7780–7781.

69. Ma, Y.; Chechik, V. Aging of Gold Nanoparticles: Ligand Exchange with Disulfides

Langmuir **2011**, *27*, 14432–14437.

70. Robinsona, I.; Alexanderb, C.; Tungc, L. D.; Fernig, D. G.; Thanhf, N. T. K. Fabrication of Water-Soluble Magnetic Nanoparticles by Ligand-Exchange with Thermo-Responsive Polymers . *J. Magn. Magn. Mater*. **2009**, *321*, 1421–1423.

71. Wang, Y.; Wong, J. F.; Teng, X.; Lin, X. Z.; Yang, H. "Pulling" Nanoparticles into Water: Phase Transfer of Oleic Acid Stabilized Monodisperse Nanoparticles into Aqueous Solutions of α-Cyclodextrin. *Nano Lett*. **2003**, *3*, 1555–1559.

72. Binder, W. H.; Weinstabl, H.; Sachsenhofer, R. Superparamagnetic Ironoxide Nanoparticles via Ligand Exchange Reactions: Organic 1,2-Diols as Versatile Building Blocks for Surface Engineering. *J. Nanomater.* **2008**, Article ID 383020.

73. Boal, A. K.; Das, K.; Gray, M.; Rotello, V. M. Monolayer Exchange Chemistry of γ-Fe2O3 Nanoparticles. *Chem. Mater.* **2002**, *14*, 2628–2636.

74. Owen, J. S.; Park, J.; Trudeau, P.-E.; Alivisatos, A. P. Reaction Chemistry and Ligand Exchange at Cadmium−Selenide Nanocrystal Surfaces. *J. Am. Chem. Soc.* **2008**, *130*, 12279–12281.

75. Lokteva, I.; Radychev, N.; Witt, F.; Borchert, H.; Parisi, J.; Kolny-Olesiak, J. Surface Treatment of CdSe Nanoparticles for Application in Hybrid Solar Cells: The Effect of Multiple Ligand Exchange with Pyridine. *J. Phys. Chem. C* **2010**, *114*, 12784-91.

76. Zhao, Y.; Li, Y.;Song, Y.; Jiang, W.; Wu, Z.; Wang, Y. A.; Sun, J.; Wang, J. Architecture of Stable and Water-soluble CdSe/ZnS Core–Shell Dendron Nanocrystals via Ligand Exchange *J. Colloid Interface Sci.* **2009**, *339*, 336–343.

77. Kim, H.; Suh, M.; Kwon, B.-H.; Jang, D. S.; Kim, S. W.; JeonIn, D. Y. In Situ Ligand Exchange of Thiol-Capped CuInS2/ZnS Quantum Dots at Growth Stage without Affecting Luminescent Characteristics. *J. Colloid interface Sci.* **2011**, *363*, 703-706.

78. Lala, N.; Lalbegi, S. P.; Adyanthaya, S. D.; Sastry, M. Transfer of Aqueous Gold Colloidal Particles Capped with Inclusion Complexes of Cyclodextrin and Alkanethiol Molecules into Chloroform. *Langmuir* **2001**, *17*, 3766–3768.

79. Alkilany, A. M.; Yaseen, A. I. B.; Park, J.; Eller, J. R.; Murphy, C. J. Facile Phase Transfer of Gold Nanoparticles from Aqueous Solution to Organic Solvents with Thiolated Poly(ethylene glycol). *RSC Adv.* **2014**, *4*, 52676-52679.

80. Liu, J.; Sutton, J.; Roberts, C. B. Synthesis and Extraction of Monodisperse Sodium Carboxymethylcellulose-Stabilized Platinum Nanoparticles for the Self-assembly of Ordered Arrays. *J. Phys. Chem. C* **2007**, *111*, 11566–11576.

81. Hong, R.; Fischer, N. O.; Emrick, T.; Rotello, V. M. Surface PEGylation and Ligand Exchange Chemistry of FePt Nanoparticles for Biological Applications. *Chem. Mater.* **2005**, *17*, 4617–4621.

82. Sun, S.; Anders, S.; Thomson, T.; Baglin, J. E. E.;Toney, M. F.; Hamann, H. F.; C. B. Murray, C. B.; Terris, B. D. Controlled Synthesis and Assembly of FePt Nanoparticles. *J. Phys. Chem. B* **2003**, *107*, 5419–5425.

83. Roberts, J. J. P.; Vuong, K. T.; Murray, R. W. Synthesis and Electrochemistry of 6 nm Ferrocenated Indium–Tin Oxide Nanoparticles. *Langmuir* **2013**, *29*, 474–479.

84. Bijanzadeh, A. R.; Vakili, M. R.; Khordad, R. A. Study of the Surface Plasmon Absorption Band for Nanoparticles. *Int. J. Phys. Sci.* **2012**, *7*, 1943–1948.

85. Creighton, A.; Eadon, D. G. Ultraviolet–visible Absorption Spectra of the Colloidal Metallic Elements. *J. Chem. Soc. Faraday Trans.* **1991**, *87*, 3881–3891.

86. Mock, J. J.; Smith, D. R.; Schultz, S. Local Refractive Index Dependence of Plasmon Resonance Spectra from Individual Nanoparticles. *Nano Lett.* **2003**, *3*, 485–491.

87. Wei, J.; Schae, N.; Pileni, M. Ag Nanocrystals: 1. Effect of Ligands on Plasmonic Properties *J. Phys. Chem. B* **2014**, *118*, 14070−14075.

88. Moores, A.; Goettmann, F.; Sanchez, C.; Le Floch, P. Phosphinine Stabilised Gold Nanoparticles; Synthesis and Immobilisation on Mesoporous Materials. *Chem. Commun*. **2004**, 2842–2843.

89. Mulvaney, P. Surface Plasmon Spectroscopy of Nanosized Metal Particles. *Langmuir* **1996**, *12*, 788–800.

90. Herrera, M. Z.; Aizpurua, J.; Kazansky, A. K.; Borisov, A. G. Plasmon Response and Electron Dynamics in Charged Metallic Nanoparticles. *Langmuir* **2016**, *32*, 2829–2840.

91. Hicks, J. F.; Miles, D. T.; Murray, R. W. Quantized Double-Layer Charging of Highly Monodisperse Metal Nanoparticles. *J. Am. Chem. Soc.* **2002**, *124*, 13322–13328.

92. Quinn, B. M.; Liljeroth, P.; Ruiz, V.; Laaksonen, T.; Kontturi, K. Electrochemical Resolution of 15 Oxidation States for Monolayer Protected Gold Nanoparticles. *J. Am. Chem. Soc.* **2003**, *125*, 6644-6645.

93. Miles, D. T.; Murray, R. W. Redox and Double-Layer Charging of Phenothiazine Functionalized Monolayer-Protected Clusters. *Anal. Chem.* **2001**, *73*, 921-929.

94. Lica, G. C.; Zelakiewicz, B. S.; Tong, Y. Y. Electrochemical and NMR Characterization of Octanethiol-Protected Au Nanoparticles. *J. Electroanal. Chem*. **2003,** *554-555*, 127-132.

95. Holm, A. H.; Ceccato, M.; Donkers, R. L.; Fabris, L.; Pace, G.; Maran, F. Effect of Peptide Ligand Dipole Moments on the Redox Potentials of Au_{38} and Au_{140} Nanoparticles. *Langmuir* **2006**, *22*, 10584-10589.

96. Su, B.; Zhang, M.; Shao, Y.; Girault, H. H. Solvent Effect on Redox Properties of Hexanethiolate Monolayer-Protected Gold Nanoclusters. *J. Phys. Chem. B* **2006**, *110*, 21460-21466.

97. Chen, S. Nanoparticle Assemblies: "Rectified" Quantized Charging in Aqueous Media. *J. Am. Chem. Soc.* **2000**, *122*, 7420-7421.

98. Guo, R.; Georganopoulou, D.; Feldberg, S. W.; Donkers, R.; Murray,R. W. Supporting Electrolyte and Solvent Effects on Single-Electron Double Layer Capacitance Charging of Hexanethiolate-Coated Au_{140} Nanoparticles. *Anal. Chem.* **2005**, *77*, 2662-2669.

99. Laaksonen, T.; Pelliniemi, O.; Quinn, B. M. Ion Permeability of SAMs on Nanoparticle Surfaces. *J. Am. Chem. Soc.* **2006**, *128*, 14341-14346.

100. Giovanni, M.; Pumera, M. Size Dependant Electrochemical Behavior of Silver Nanoparticles with Sizes of 10, 20, 40, 80 and 107 nm. *Electroanalysis* **2012**, *24*, 615 – 617.

101. Ung, T.; Giersig, M. Dunstan, D.; Mulvaney, P. Spectroelectrochemistry of Colloidal Silver. *Langmuir* **1997**, *13*, 1773–178.

102. Li, D.; Zhang, Y.; Jiang, J.; Li, J. Electroactive Gold Nanoparticles Protected by 4-Ferrocene Thiophenol Monolayer. *J. Colloid Interface Sci.* **2003**, *264*, 109–113.

103. Hostetler, M. J.; Green, S. J.; Stokes, J. J.; Murray, R. W. Monolayers in Three Dimensions: Synthesis and Electrochemistry of ω-Functionalized Alkanethiolate-Stabilized Gold Cluster Compounds. *J. Am. Chem. Soc.* **1996**, *118*, 4212-4213.

104. Daniel, M.-C.; Ruiz, J.; Nlate, S.; Palumbo, J.; Blais, J.-C.; Astruc, D. Gold Nanoparticles Containing Redox-Active Supramolecular Dendrons that Recognize $H_2PO_4^-$. *Chem. Commun.* **2001**, 2000-2001.

105. Yamada, M.; Quiros, I.; Mizutani, J.; Kubo, K.; Nishihara, H. Preparation of Palladium Nanoparticles Functionalized with Biferrocene thiol Derivatives and their Electro-Oxidative Deposition. *Phys. Chem. Chem.Phys*.**2001**, *3*, 3377-3381.

106. Horikoshi, T.; Itoh, M.; Kurihara, M.; Kubo, K.; Nishihara, H.; Synthesis, Redox Behavior and Electrodeposition of Biferrocene-Modified Gold Clusters. *J. Electroanal. Chem.***1999**, *473*, 113-116.

107. Ingram, R. S.; Murray, R. W. Electroactive three-dimensional monolayers. Anthraquinone alkanethiolate-stabilized gold clusters. *Langmuir* **1998**, *14*, 4115-4121.

108. Pietron, J. J.; Murray, R. W. Mediated Electrocatalysis with Polyanthraquinone-Functionalized Monolayer-Protected Clusters. *J. Phys. Chem. B* **1999**, *103*, 4440-4446.

109. Yamada, M.; Kubo, K.; Nishihara, H. Electroreductive Deposition of Au Clusters Modified with Ananthraquinone Derivative. *Chem. Lett.* **1999**, *28*, 1335-1336.

110. Yamada, M.; Tadera, T.; Kubo, K.; Nishihara, H. Electroreductive Deposition of Anthraquinone Derivative Attached Au Clusters: Optical Properties and Scanning Tunneling Microscopy Observation of the Electrodeposited Cluster Film *Langmuir* **2001**, *17*, 2363-2370.

111. Templeton, A. C. Cliffel, D. E.; Murray, R. W. Redox and Fluorophore Functionalization of Water Soluble, Tiopronin-Protected Gold Clusters. *J. Am. Chem. Soc.* **1999**, *121*, 7081-7089.

112. Xue, C.; Birel, O.; Gao, M.; Zhang, S.; Dai, L.; Urbas, A.; Li, Q. Perylene Monolayer Protected Gold Nanorods: Unique Optical, Electronic Properties and Self-Assemblies. *J. Phys. Chem. C* **2012**, *116*, 10396–10404.

113. Sun, N.; Wang, Y.; Song, Y.; Quo, Z.;Dai, L.; Zhu, D. Novel [60] fullerene-silver Nanocomposite with Large Optical Limiting Effect. *Chem. Phys. Lett.* **2001**, *344*, 277-282.

114. Fujihara, H.; Nakai, H. Fullerenethiolate-Functionalized Gold Nanoparticles: A New Class of Surface Confined Nanocomposites. *Langmuir* **2001**, *17*, 6393-6395.

115. Sudeep, P. K.; Ipe, B. I.;Thomas, K. G.; George, M. V. Fullerene-Functionalized Gold Nanoparticles. A Self-Assembled Photoactive Antenna-Metal Nanocore Assembly. *Nano Lett* **2002**, *2*, 29-35.

116. Chen, S.; Huang, K. Electrochemical Studies of Water-Soluble Palladium Nanoparticles. *J Cluster Sci.* **2000**, *11*, 405-422.

117. Kamat, P. V. Photophysical, Photochemical and Photocatalytic Aspects of Metal Nanoparticles. *J. Phys. Chem. B* **2002**, *106*, 7729–7744.

118. Thomas, K. G.; Kamat, P. V. Making Gold Nanoparticles glow: Enhanced eEmission from a Surface Bound Fluoroprobe. *J. Am. Chem. Soc.***2000**, *122*, 2655-2656.

119. Chen, M. M. Y.; Katz, A. Steady-state Fluorescence-based Investigation of the Interaction between Protected Thiols and Gold Nanoparticles. *Langmuir* **2002**, *18*, 2413-2420.

120. Aguila, A.; Murray, R. W. Monolayer-Protected Clusters with Fluorescent Dansyl Ligands. *Langmuir* **2000**, *16*, 5949–5954.

121. Hu, J.; Zhang, J.; Liu, F.; Kittredge, K.; Whitesell, J. K.; Fox, M. A. Competitive Photochemical Reactivity in a Self-Assembled Monolayer on a Colloidal Gold Cluster. *J. Am. Chem. Soc.* **2001**, *123*, 1464-1470.

122. Imahori, H.; Fukuzumi, S. Porphyrin Monolayer-Modified Gold Clusters as Photoactive Materials. *Adv. Mater.* **2001**, *13*, 1197-1199.

123. Imahori, H.; Arimura, M.; Hanada, T.; Nishimura, Y.; Yamazaki, I.; Sakata, Y.; Fukuzumi, S. Photoactive Three-Dimensional Monolayers: Porphyrin−Alkanethiolate-Stabilized Gold Clusters*J. Am. Chem. Soc.* **2001**, *123*, 335-336.

124. Evans, S. D.; Johnson, S. R.; Ringsdorf, H.; Williams, L. M.; Wolf, H. Photoswitching of Azobenzene Derivatives Formed on Planar and Colloidal Surfaces. *Langmuir* **1998**, *14*, 6436-6440.

125. Kamat, P. V.; Barazzouk, S.; Hotchandani, S. ElectrochemicalModulation of Fluorophore Emission at a Nanostructured Gold Film. *Angew. Chem., Int. Ed.* **2002**, *41*, 2764-2767.

126. Stellacci, F.; Bauer, C. A.; Meyer-Friedrichsen, T.; Wenseleers, W.; Marder, S. R.; Perry, J. W. Ultrabright Supramolecular Beacons Based on the Self-Assembly of Two-Photon Chromophores on Metal Nanoparticles. *J. Am. Chem. Soc.* **2003**, *125*, 328-329.

127. Shibu, E. S.; Sonoda, A.; Tao, Z.; Feng, Q.; Furube, A.; Masuo, S.; Wang, L.; Tamai, N.; Ishikawa, M.; Biju, V. Photofabrication of Fullerene-Shelled Quantum Dots Supramolecular Nanoparticlesfor Solar Energy Harvesting. *ACS nano* **2012**, *6*, 1601–1608.

128. Gu, T.; Whitesell, J. K.; Fox, M. A. Energy Transfer from a Surface-Bound Arene to the Gold Core in ω-Fluorenyl-Alkane-1-ThiolateMonolayer-Protected Gold Clusters. *Chem. Mater.* **2003**, *15*, 1358-1366.

129. Lee, S.H.; Jang, B.B.; Tsutsui, T. Sterically Hindered Fluorenyl Substituted Poly(p-phenylenevinylenes) for Light-Emitting Diodes. *Macromolecules* **2002**, *35*, 1356-1364.

130. Winder, C.; Matt, G.; Hummelen, J.C.; Janssen, R.A.J.; Sariciftci, N.S.; Brabec, C.J. Sensitization of Low Bandgap Polymer Bulk Heterojunction Solar Cell. *Thin Solid Films* **2002**, *403*, 373-379.

131. Winsberg, J.; Hagemann, T.; Muench, S.; Friebe, C.; Häupler, B.; Janoschka, T.; Morgenstern, S.; Hager, M. D.; Schubert , U. S. Poly(boron-dipyrromethene)-A Redox-Active Polymer Class for Polymer Redox-Flow Batteries. *Chem. Mater.* **2016**, *28*, 3401–3405.

132. Ates, M.; Karazehir, T.; Sarac, A. S. Conducting Polymers and their Applications. *Current Phys. Chem.* **2012**, *2*, 224-240.

133. Anderson, P. E.; Badlani, R. N.; Mayer, J.; Mabrouk, P. A. Electrochemical Synthesis and Characterization of Conducting Polymers in Supercritical Carbon Dioxide. *J. Am. Chem. Soc.* **2002**, *124*, 10284-10285.

134. Gurunathan, K.; A. Murugan, V. A.; Marimuthu, R. Mulik, U. P., Amalnerkar, D. P. Electrochemically Synthesised Conducting Polymeric Materials for Applications Towards Technology in Electronics, Optoelectronics and Energy Storage Devices. *Mater. Chem. Phys.* **1999**, *61*, 173-191.

135. Nyholm , L.; Nyström, G.; Mihranyan, A.; Strømme, M. Toward Flexible Polymer and Paper-Based Energy Storage Devices. *Adv. Mater.* **2011**, *23*, 3751–3769.

136. Häupler, B.; Rössel, C.; Schwenke, A. M.;Winsberg, J.; Schmidt, D.; Wild, A.;Schubert, U. S. Aqueous Zinc-Organic Polymer Battery with a High rate Performance and Long Lifetime. *NPG Asia Mater.* **2016**, *8*, 1-7.

137. Chen, Z.; Zheng, Y.; Yan, H.; Facchetti, A. Naphthalene dicarboximide- vs Perylenedicarboximide-Based Copolymers. Synthesis and Semiconducting Properties in Bottom-Gate N-Channel Organic Transistors. *J. Am. Chem. Soc.* **2009**, *131*, 8-9.

138. Zhan, X.; Tan, Z. A.; Domercq, B.; An, Z.; Zhang, X.; Barlow, S.; Li, Y.; Zhu, D.; Kippelen, B.; Marder, S. R. A High-Mobility Electron-Transport Polymer with Broad Absorption and Its Use in Field-Effect Transistors and All-Polymer Solar Cells. *J. Am. Chem. Soc.* **2007**, *129*, 7246-7247.

139. Zhan, X. W.; Tan, Z. A.; Zhou, E. J.; Li, Y. F.; Misra, R.; Grant, A.; Domercq, B.; Zhang, X. H.; An, Z. S.; Zhang, X.; Barlow, S.; Kippelen, B.; Marder, S. R. Copolymers of Perylene Diimide with Dithienothiophene and Dithienopyrrole as Electron-Transport Materials for all-Polymer Solar Cellsand Field-Effect Transistors. *J. Mater. Chem.* **2009**, *19*, 5794-5803.

140. Sadki, S.; Schottland, P.; Brodiec, N.; Sabouraud, G. The mechanisms of Pyrrole Electropolymerization. *Chem. Soc. Rev.***2000**, *29*, 283–293.

141. Patel, R. J.; Tighe, T. B.;Ivanov, I. N.; Hickner, M.A. Electro-Optical Properties of Electropolymerized Poly(3-hexylthiophene)/Carbon Nanotube Composite Thin Films. *J. Polym. Sci. Pol. Phys.* **2011**, *49*, 1269–1275.

142. de Surville, R., Jozefowicz, M., Yu, L.T., Perichon, J., and Buvet, R. Electrochemical Chains using Protolytic Organic Semiconductors. *Electrochim.Acta.* **1968**, *13*, 1451-1458.

143. Wei, Y.; Chan, C.C.;Tian, J.; Jang, G. W.; Hsueh, K.F. Electrochemical polymerization of Thiophenes in the Presence of Bithiophene or Terthiophene: Kinetics and Mechanism of the Polymerization. *Chem. Mater.***1991**, *3*, 888–897.

144. Demirboğa, B.; Önal, A. M. Electrochemical Polymerization of Furan and 2-Methylfuran. *Synthetic Met.***1999**, *99*, 237–242.

145. Saraji, M.; Bagheri, A. Electropolymerization of Indole and Study of Electrochemical Behavior of the Polymer in Aqueous Solutions. *Synthetic Met.* **1998**, *98*, 57–63.

146. Wang, F.; Shi, G.; Chen, F.; Xu, J.; Zhang, J. Electrochemical Polymerization of Thianaphthene. *J. Electroanal. Chem.* **2001**, *510*, 29–34.

147. Wei, Z.; Xu, J.; Nie, G.; Du, Y.; Pu, S. Low-potential Electrochemical Polymerization of Carbazole and its Alkyl Derivatives. *J. Electroanal. Chem.* **2006**, *589*, 112–119.

148. Pandey, P. C.; Singh, V. Electrochemical polymerization of aniline over tetracyanoquinodimethane encapsulated or mosil matrix: application in the electrocatalytic oxidation of ascorbic acid and acetylthiocholine. *Analyst* **2011**, *136*, 1472-1480.

149. Bidan, G. Electropolymerized Films of π-Conjugated Polymers. A Tool for Surface Functionalization: a Brief Historical Evolution and Recent Trends. *Electropolymerization, WILEY-VCH Verlag & Co. KGaA, Weinheim* .**2010**, 1–26.

150. Wang, L. Synthesis, Polymerization and Langmuir-Schaefer films of novel Electroactive compounds with Diphenylamine end groups. PhD Dissertation. Auburn University. **1997**.

151. Liang, J. Preparation, Characterization and Application of Electroactive polymers in Electrochromism and Sensors. PhD Dissertation. Auburn University. **2003**.

152. Efimov, I.; Winkels, S.; Schultze, J. W. EQCM Study of Electropolymerization and Redox Cycling of 3,4-Polyethylenedioxythiophene. *J. Electroanal. Chem.* **2001**, *499*, 169–175.

153. Sezer, E.; Skompska , M.; Heınze, J. Voltammetric, EQCM, and In Situ Conductance Studies of p- and n-dopable Polymers based on Ethylenedioxythiophene and Bithiazole. *Electrochim Acta* **2008**, *53*, 2008, 4958–4968.

154. Lu, W.; Gao, J. P.; Wang, Z. Y.; Qi, Y.; Sacripante, G. G.; Duff, J. D.; Sundararajan, P. R. Electrochemical Characterization, Electrochroism, and Voltage-Dependent Fluorescence of Novel Perylene-Containing Polyimides. *Macromolecules* **1999**, *32*, 8880–8885.

155. Milesa, M. J.; Smithb, W. T.; Shapirob, J. S. Morphological Investigation by Atomic Force Microscopy and Light Microscopy of Electropolymerised Polypyrrole Films. *Polymer* **2000**, *41*, 3349–3356

156. Gordon, M. P.; Lloyd, L. T.; Boucher, D. S. Poly(3-hexylthiophene) Films Prepared Using Binary Solvent Mixtures. *J. Polym. Sci., Part B: Polym. Phys* .**2016**, *54*, 624–638.

157. Dufour, B.; Rannou, P.;Travers, J. P.; Pron, A.; Zagórska, M.; Korc, G.;Kulszewicz-Bajer, I.; Quillard, S.; Lefrant, S. Spectroscopic and Spectroelectrochemical Properties of a Poly(alkylthiophene)−Oligoaniline Hybrid Polymer. *Macromolecules*, **2002**, *35*, 6112–6120.

158. Bozzini, B.; Fanigliulo, A. An In Situ Spectroelectrochemical Raman Investigation of Au Electrodeposition and Electrodissolution in $KAu(CN)_2$ Solution. *J. Applied Electrochem.* **2002**, *32*, 1043–1048.

159. de Santana, H.; Temperini, M. L. A.; Rubim, J. C. In Situ Resonance Raman and Reflectance Spectroscopic Study of the Electrochemical Oxidation of Diphenylamine. *J. Electroanal. Chem.* **1993**, *356*, 145-155.

160. Giorgetti, M.1.; Ascone, I.; Berrettoni, M.; Conti, P.; Zamponi, S.; Marassi, R. In Situ X-Ray Absorption Spectroelectrochemical Study of Hydroxocobalamin. *J. Biol. Inorg. Chem.* **2000**, *5*, 156-166.

161. Kondo, T.; Tamura, K.; Takahasi, M.; Mizuki, J.-I.; Uosaki, K. A Novel Spectroelectrochemical Cell for In Situ Surface X-ray Scattering Measurements of Single Crystal Disk Electrodes. *Electrochim Acta* **2002**, *47*, 3075-3080.

162. Wang, Q. Copolymerization and Characterization of novel Bis(Diphenylamine) monomers. M S Thesis. Auburn University. **1999**.

163. Wang, L.; Wang, Q.; Cammarata, V. Electro-oxidative Polymerization and Spectroscopic Characterization of Novel Amide Polymers Using Diphenylamine Coupling. *J. Electrochem. Soc.* **1998**, *145*, 2648-2654.

164. Wang, L.; Cammarata, V. Electropolymers based on Diphenylamine II-Stacking in Cationic Benzidine Units. *Thin Solid Films* **1996**, *284-285*, 297-300.

165. Li, Y. Organic Electronic and Optoelectronic Devices Based on Diphenylamine End-group Polymers. PhD dissertation. Auburn University. **2010**.

166. Fusalba, F.; Gouerec, P.; Villers, D.; Belanger, D. Electrochemical Characterization of Polyaniline in Nonaqueous Electrolyte and its Evaluation as Electrode Material for Electrochemical Supercapacitors. *J. Electrochem. Soc.* **2001**, *148*, A1-A6.

167. Belanger, D.; Ren, X.; Davey, J.; Uribe, F.; Gottesfeld, S. Characterization and Long-Term Performance of Polyaniline-Based Electrochemical Capacitors. *J. Electrochem. Soc.* **2000**, *147*, 2923-2929.

168. de Oliveira, H. P.; Sydlik, S. A.; Swager, T. M. Supercapacitors from Free-Standing Polypyrrole/Graphene Nanocomposites. *J. Phys. Chem. C* **2013**, *117*, 10270–10276.

169. Song, Z.; Zhan, H.; Zhoua, Y. Anthraquinone Based Polymer as High Performance Cathode Material for Rechargeable Lithium Batteries. *Chem. Commun.* **2009**, 448-450.

170. Shown, I.; Ganguly, A.; Chen, L-C.; Chen, K-H.Conducting Polymer-Based Flexible Supercapacitor. *Energy Sci. Eng*. **2015**, *3*, 2-26.

171. Mortimer, R. J.; Dyer, A. L.; Reynolds, J. R. Electrochromic organic and Polymeric Materials for Display Applications. *Displays* **2006**, *27*, 2–18.

172. Avellaneda, C. O.; Bulhões, L. O. Electrochromic properties of WO3 and WO3:P Thin Films. *J. Solid State Electrochem.* **2003**, *7*, 183-186.

173. Green, M.; Pita, K. Lithium Vanadium Bronze Thin Films for Electrochromic Applications. *J. Appl. Phys.***1997**, *81*, 3592-3600.

174. Švegl, F.; Orel, B.; Hutchins, M. G.; Kalcher, K. Structural and Spectroelectrochemical Investigations of Sol-Gel Derived Electrochromic Spinel Co_3O_4 Films. *J. Electrochem Soc.* **1996**, *143*, 1532-1539.

175. Laperrière, G.; Lavoie, M.-A.; Bélange, D. Electrochromic Behavior of Molybdenum Trioxide Thin Films, Prepared by Thermal Oxidation of Electrodeposited Molybdenum

Trisulfide, in Mixtures of Nonaqueous and Aqueous Electrolytes. *J. Electrochem. Soc.***1996**, *143*, 3109-3117.

176. Pei, Q.; Zuccarello, G.; Ahlskogt, M.; Inganas, O. Electrochromic and Highly Stable Poly(3,4-ethylenedioxythiophene) Switches between Opaque Blue-Black and Transparent Sky Blue. *Polymer* **1994**, *35*, 1347-1351.

177. Rourke, F.; Crayston, J. A. Cyclic Voltammetry and Morphology of Polyaniline-coated Electrodes containing $[Fe(CN),]^{3-/4-}$ Ions. *J. Chem. Soc. Farad. Trans.***1993**, *89*, 295-302.

178. Ebisawa, F.; Kurokawa, T.; Nara, S. Electrical-Properties of Polyacetylene Polysiloxane Interface. *J. Appl. Phys.***1983**, *54*, 3255-3259.

179. Ito, H.; Niimi, Y.; Suzuki, A.; Marumoto, K.; Kuroda, S. Photocurrent of Regioregular Poly(3-alkylthiophene)/Fullerenecomposites in Surface-type Photocells. *Thin Solid Films* **2008**, *516*, 2743-2746.

180. Sirringhaus, H.; Brown, P.J.; Friend, R.H.; Nielsen, M.M.;Bechgaard, K.; Langeveld-Voss, B.M.W.; Spiering, A.J.H.;Janssen, R.A.J.; Meijer, E.W.; Herwig, P.; de Leeuw, D.M. Two Dimensional Charge Transport in Self-Organized, High-mobility Conjugated Polymers. *Nature* **1999**, *401*, 685-688.

181. Park, Y.D.; Kim, D.H.; Jang, Y.; Cho. J.H.; Hwang, M.; Lee, H.S.; Lim, J.A.; Cho, K. Effect of Side Chain Length on Molecularordering and Field-Effect Mobility in Poly(3-alkylthiophene) Transistors. *Org. Electron.* **2006**, *7*, 514-520.

182. Abruna, H. D.; Denisevich, P.; Umana, M.; Meyer, T. J.; Murray, R. W. Rectifying Interfaces Using Two-Layer Films ofElectrochemically Polymerized Vinylpyridine and

Vinylbipyridine Complexes of Ruthenium and Iron onElectrodes. *J. Am. Chem. Soc.* **1981**, *103*, 1-5.

183. Denisevich, P.; Willman, K. W.; Murray, R. W. Unidirectional Current Flow and Charge State Trapping atRedox Polymer Interfaces on Bilayer Electrodes:Principles, Experimental Demonstration, and Theory. *J. Am. Chem. Soc.***1981**, *103*, 4727-4737.

184. Leidner, C. R.; Murray, R. W. Estimation of the Rate of Electron Transfers between Two Contacting Polymer Surfaces. *J. Am. Chem. Soc.***1985**, *107*, 551-6.

185. Aizama, M.; Shinohara, H. Electrochemical Fabrication of a Polypyrrole/Polythiophene p-n Junction Diode. *Synth. Metal* **1987**, *18*, 711-714.

186. Robinson, S. G.; Lonergan, M. C. Polyacetylene p−n Junctions with Varying Dopant Density by Polyelectrolyte-Mediated Electrochemistry. *J. Phys. Chem. C* **2013**, *117*, 1600−1610

187. Lin, F.; Walker, E. M.; Lonergan, M. C. Photochemical Doping of an Adaptive Mix-Conducting p-n Junction. *J. Phys. Chem. Lett.* **2010**, *1*, 720–723.

188. Hoven, C. V.;Wang, H.; Elbing, M.;Garne, L.;Winkelhaus, D.; Bazan, G. C. Chemically Fixed p–n Heterojunctions for Polymer Electronics by Means of Covalent B–F Bond Formation. *Nat. Mater.* **2010**, *9*, 249-252.

189. Cammarata, V.; Hao, N.; Metz, J.; Liang, J. Electrochemical Quartz Crystal Microbalance Studies of the Growth of Perylene-Containing Films. *ACS Symposium Series 832. Conducting Polymers and Polymer Electrolytes* **2009**, *5*, 59–74.

190. Wang, L.; Goodloe, W. G.; Stallman, B. J.; Cammarata, V. Synthesis, Electrooxidation, and Characterization of Bis(diphenylamine)naphthalene Diimide. *Chem Mate*r. **1996**, *8*, 1175-1181

Chapter Two

NAPHTHALENE DIIMIDE LINKER ON SILVER AND GOLD NANOPARTICLES: SYNTHESIS AND CHARACTERIZATION

2.1 Introduction

Synthetic procedures for metal nanoparticles are not limited to just tuning their shape, size and stability. Functionalizing their surfaces with important organic molecules can control the optical and electronic properties of metal nanoparticles.[1,2] The surface electrons of metal nanoparticles oscillate and a distinct strong plasmon absorption band can be observed in the UV-visible region.[3] Organic molecules on the surface interact with the surface electrons and can change the optical behavior because of changes in dielectric constant.[1,3] This property has created a wide range of research opportunities in device development using metal nanoparticles in the areas of photonics, electronics and biology.[4–6] All areas of nanoparticle applications can take advance of surface functionalization because this modification can result in a controlled particle assembly or in the delivery of nanoparticles to a target.

The use of organosulfur compounds like thiols or disulfides for modification of the metal nanoparticle surface has been studied extensively because of the strong binding affinity of sulfur to noble metal atoms.[7–9] Other functional groups, including carboxylic acids,[10] amines,[11] and phosphines,[12] have been employed as capping agents. Organic-inorganic donor –acceptor building blocks with chromosphore-functionalized metal nanoparticles have showed improved photochemical conversion of light into energy.[13–15] Photoactive fullerene and pyrene molecules attached to the Au nanoparticles surface have improved photoinduced charge separation for energy transfer from the fluorophore to the gold nanocore.[13,14] Fluorescence quenching was also observed when tiopronine and dansyl were anchored on the surface of Au clusters.[16,17] Murray's

research group has studied ferrocene functionalized Au, SiO_2, and ITO nanoparticles as electroactive nanomaterials.[18–22]

Naphthalene and perylene diimides are redox active molecule that have interesting properties for potential application as photorefractive media for optical signal processing, electron transporting components in organic light emitting diodes and semiconducting materials for solar energy conversion.[23] Perylene diimide coated gold nanoparticles and perylene diimide –silicon hybrid nanocomposites and their photophysical properties have been discussed earlier.[24–27] Different electropolymerizable monomers containing diphenylamine (DPA) with electroactive groups including naphthalene diimide, ferrocene, benzimide and perylene diimide have been reported from our lab.[28–33] For the first time here we report the synthesis of naphthalene diimide (NDI) functionalized silver and gold nanoparticles (Scheme 2.1). Asymmetric naphthalene diimide (DPA-NDI-SH) was synthesized with benzenethiol and diphenylamine end group according to the literature.[29,34] Nanoparticles were synthesized using a high temperature method in DMSO and DMF as both solvents and reducing agents.

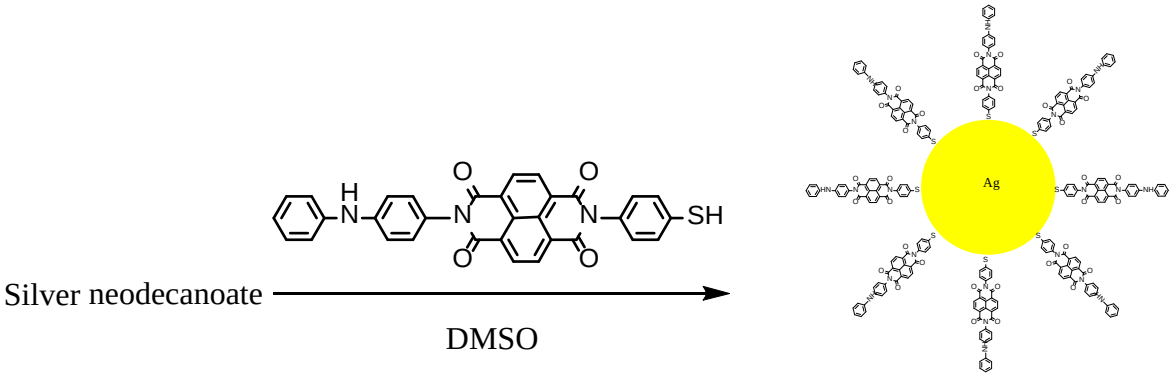

Scheme 2.1: Naphthalene diimide linked nanoparticle formation.

2.2 Experimental

2.2.1 Materials:

Silver neodecanoate and gold (I) sodium thiosulfate were purchased from Strem Chemicals and Alfa Aesar respectively and used as received. Dimethyl sulfoxide (DMSO) and dimethyl formamide (DMF) were obtained from Macron fine chemicals and Fisher, respectively. Dichloromethane (BDH Chemicals) was freshly distilled from calcium hydride (Aldrich) before use. Tetrabutyl ammonium tetrafluoroborate($TBABF_4$) was synthesized as described in the literature.[35]

2.2.2 Synthesis of DPA-NDI-SH:

DPA-NDI-SH has been synthesized according to the process described earlier.[29,34] Briefly the synthetic procedure for DPA-NDI-SH is as follows (Scheme 2.2): 0.30 g of 1,4,5,8-naphthalene tetracarboxylic dianhydride was placed in a flask and 10 mL of DMA was added to the flask and heated to 90^{o} C to dissolve the dianhydride. Then a solution of 4-aminothiophenol (0.14 g in 6 mL of DMA) was added dropwise over 10 min. Then the solution was heated at 135^{o} C for 20 h. The product was precipitated out with diethyl ether, filtered and washed with copius amounts of acetone and diethyl ether. 0.24 g of the intermediate product, N-(p-aminothiophenyl)-1,4,5,8-naphthalene tetracarboxylic imide was obtained. Yield = 56%.

FT-IR (KBr): (cm^{-1}) = 1786, 1746, 1715, 1673, 1587, 1490, 1447, 1346, 1247, 1195, 854, 766, 744.

0.24 g N-(p-aminothiophenyl)-1,4,5,8-naphthalene tetracarboxylic imide was dissolved in10 mL of DMA and the temperature is raised to 135^{o} C. Then 0.26 g of N-phenyl-1,4 phenylenediamine was added portion wise over 10 min. The temperature of the reaction mixture was held at 135^{o} C for 24 h. The product was precipitated out with diethyl ether, filtered and washed with copious amounts of acetone and diethyl ether. 0.23 g of the final product were obtained. Yield = 68%.

FT-IR (KBr): (cm^{-1}) = 1714, 1671, 1591, 1511, 1493, 1345, 1248, 1191, 767, 746.

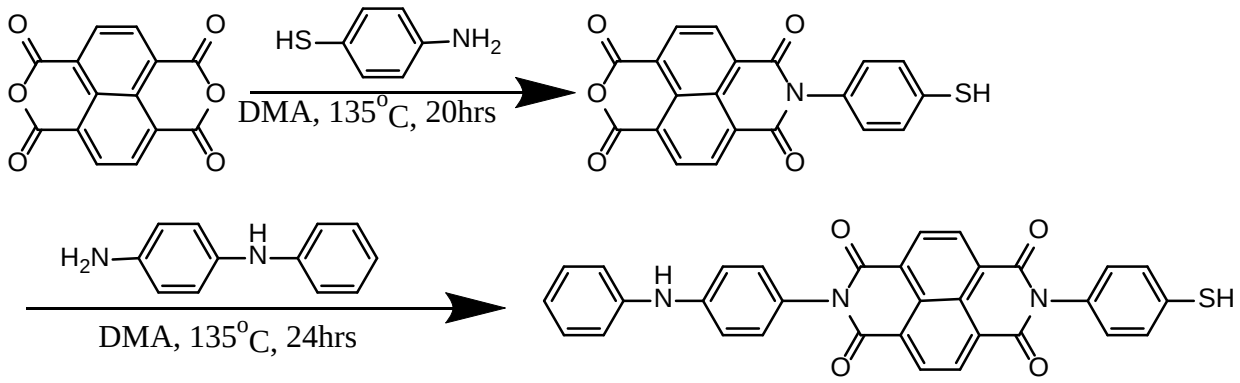

Scheme 2.2: Synthesis of DPA-NDI-SH.

2.2.3 Nanoparticles synthesis:

Ag nanoparticles:

Ag nanoparticles were synthesized by a very simple method in a single reaction vessel. In a typical synthesis, 0.0027 g ($5x10^{-3}$ mmol) of DPA-NDI-SH were dissolved in 100 mL of DMSO in a round bottom flask. Then 0.0279 g of Silver neodecanoate was added to the DPA-NDI-SH solution in DMSO and heated at 100^{o} C for 3 h. The final concentration of silver neodecanoate was 1 mM.

Surface modification:

The process was performed by mixing butanethiol ($50x10^{-3}$ mmol) to the synthesized 1 mM Ag nanoparticles in DMSO (50 mL) and stirred overnight and then the particles were collected through centrifugation and dried.

Au nanoparticles:

Au nanoparticles were also synthesized via a single step in DMF. 0.0027 g DPA-NDI-SH and 0.0061 g gold (I) sodium thiosulfate were added to 100 mL DMF and heated at 140^0 C for 4 h.

To collect the particles from the reaction mixture, centrifugation was utilized at 7000 and 12500 rpm for Ag and Au nanoparticles respectively for about 25 min after adding methanol (EMD Millipore Corporation). The collected precipitates were washed two times with methanol, centrifugating the suspensions after every wash and finally dried using N_2 for XRD, FT-IR and TGA characterization.

2.2.4 Nanoparticles Characterization:

UV-Visible:

UV-Visible spectroscopic measurements of the Ag and Au nanoparticles at different dilutions in DMSO and DMF, respectively, were carried out using a HP 8453 UV-Visible spectrophotometer.

TEM:

The prepared nanoparticles were diluted using methanol and drop cast onto carbon coated copper grids (400 mesh) (Electron microscopy Sciences) and then dried. The measurements were carried out by ZEISS EM10 instrument operating at 200 kV. The particles size distribution was determined by ImageJ software.

FT-IR:

Fourier transform infrared spectroscopic measurements were carried out by means of a FT-IR spectrophotometer (Shimadzu IR Prestige -21) at 2 cm^{-1} resolution. Prior to the measurements, the dried solid nanoparticles were mixed with potassium bromide and compressed into pellets.

XRD Analysis:

Bruker D-8 Discover Diffractometer was used to analyze the prepared nanoparticles. Samples were drop cast in a glass slide and then dried in air. The powder diffractometer was operated at a voltage of 40 kV and a current of 40 mA with Cu Kα radiation in ambient temperature.

TGA Analysis:

The thermogravimetric analysis was performed by Q500 from TA Instruments Inc (DE, USA). A 10 mg sample was placed in an aluminum sample pan and then the analysis was carried out in a N_2 atmosphere at a heating rate of 10^{o} C min^{-1}, from 0^{o} C to 800^{o} C to evaluate the organic content in the nanoparticles samples.

Electrochemistry:

Cyclic Voltammetry was performed on a modified AFRDE4 Bi-Potentiostat (Pine Instrument Co.) electrochemistry workstation. The experiments were performed on a three electrode electrochemical cell with a spiral Pt wire counter electrode and a Ag/AgCl reference electrode saturated with KCl. The working electrodes were glassy carbon disk (3mm diameter), An Au disk (1.5mm diameter) and an Indium Tin Oxide (ITO) coated glass (variable dimension) electrodes. The Au and GC disk electrodes were cleaned by polishing using alumina powder and

sonicated for one minute in water and then cleaned with hydrogen peroxide and finally rinsed with CH_2Cl_2. The solutions were degassed with argon gas before the measurements.

2.3 Results and discussions

2.3.1 Silver nanoparticles formation:

For silver particle synthesis with DPA-NDI-SH, the solvent selection is critical since DPA-NDI-SH is insoluble in aqueous solutions as well as in most organic solvents. In DMSO, SH-NDI-DPA exhibits a low solubility (solubility ~ 0.10 mM). Most of the metal nanoparticle synthetic methods in both aqueous and organic medium used sodium borohydride as reducing agent.[7,8,36] Patakfalvi et al. used DMSO as solvent and reducing agent in the synthesis of Ag nanoparticles .[37] As the DMSO plays a dual role in the synthetic process, the number of reactants and byproducts decrease. The high viscosity of DMSO can reduce particle aggregation as the diffusion of particles became slower.[37] The reduction of the starting material, silver neodecanoate, by DMSO is postulated as follows according to the literature:[37,38]

$$2\ AgO_2CR + (CH_3)_2SO + H_2O \longrightarrow 2Ag(s) + (CH_3)_2SO_2 + 2H^+ + 2\ [RCO_2]^- \qquad (2.1)$$

R= $C(CH_3)_2$-CH_2-CH_2-CH_2-CH_2-CH_2-CH_3

The formation of silver colloids were characterized by its characteristic yellow color. DPA-NDI-SH coated silver particles exhibited a color dark brown as prepared because of the solutions high concentration. When the reaction solution was diluted to 0.1 mM, a resulting yellow color was observed (Figure 2.1). The particle formation was monitored by UV-visible spectroscopy

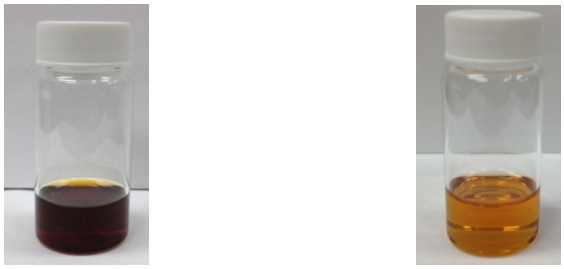

Figure 2.1: Ag nanoparticles as prepared in DMSO (1 mM) (left) and after dilution (0.1 mM) (right)

because dispersed Ag nanoparticles exhibit an absorption in the UV-visible region due to their plasmon resonance transition.[39] The UV-visible spectrum of the silver particles is shown in Figure 2.2. The full width half maxima (FWHM) for the peak of silver plasmon band is about 100 nm, indicating that the particles are monodispersed .[40,41] Control of size distribution of the nanoparticles depends on the concentration of starting materials, temperature and duration of reaction. Silver 2-ethylhexanoate was used as Ag^+ source in the literature which was reduced by DMSO for nanoparticles synthesis.[37] These authors made particles at an elevated temperature (60^0 C). In the present study, we investigated the concentration ratio of silver neodecanoate and DPA-NDI-SH as well as the optimum temperature, duration of reduction to optimize the stability of particles and completness of silver salt reduction using UV-Visible spectroscopy. The molar ratio of Ag^+/ DPA-NDI-SH= 1/0.05 was chosen since it leads to stable particles. Silver salt concentrations higher than 1 mM results in precipitation of metallic silver and a red shift of the plasmon band from 445 nm to 460 nm. Higher concentrations of stabilizer induced the same fate, i.e aggregation of particles. To determine the optimum temperature, the oil bath temperature was varied from at 60^o, 80^o, 100^0 and 140^o C. The absorbance change at λ_{max} (nm) with time is shown in Figure 2.3. The data showed thatat 100^o C the reduction of the silver salt was complete in 3h.

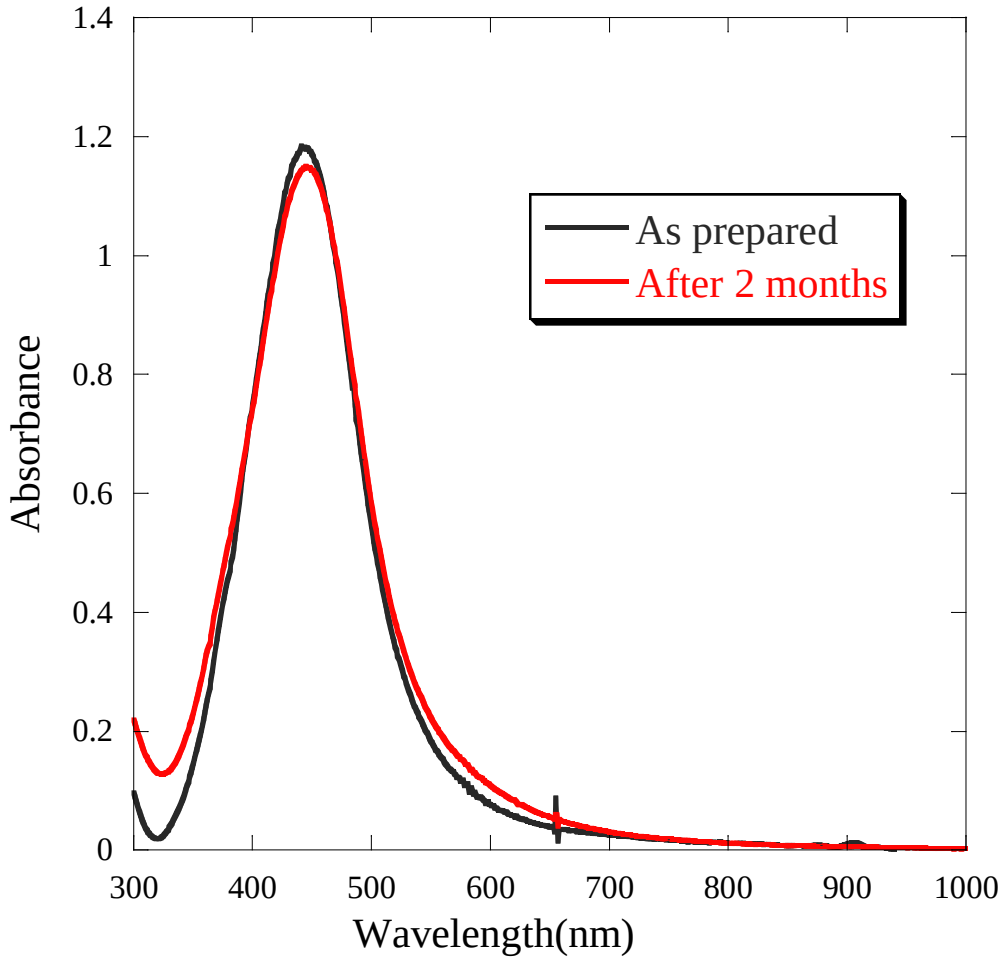

Figure 2.2: UV-visible spectrum of Ag nanoparticles mixture in DMSO (0.1 mM).

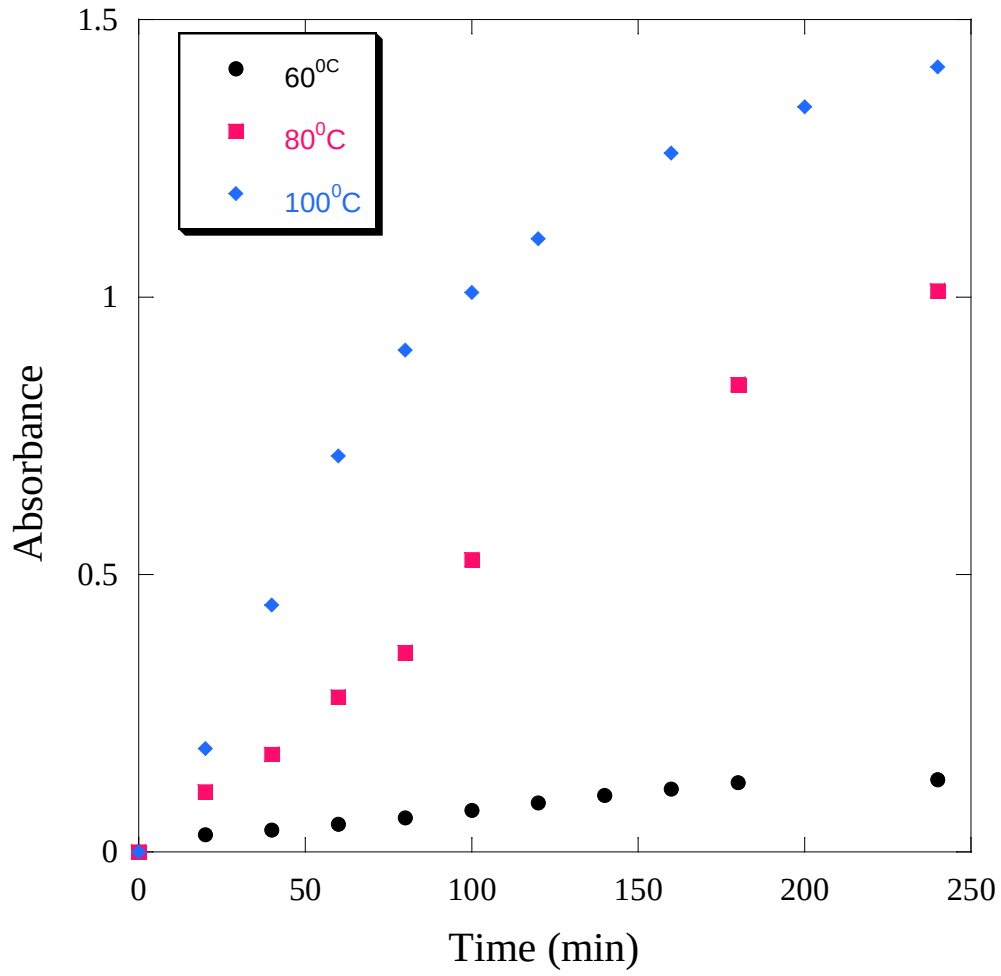

Figure 2.3: Reaction Temperature effect on the formation of Ag nanoparticles from Ag neodecanoate.

The synthetic process at 140^{o} C was not shown in the figure because the resulting absorption band was not symmetric indicating a polydispersed size distribution. Also after 40 days, the absorption band was broadened and the particles precipitated out. We concluded that the particles prepared at 140^{o} C were not stable. However, the particles prepared at100^{o} C, are stable even after 60 days (Figure 2.2). Ag nanoparticles were also synthesized without DPA-NDI-SH at 100^{o} C. After 2 h of reaction, metallic silver formed and precipitated out. However, at the beginning of the reaction, the color of the reaction mixture was pale yellow. The UV-visible spectrum of reaction mixture obtained after one hr of reaction shows two absorption band at 438 and 723 nm indicating a broad size distribution of particles (Figure 2.4). This means the surface-bound ligand DPA-NDI-SH provides significant control of the size distribution and stability of the Ag nanoparticles.

2.3.2 Gold nanoparticles formation:

Thesynthesis of Au nanoparticles in both DMSO and DMF have been reported in literatures.[42–46] The most used starting material for Au particles synthesis is chloroauric acid.[5-6,8,18] Here we used gold (I) sodium thiosulfate as the starting material for gold nanoparticles which has not been reported elsewhere. By dissolving both starting material and capping agent DPA-NDI-SH in DMF in a reaction flask and heating at 140^{0}C, we were able to produce particles. Chen, et al. have claimed that DMF acts as a reducing agent during Au nanoparticles synthesis.[45] However, they have not determined the reduction mechanism of chloroauric acid by DMF. The reduction of Ag^{+} has been discussed in literature,[47] involving formation of carbamic acid and metallic silver. We propose here that the thermal reduction of Au^{+} complex by DMF occurs via the reaction as follows:

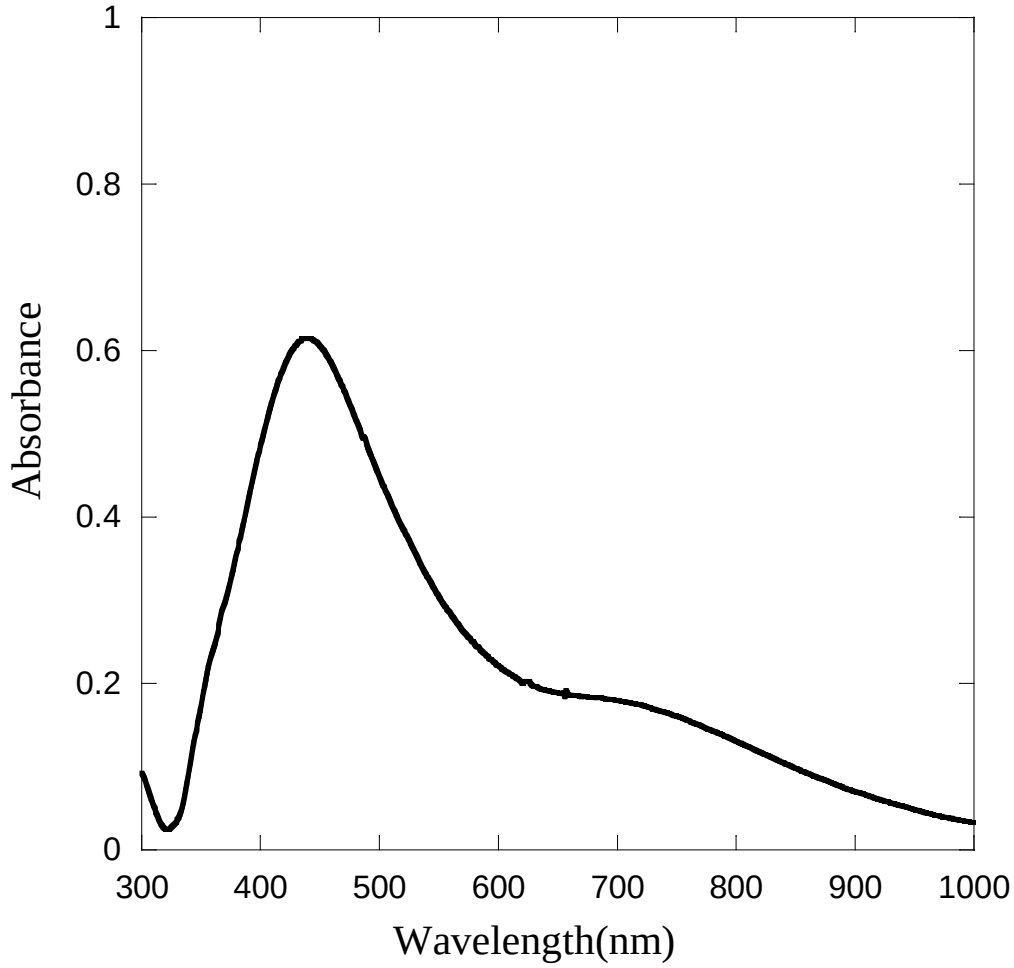

Figure 2.4: UV-visible spectrum of Ag nanoparticles mixture without DPA-NDI-SH in DMSO (0.1 mM).

$$[Au(S_2O_3)_2]^{3-} + HCON(CH_3)_2 + H_2O \longrightarrow Au(s) + (CH_3)_2NCOOH + 2H^+ + 2S_2O_3^{2-}$$

$S_2O_3^{2-}$ also form during the gold (I) sodium thiosulfate reduction by ascorbate ions used in gold baths.[48] The growth of gold particles was monitored by the evalution of the reddish brown color. Due to the intense dark blue color of DPA-NDI-SH, the red color of the prepared particles cannot be observed. However, for Au particles in DMF without DPA-NDI-SH, the characteristic red-colored was observed (Figure 2.5). The UV-visible spectrum of Au nanoparticles is shown in Figure 2.6 and the plasmon band for Au particles are observed at 574 and 564 nm with DPA-NDI-SH and without DPA-NDI-SH, respectively. The red shift of the plasmon band might be due to the presence of DPA-NDI-SH on the surface of the particles.[1,2] In both cases, the

Figure 2.5: Au nanoparticles as prepared (left) and after dilution (2 times) (middle) and without SH-NDI-DPA (right).

particles are stable and well-dispersed in solution as the FWHM of the UV-visible spectrum is ~100 nm. The stability of the Au particles without surface ligand will be discussed in the surface characterization section.

2.3.3. XRD Analysis:

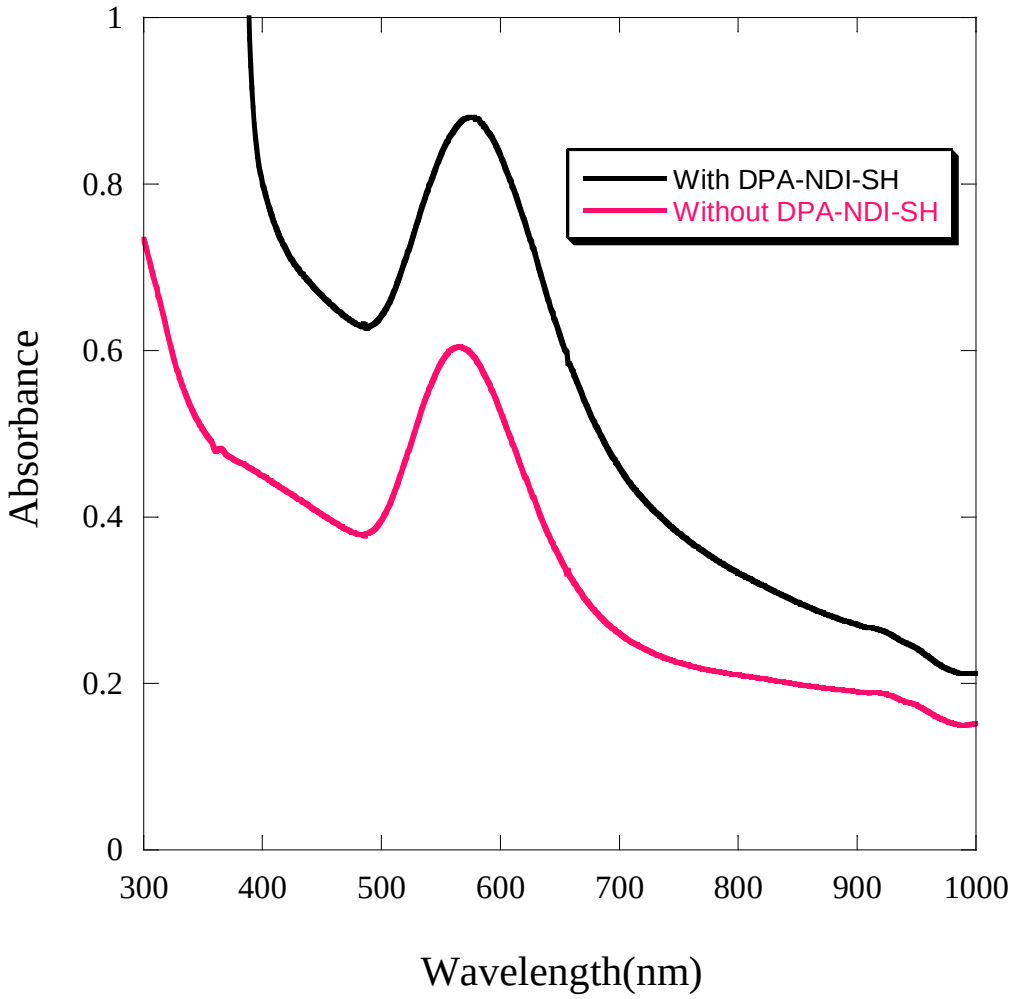

Figure 2.6: UV-Visible Spectrum of Au nanoparticles mixture in DMF (0.25mM).

X-ray diffraction is one of the important tools in nanomaterials chemistry for investigating the reduction of a metal salt to the metallic state. Lattice parameters, size and shape of the unit cell of a crystalline material can be obtainedfrom XRD analysis. The X-ray diffraction patterns of the synthesized Ag and Au nanoparticles are shown in Figures 2.7 and 2.8. The Bragg reflections correspond to the 2θ values at 37.2^o, 43.6^o, 63.7^o and 76.9^o of corresponding to diffractions from the (111), (200), (220) and (311) lattice planes respectively for Ag nanoparticles showing fcc structure of this metal nanoparticles (JCPDF 4-785). The 2θ values of Au fcc structure (Figure 2.8) at 37.4^o, 43.7^o, 64.1^o and 77.2^o from the (111), (200), (220) and (311) lattice plane respectively (JCPDF 4-784). There are some low intensity diffraction signals in the Au pattern that are not matching with the known metallic Au reflections. We assumed that these peaks originate from the presence of $Au(S_2O_3)_x$ that remained unreduced. This will be discussed in the FT-IR analysis section. The particle sizes were determined from the peak width at half the maximum intensity (FWHM) using theScherrer equation.[49] The average sizes of the Ag and Au nanoparticles were 8.0 ±1.6 and 6.9 ±2.9 nm respectively. The particle dimensions derived from the Scherrer equation were in rough agreement with the more accurate sizes evaluated using TEM.

2.3.4 TEM images:

The size distribution of the silver and gold particles were evaluated using TEM images. Figure 2.9 shows that the average particles sizes were 5.7 ± 4.9 nm for Ag nanoparticles whereas the particles sizes are 4.1 ± 3.8 nm for Au nanoparticles (Figure 2.10). The histogram depicts that the size distribution of Au nanoparticles was narrower than that for the Ag nanoparticles.

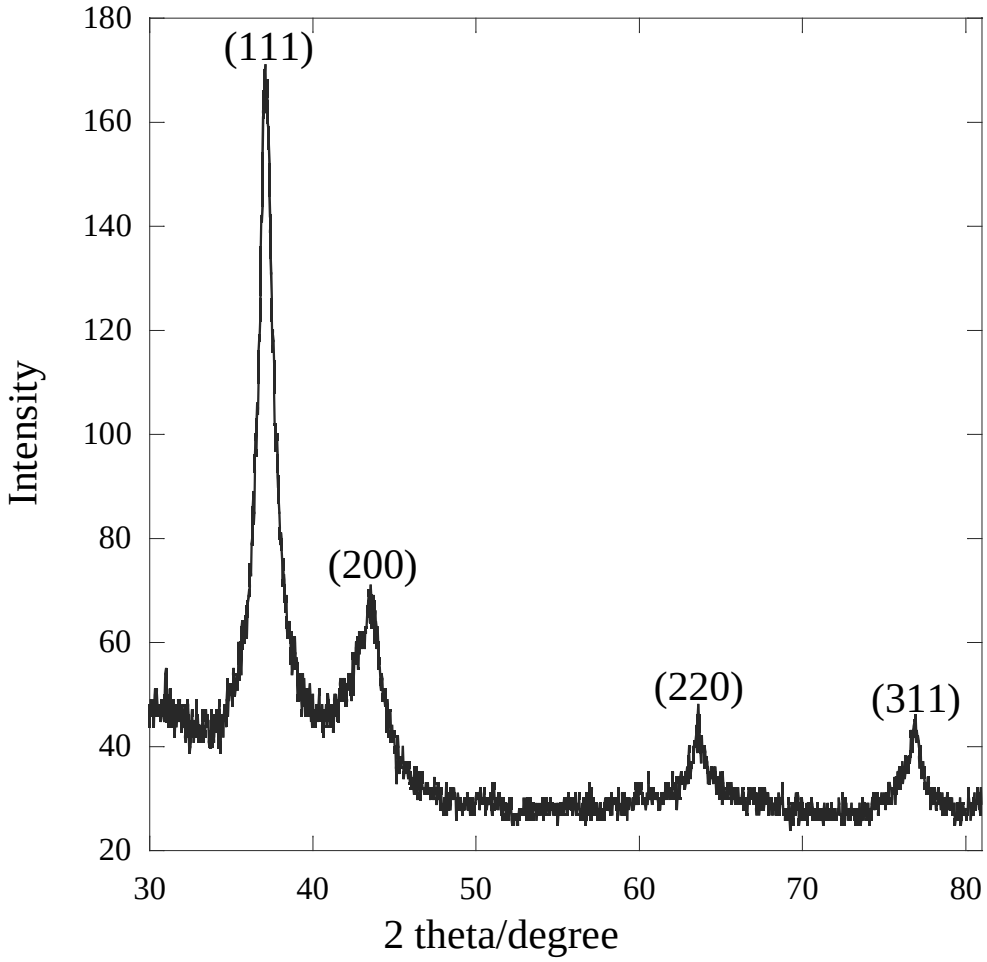

Figure 2.7: X-ray diffractogram of Ag nanoparticles.

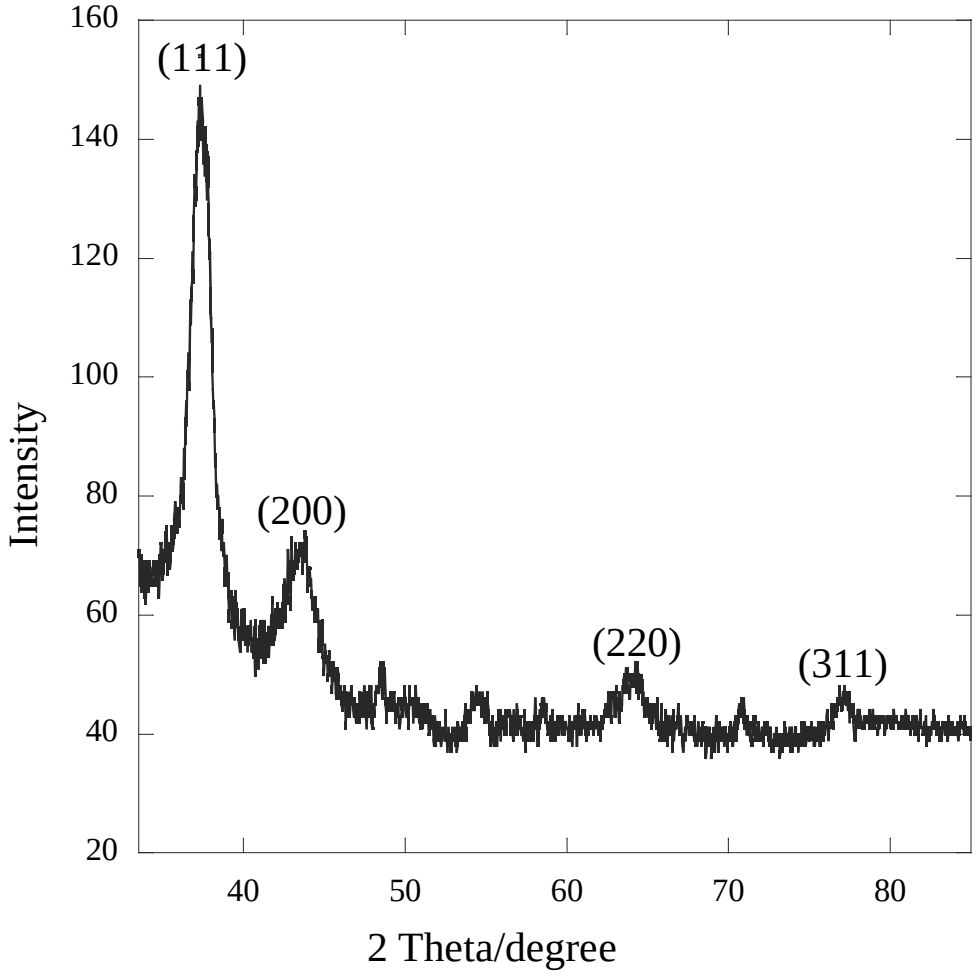

Figure 2.8: X-ray diffractogram of Au nanoparticles.

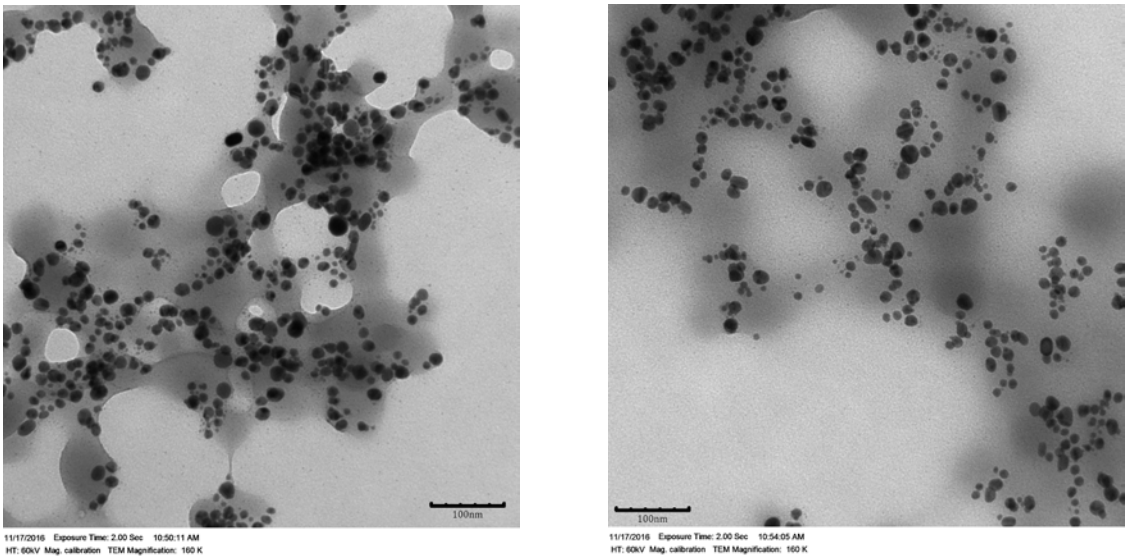

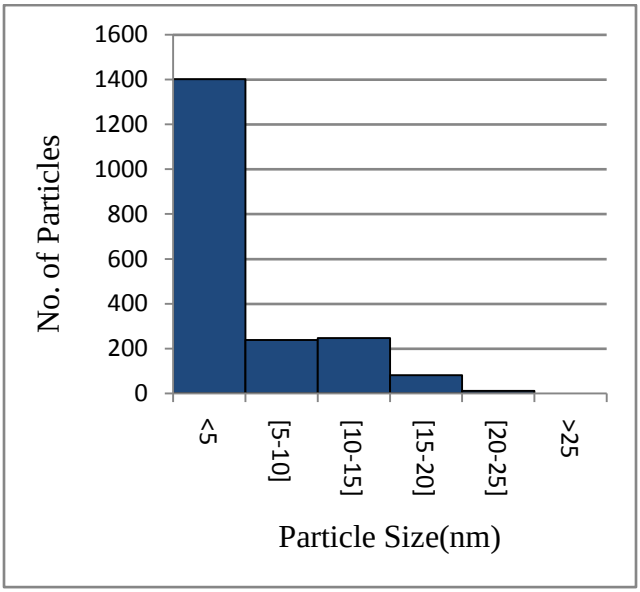

Figure 2.9: TEM images of Ag nanoparticles with histogram for different particles size distribution. Dimension bar is 100 nm.

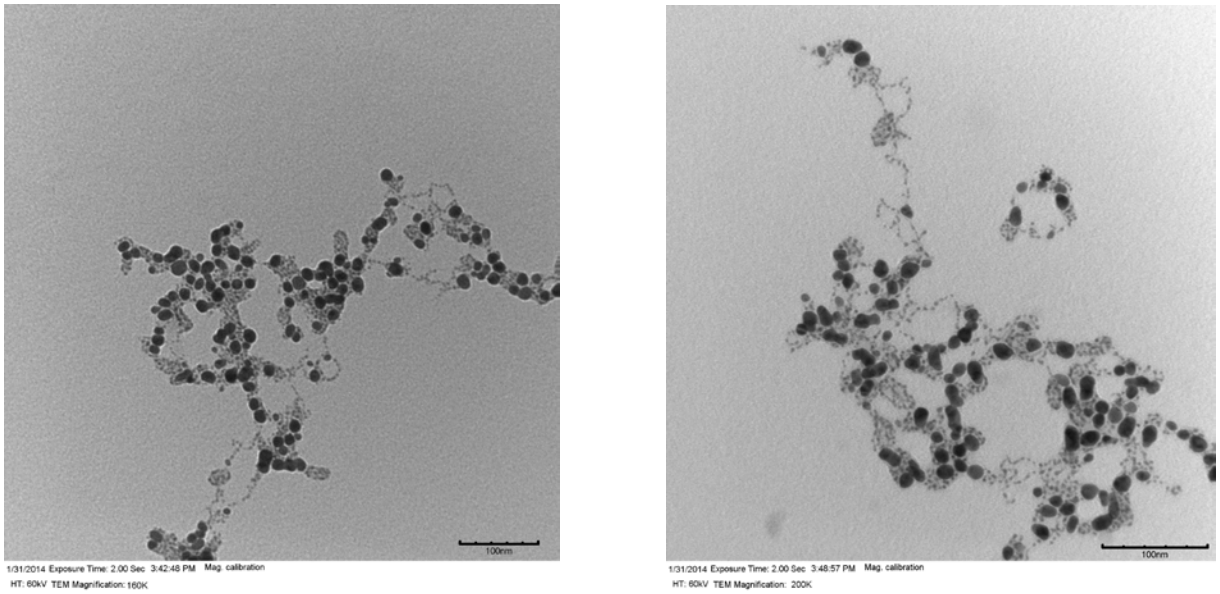

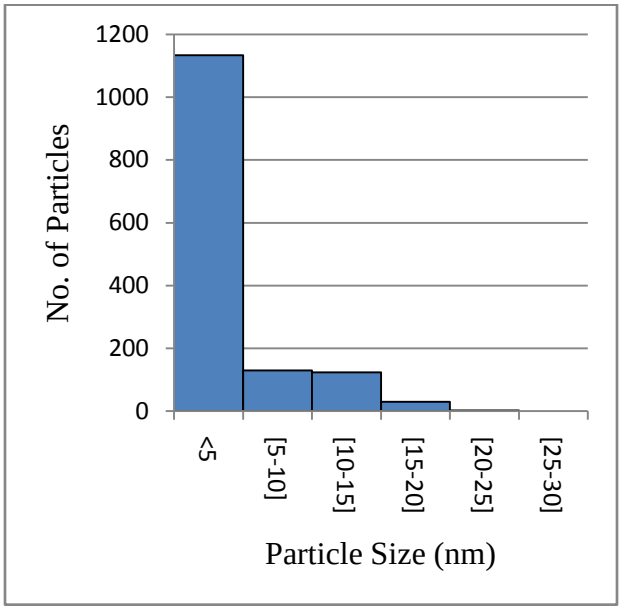

Figure 2.10: TEM images of Au nanoparticles with histogram for different particles size distribution. Dimension bar is 100 nm.

2.3.5 Surface Characterization:

The surface characterization of Ag and Au nanoparticles was performed by FT-IR. FTIR spectra of DPA-NDI-SH and DPA-NDI-SH coated nanoparticles are shown in Figure 2.11 and 2.11. The symmetric and asymmetric carboxylic group (C=O) vibration stretching band are located at 1714 cm^{-1} and 1671 cm^{-1} for DPA-NDI-SH and for DPA-NDI-SH coated Ag and Au particles respectively. When the ligand DPA-NDI-SH is incorporated into the surface, the peak position of the C=O bond remains unchanged. This might be due to the position of the imide group in the compound DPA-NDI-SH being far away from the surface of the particles. However, when SAM of DPA-NDI-SH deposited on gold surfaces were studied, A small shift of the carboxyl group stretching vibration was observed.[29] Kwan et al. observed a small shift only for the asymmetric C=O vibration in thiol-terminated oligoimides attached to gold.[34] Moreover, a very small shift for both symmetric and asymmetric C=O stretching band has been observed for monolayers of thiol-terminated polyimide on gold.[50] The other characteristic signals in the IR spectrum of DPA-NDI-SH such as the C-N-C symmetric and asymmetric stretching bands at 1345 and 1248 cm^{-1}[29] and the benzene ring quadrant and semicircle stretching mode bands at 1583 and 1493 cm^{-1} respectively, also remained unchanged in the case of the synthesized Ag and Au nanoparticles.[51] To confirm the presence of naphthalene diimide on the surface of the nanoparticles, we have synthesized both Ag and Au nanoparticles without naphthalene diimide. As mentioned before Ag nanoparticles are not stable without DPA-NDI-SH and metallic silver precipitation form within 2 h after the reaction ended. But with DPA-NDI-SH, Ag particles are stable for a long time. Therefore, it proves that the absorbrd DPA-NDI-SH molecules provide stability to the Ag particles by incorporating on the surface. However, a different feature was observed in the FT-IR spectrum of Au nanoparticles without DPA-NDI-SH. Also as discussed earlier, the Au particles are stable even without DPA-NDI-SH. The FTIR spectrum

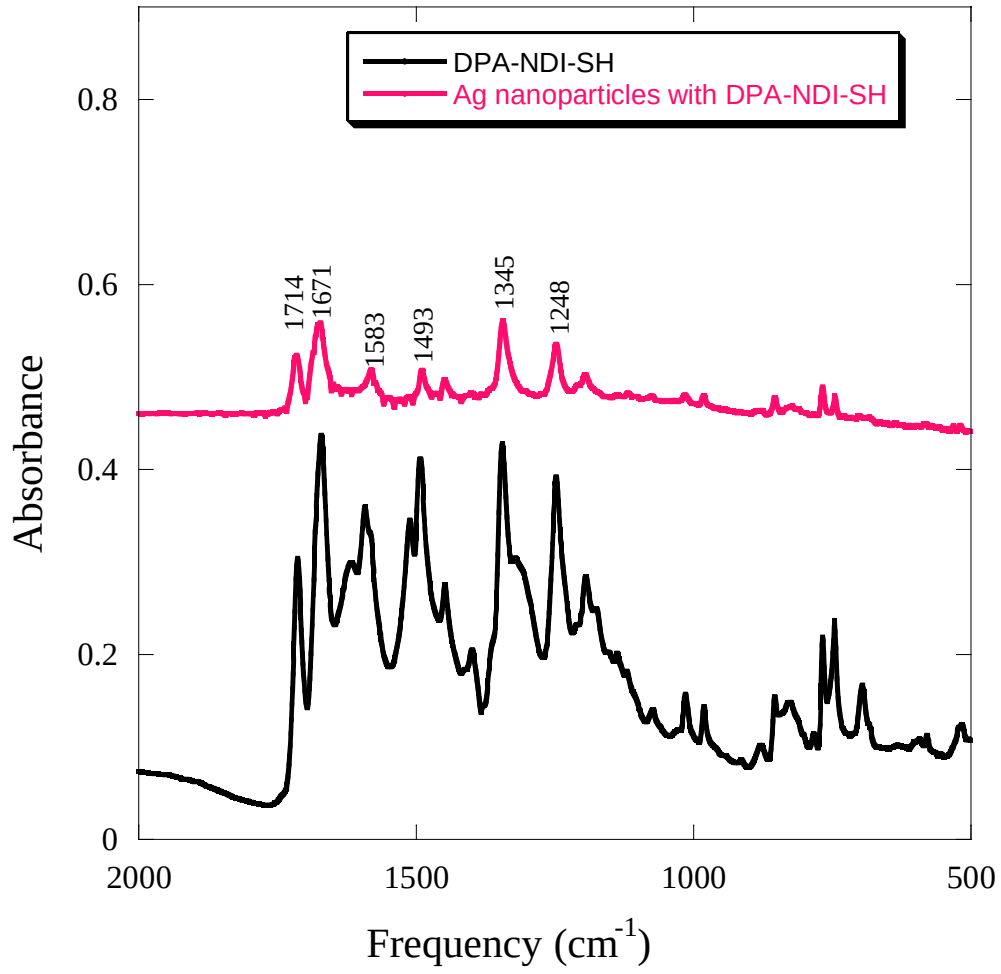

Figure 2.11: FT-IR spectrum of DPA-NDI-SH (bottom) and Ag nanoparticles with DPA-NDI-SH (top).

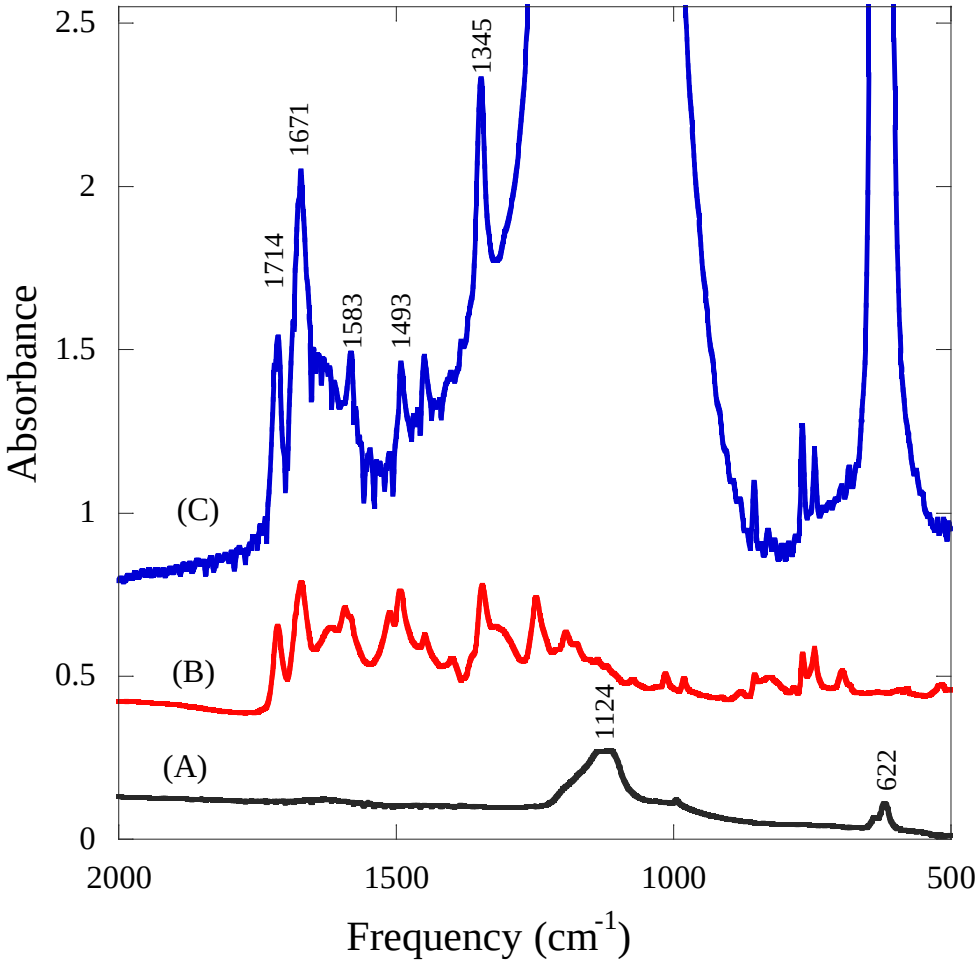

Figure 2.12: FT-IR spectrum of (A) Au nanoparticles without DPA-NDI-SH, (B) DPA-NDI-SH, (C) Au nanoparticles with DPA-NDI-SH.

of Au nanoparticles shows an intense broad peak at 1124 cm^{-1} along with a sharp peak at 622 cm^{-1} (Figure 2.11). The characteristic S=O stretching and bending frequencies are at 1308-1108 cm^{-1} and 610-545 cm^{-1} respectively.[51] Without DPA- NDI-SH group, Au nanoparticles are stabilized by S=O group. Moreover, in the XRD pattern of Au nanoparticles, we found some diffraction peaks other than those from the fcc Au structure. This explanation also is supported by the fact that when we synthesized Au nanoparticles in DMF from the chloroauric acid as a starting material,[45] there were no stretching and bending frequencies other than those present for the DPA-NDI-SH (Figure 2.13).

2.3.6 Thermal Gravimetric Analysis:

A thermogram of dried Ag nanoparticles is shown in Figure 2.14. The weight loss is about 12% between 80-800^{o} C. Three steps of weight loss can be distinguished in the thermogram of the Ag nanoparticles. The first weight step appeared at about 122^{o} C which corresponds to moisture and solvent loss. The second and third steps are seen at about 338^{o} C and 646^{o} C, these weight loss processes might be due to the loosely and tightly bonded DPA-NDI-SH to the surface of Ag nanoparticles.[52]

2.3.7 Surface modification:

After collecting the Ag nanoparticles through centrifugation, the particles were unstable upon redispersion in methanol or dichloromethane. Figure 2.14 shows the UV-visible spectrum of Ag nanoparticles in both methanol and dichloromethane. The UV-visible peak shapes are not symmetric and also a red shift of the plasmon band occurs indicating that the particles became

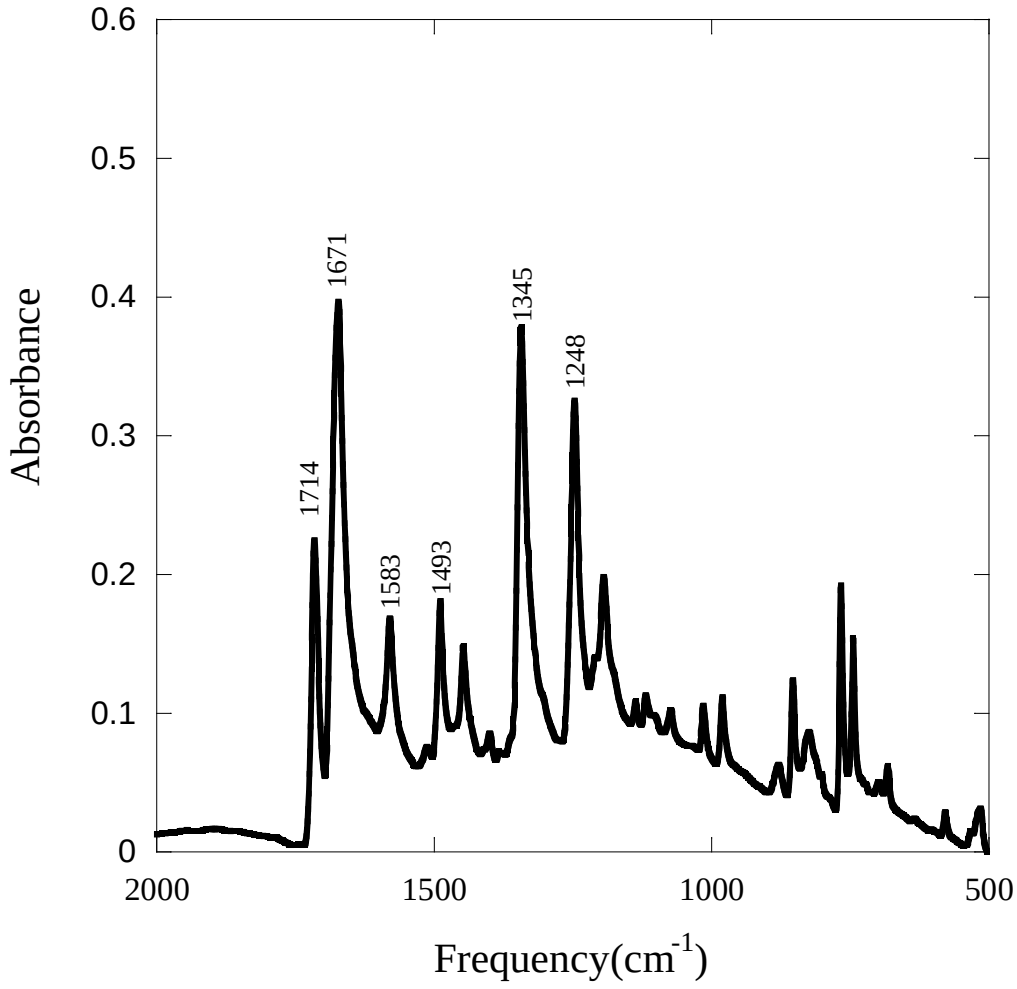

Figure 2.13: FT-IR spectrum of Au nanoparticles from chloroauric acid in presence of DPA-NDI-SH (KBr pellets).

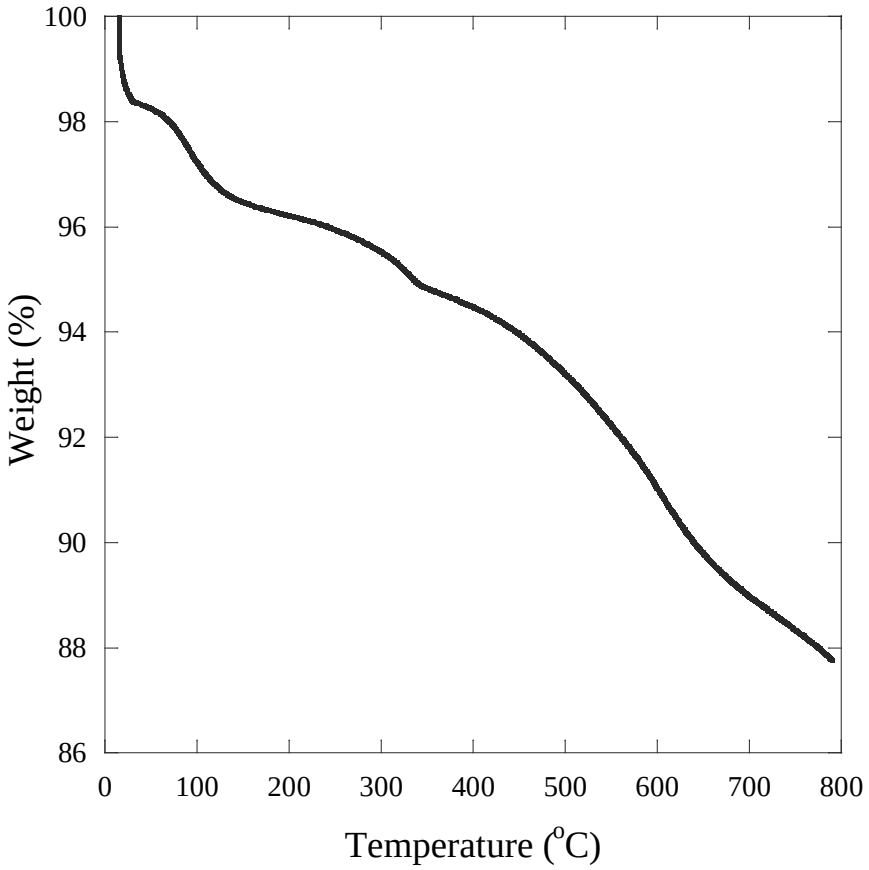

Figure 2.14: Thermal gravimetric analysis of DPA-NDI-SH coated Ag nanoparticles.

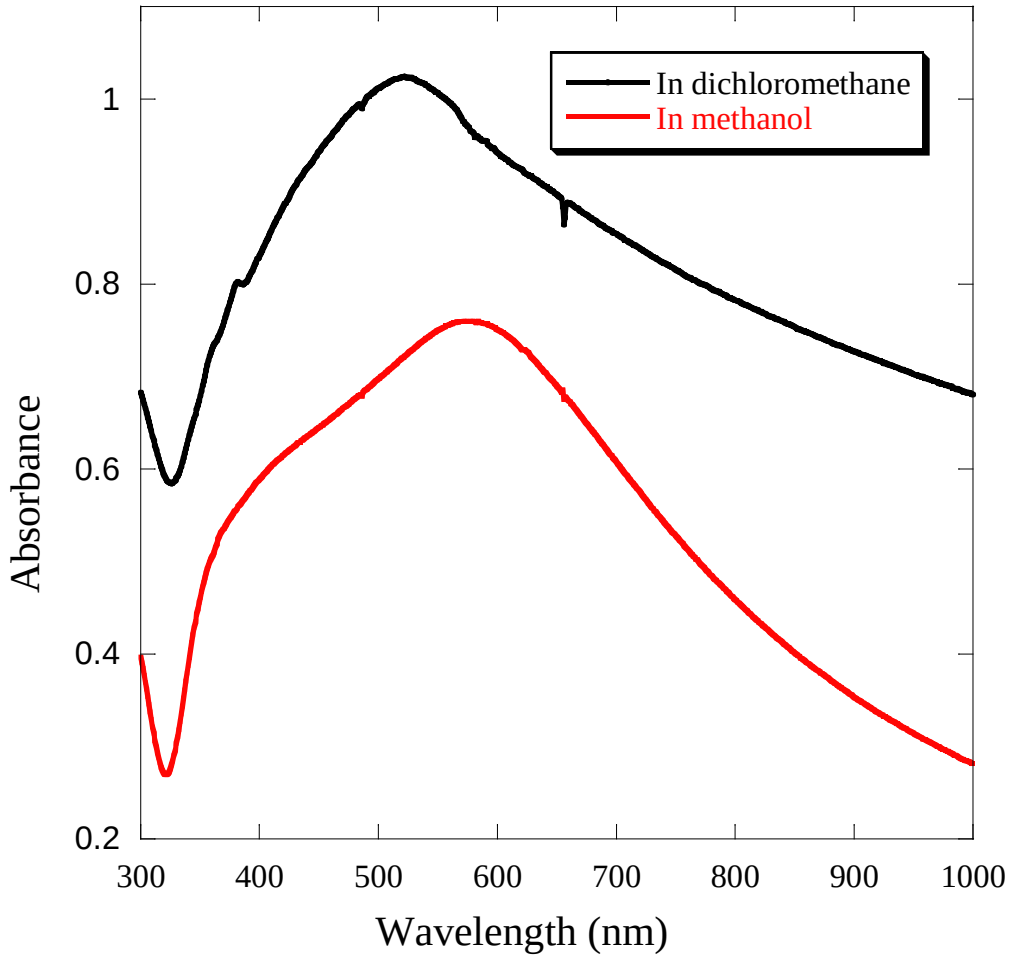

Figure 2.15: UV-visible spectrum of Ag nanoparticles in dichloromethane and methanol (5 mM).

larger in size as compared to the original particle size. In Chapter One, we have discussed that surface ligands provide solvent compatibility. It has also been reported that Au nanoparticles are stable in dichloromethane, chloroform and toluene when the particles are coated with alkyl thiols.[8,18] Here we have modified the surface of the naphthalene diimide stabilized Ag nanoparticles surfaces with butanethiol. The modified particles are redispersed in dichloromethane and UV-visible spectrum of the redispered particles is shown in Figure 2.15(A).The UV-visible spectrum is symmetric but a red shift (λ_{max} = 461nm) was detected. So the particles are stable in dichloromethane. The FT-IR spectrum of the butanethiol modified Ag nanoparticles is shown in Figure 2.15(B). The alkyl chain vibrational frequencies at 2954, 2920, 2870, 2853 and 1465 cm^{-1} were found in the spectrum indicating the presence of butanethiol on the particles surface. The symmetric and asymmetric stretching frequencies of C=O and C-N-C bond from DPA-NDI-SH are also present in the spectrum indicating that the naphthalene diimide molecules are not fully replaced by butanethiol. It has been reported that the ligand exchange of thiol by thiol produces mixed ligand capped nanoparticles.[53]

2.3.8 Electropolymerization of DPA-NDI-SH and DPA-NDI-SH linked Ag nanoparticles:

The symmetric naphthalene diimide with diphenylamine group at the imide position (DNTD) has been electropolymerized onto different electrode surfaces, Au, glassy carbon(GC), and ITO.[28] Here we report that the asymmetric naphthalene diimide, DPA-NDI-SH also can be electropolymerized. The cyclic voltammogram of the electropolymerization of DPA-NDI-SH monomer in dichloromethane with 0.1 M $TBABF_4$ and 0.4% TFA is shown in the Figure 2.17(A). In this voltammogram, the first scan shows one oxidation peak at 1.10 V vs Ag/AgCl

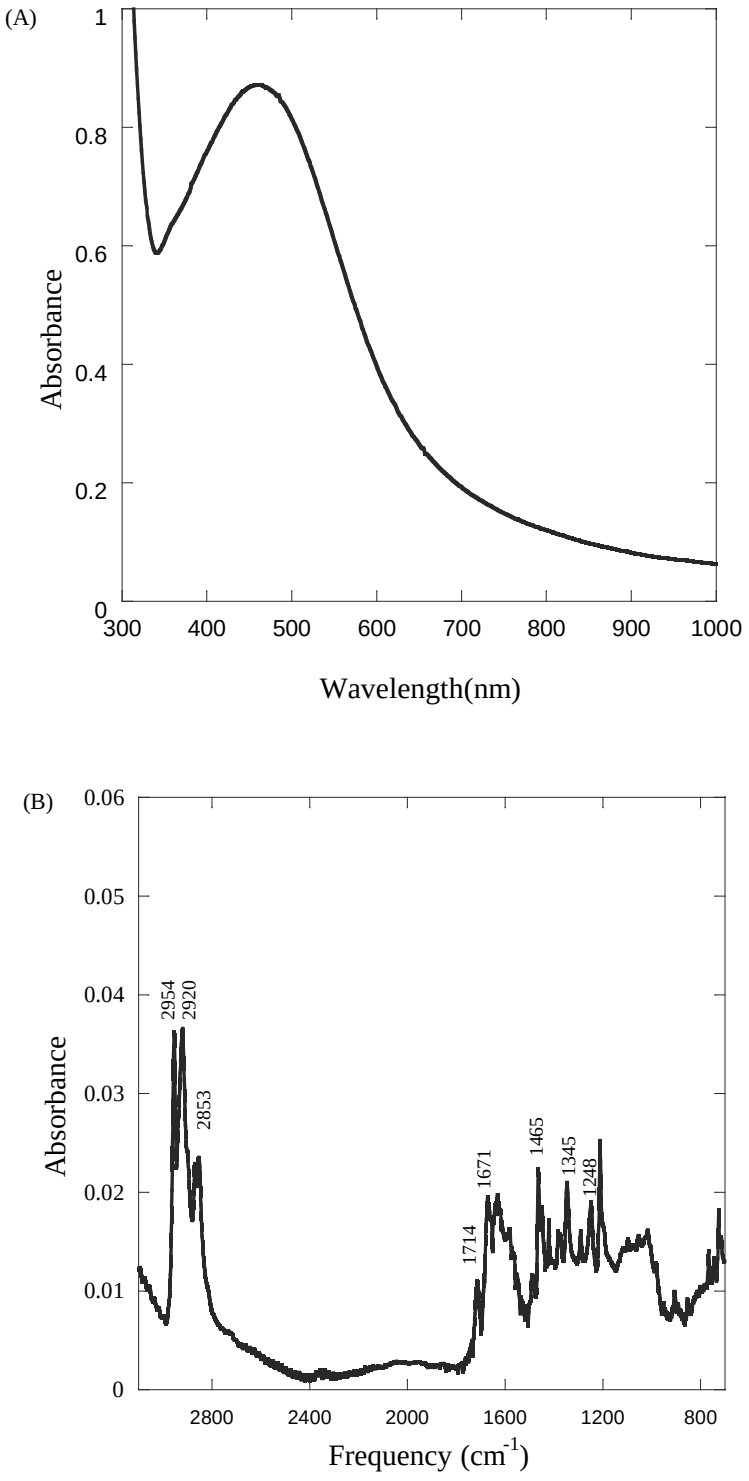

Figure 2.16: (A) UV-visible spectrum of butanethiol modified DPA-NDI-SH linked Ag nanoparticles in CH_2Cl_2 (5 mM), (B) FT-IR spectrum of butanethiol modified DPA-NDI-SH linked Ag nanoparticles (KBr pellet).

and the corresponding reduction shows two peaks at 0.92 and 0.78 V. These two peaks are assigned for the reduction of diphenylbenzidine (DPB) unit. The subsequent scans show the two sets of oxidation and reduction peaks and a gradual increase in the peak currents as the number of scan increases. Then the electrode was withdrawn from the cell and rinsed with dichloromethane, following by immersion into a fresh electrolyte solution of 0.1 M $TBABF_4$. Upon scanning from 0 to 1.4 V, the voltammogram shows two reversible redox peaks for the DPB unit and also scanning negative from 0.0 V yielded two sets redox of peaks which are assigned to the reduction and oxidation waves of the tetracarboxylic group of DPA-NDI-SH (Figure 2.17 (B).[28,31,32]

Although DPA-NDI-SH containing Ag and Au nanoparticles are not very soluable in dichloromethane, we attempted to polymerize the particles. Cyclic voltammograms of 5 mM Ag nanoparticles in dichloromethane with 0.1M $TBABF_4$ were free of oxidation peaks associated with the diphenylamine groups (Figure 2.18(A). Similar results were obtained with butanethiol-modified DPA-NDI-SH linked Ag nanoparticles although these particles are soluble in dichloromethane (Figure 2.18 (B). From the FT-IR of butanethiol modified Ag nanoparticles, it was observed that DPA-NDI-SH molecules were replaced by butanethiol, so that the number of DPA-NDI-SH molecules on the nanoparticles surfaces decreased. Consequently, the availability of diphenylamine group was decreased in solutions containing butanethiol modified DPA-NDI-SH linked Ag nanoparticles. Also, the particles become unstable after addition of supporting electrolytes such as $TBABF_4$, $TBAPF_6$ and BMIM TFSI. Therefore, DPA-NDI-SH capped nanoparticles cannot be polymerized due to low concentration of DPA-NDI-SH or poor stability of the particles in dichloromethane containing supporting electrolyte.

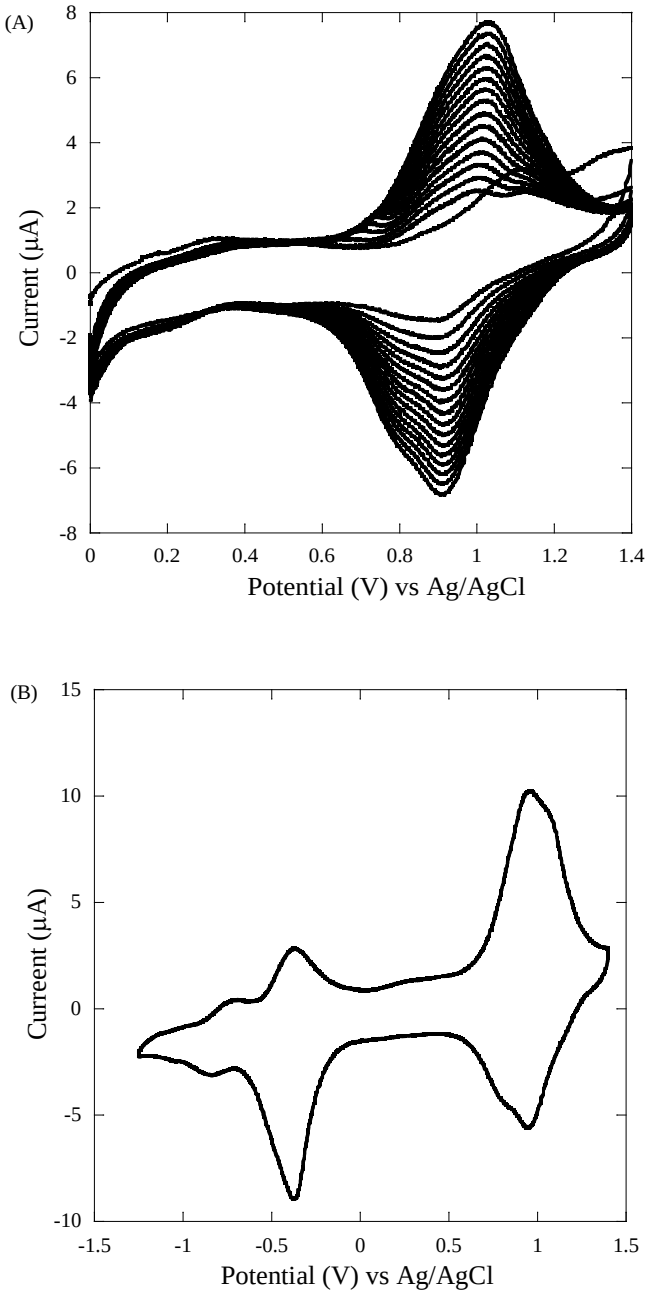

Figure 2.17: (A) Cyclic voltammetry of 0.25 mM DPA-NDI-SH in CH_2Cl_2 containing 0.1 M $TBABF_4$ and 0.4% TFA at Au electrode (0.0314 cm^2). (B) Cyclic voltammetry of DPA-NDI-SH polymer film at the same electrode containing 0.1 M $TBABF_4$.

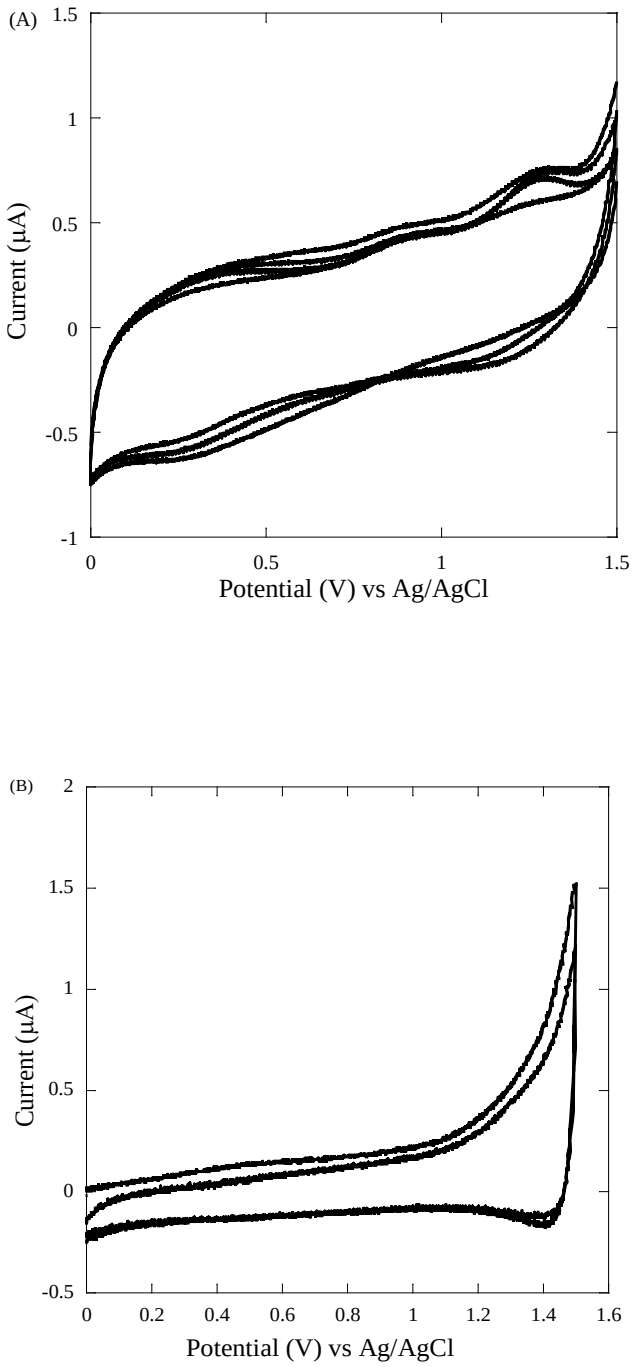

Figure 2.18: (A) Cyclic voltammetry of 5 mM DPA-NDI-SH capped Ag nanoparticles (B) Cyclic voltammetry of 10 mM butanethiol modified DPA-NDI-SH capped Ag nanoparticles in CH_2Cl_2 containing 0.1 M $TBABF_4$ at Au electrode (0.0314 cm^2). Scan rate 200 mV/s.

2.4 Conclusions

Ag and Au nanoparticles containing naphthalene diimide on their surfaces were successfully synthesized in DMSO and DMF. To stabilize the particles in dichloromethane, butanethiol was incorporated on the particle surface. Naphthalene diimide, DPA-NDI-SH can be polymerized through oxidative electropolymerization in dichloromethane. We have attempted to polymerize the DPA-NDI-SH coated Ag and Au nanoparticles, but the reaction was unsuccessful. This might be due to the low amount of DPA-NDI-SH in the solution to be polymerized or because the particles become larger when the supporting electrolyte was added. Now our goal is to stabilize the synthesized particles in dichloromethane containing supporting electrolyte. In this way we could fabricate a nanoparticle organic framework via electropolymerization of naphthalene diimide liked to the metal nanoparticles that might have interesting optical and electronic properties. A different synthetic approach needs to be found that provides better stability of the particles in dichloromethane containing supporting electrolyte.

2.5 References

1. Moores, A.; Goettmann, F. The Plasmon Band in Noble Metal Nanoparticles: An Introduction to Theory and Applications. *New J. Chem.* **2006**, *30*, 1121–1132.

2. Ghosh, S. K.; Nath, S.; Kundu, S.; Esumi, K.; Pal, T. Solvent and Ligand Effects on the Localized Surface Plasmon Resonance (LSPR) of Gold Colloids. *J. Phys. Chem. B* **2004**, *108*, 13963–13971.

3. Eustis, S.; El-Sayed, M. A. Why Gold Nanoparticles Are More Precious than Pretty Gold: Noble Metal Surface Plasmon Resonance and Its Enhancement of the Radiative and Nonradiative Properties of Nanocrystals of Different Shapes. *Chem. Soc. Rev.* **2006**, *35*, 209-217.

4. Thomas, K. G.; Kamat, P. V. Chromophore-Functionalized Gold Nanoparticles. *Acc. Chem. Res.* **2003**, *36*, 888–898.

5. Tan, E.; Yin, P. Lang, X. Wang, X., Youa T.; Guo, L. Functionalized Gold Nanoparticles as Nanosensor for Sensitive and Selective Detection of Silver Ions and Silver Nanoparticles by Surface-Enhanced Raman Scattering. *Analyst*, **2012**, *137*, 3925-3928.

6. Jain, S.; Hirst, D. G.; O'Sullivan, J. M. Gold Nanoparticles as Novel Agents for Cancer Therapy. *B.r J. Radiol.* **2012**, *85*, 101–113.

7. He, S.; Yao, J.; Jiang, P.; Shi, D.; Zhang ,H.; Xie, S.; Pang, S.; Gao, H. Formation of Silver Nanoparticles and Self-Assembled Two-Dimensional Ordered Superlattice. *Langmuir* **2001**, *17*, 1571–1575.

8. Brust, B.; Walker, M.; Bethell, D.; Schiffrin, D. J.; Whyman, R. Synthesis of Thiol-derivatised Gold Nanoparticles in a Two-phase Liquid-Liquid System**.** *J. Chem. Soc., Chem. Commun.* **1994**, 801-802.

9. Roux, S.; Garcia, B.; Bridot, J.; Salomé, M.; Marquette, C.; Lemelle, L.; Gillet, P.; Blum , L.; Perriat, P.; Tillement, O. Synthesis, Characterization of Dihydrolipoic Acid Capped Gold Nanoparticles, and Functionalization by the Electroluminescent Luminol. *Langmuir* **2005**, *21*, 2526–2536.

10. Ojea-Jiménez, I.; Romero, F. M.; Bastús, N. G.; Puntes, V.; Small Gold Nanoparticles Synthesized with Sodium Citrate and Heavy Water: Insights into the Reaction Mechanism. *J. Phys. Chem. C* **2010**, *114*, 1800–1804.

11. Lee, S. H.; Bae, K. H.; Kim, S. H.; Lee, K. R.; Park, T. G. Amine-Functionalized Gold Nanoparticles as Non-Cytotoxic and Efficient Intracellular siRNA Delivery Carriers. *Int. J. Pharm.* **2008**, *364*, 94–101.

12. Shem, P.M.; Sardar, R.; Shumaker-Parry, J. S. One-Step Synthesis of Phosphine-Stabilized Gold Nanoparticles Using the Mild Reducing Agent 9-BBN. *Langmuir* **2009**, *25*, 13279–13283.

13. Sudeep, P. K.; Ipe, B. I.; Thomas, K. G.; George, M. V. Fullerene-Functionalized Gold Nanoparticles. A Self-Assembled Photoactive Antenna-Metal Nanocore Assembly. *Nano Lett.* **2002**, *2*, 29-35.

14. Ipe, B. I.; Thomas, K. G. Photoinduced Charge Separation in a Fluorophore−Gold Nanoassembly. *J. Phys. Chem. B* **2002**, *106*, 18–21.

15. Stamplecoskie, K. G.; Kamat, P. V. Size-Dependent Excited State Behavior of Glutathione-Capped Gold Clusters and Their Light-Harvesting Capacity. *J. Am. Chem. Soc.* **2014**, *136*, 11093–11099.

16. Aguila, A.; Murray, R. W. Monolayer-Protected Clusters with Fluorescent Dansyl Ligands *Langmuir* **2000**, *16*, 5949–5954.

17. Templeton, A. C.; Cliffel, D. E.; Murray, R. W. Redox and Fluorophore Functionalization of Water-Soluble, Tiopronin-Protected Gold Clusters. *J. Am. Chem. Soc.* **1999**, *121*, 7081–7089.

18. Wolfe, R. L.; Balasubramanian, R.; Tracy, J.B.; Murray, R. W. Fully Ferrocenated Hexanethiolate Monolayer-Protected Gold Clusters. *Langmuir* **2007**, *23*, 2247–2254.

19. Roberts, J. J. P.; Vuong, K. T.; Murray, R. W. Synthesis and Electrochemistry of 6 nm Ferrocenated Indium–Tin Oxide Nanoparticles. *Langmuir* **2013**, *29*, 474–479.

20. Green, S. J.; Pietron, J.J.; Stokes, J.J.; Hostetler, M.J.; Vu, H.; Wuelfing, W.P.; Murray, R.W. Three-Dimensional Monolayers: Voltammetry of Alkanethiolate-Stabilized Gold Cluster Molecules *Langmuir* **1998**, *14*, 5612-5619.

21. Ingram, R.S.; Hostetler, M.J.; Murray, R. W. Poly-hetero-ω-Functionalized Alkanethiolate-Stabilized Gold Cluster Compounds. *J. Am. Chem. Soc.* **1997**, *119*, 9175-9178.

22. Beasley, C. A.; Murray, R. W. Voltammetry and Redox Charge Storage Capacity of Ferrocene-Functionalized Silica Nanoparticles. *Langmuir* **2009**, *25*, 10370–10375.

23. Asır, S.The Synthesis of Chiral Perylene and Naphthalene diimides. PhD Dissertation. Eastern Mediterranean University, Gazimagusa, North Cyprus. **2009**.

24. Santosh, G.; Shirman, E.; Weissman, H.; Shimoni, E.; Pinkas, I.; Rudich, Y.; Rybtchinski, B. J. Photofunctional Self-Assembled Nanostructures Formed by Perylene Diimide−Gold Nanoparticle Hybrids. *J. Phys. Chem. B* **2010**, *114*, 14389−14396.

25. Xue, C.; Birel, O.; Gao, M.; Zhang, S.; Dai, L.; Urbas, A.; Li, Q. Perylene Monolayer Protected Gold Nanorods: Unique Optical, Electronic Properties and Self-Assemblies. *J. Phys. Chem. C* **2012**, *116*, 10396−10404.

26. Liu, N.; Shi, M.-M.; Pan, X.-W.; Qiu, W.-M.; Zhu, J.-H.; He, H.- P.; Chen, H.-Z.; Wang, M. Photoinduced Electron Transfer and Enhancement of Photoconductivity in Silicon Nanoparticles/Perylene Diimide Composites in a Polymer Matrix. *J. Phys. Chem. C* **2008**, *112*, 15865−15869.

27. Rathnayake, H.; Binion, J.; McKee, A.; Scardino, D.J.; Hammer, N.I. Perylene DiimideFunctionalized Bridged-Siloxane Nanoparticles for Bulk Heterojunction Organic Photovoltaics, *Nanoscale* **2012**, *4*, 4631-4640.

28. Wang, L.; Goodloe, W. G.; Stallman, B. J.; Cammarata, V. Synthesis, Electrooxidation, and Characterization of Bis(diphenylamine)naphthalene Diimide. *Chem. Mate*r. **1996**, *8*, 1175-1181.

29. Wang, Q. Copolymerization and Characterization of novel Bis(Diphenylamine) Monomers. M S Thesis. Auburn University.**1999**.

30. Liang, J. Preparation, Characterization and Application of Electroactive Polymers in Electrochromism and Sensors. PhD Dissertation. Auburn University. **2003**.

31. Wang, L.; Wang, Q. Q.; Cammarata, V. Electro-oxidative Polymerization and Spectroscopic Characterization of Novel Amide Polymers Using Diphenylamine Coupling. *J. Electrochem. Soc.* **1998**, *145*, 2648-2654.

32. Wang, L.; Cammarata, V. Electropolymers based on Diphenylamine II-Stacking in Cationic Benzidine Units. *Thin Solid Films* **1996**, *284-285*, 297-300.

33. Cammarata, V.; Hao, N.; Metz, J.; Liang, J. Electrochemical Quartz Crystal Microbalance Studies of the Growth of Perylene-Containing Films *ACS Symposium Series 832. Conducting Polymers and Polymer Electrolytes* **2009**, *5*, 59–74.

34. Kwan, W.; Atanasoska, L.; Miller, L.L. Oligoimide Monolayers Covalently Attached to Gold. *Langmuir* **1991**, *7*, 1419-1425.

35. Sawyer, D. T.; Roberts Jr., J. L. Experimental Electrochemistry for Chemist. *John Wiley & Sons.* **1974**.

36. Mazumder, A.; Davis J.; Rangari, V.; Curry M. Synthesis, Characterization, and Applications of Dendrimer-Encapsulated Zero-Valent Ni Nanoparticles as Antimicrobial Agents. *ISRN Nanomater.* **2013**, Article ID 843709, 9.

37. Patakfalvi, R.; Diaz, D.; Velasco-Arias,D.; Rodriguez-Gattorno, G.; Santiago-Jacinto, P. Synthesis and Direct Interactions of Silver Nanoparticles with Pollutant Gases. *Colloid Polym. Sci.* **2008**, *286*, 67–77.

38. Rodríguez-Gattorno, G.; Díaz, D.; Rendón , L.; Hernández-Segura, O.G. Metallic Nanoparticles from Spontaneous Reduction of Silver(I) in DMSO. Interaction between Nitric Oxide and Silver Nanoparticles. *J. Phys. Chem. B* **2002**, *106*, 2482-2487.

39. Creighton, J. A.; Eadont, D. G. Ultraviolet-Visible Absorption Spectra of the Colloidal Metallic Elements. *J. Chem. Soc. Faraday Trans.***1991**, *87*, 3881-3891.

40. Wang, W.; Chen, X.; Efrima, S. Silver Nanoparticles Capped by Long-Chain Unsaturated Carboxylates. *J. Phys. Chem. B* **1999**, *103*, 7238-7237.

41. Leopold, N.; Lendl, B. A New Method for Fast Preparation of Highly Surface-Enhanced Raman Scattering (SERS) Active Silver Colloids at Room Temperature by Reduction of Silver Nitrate with Hydroxylamine Hydrochloride. *J. Phys. Chem. B* **2003**, *107*, 5723-5727.

42. Duggan, J. N.; Roberts, C.B. Aggregation and Precipitation of Gold Nanoparticle Clusters in Carbon Dioxide-Gas-Expanded Liquid Dimethyl Sulfoxide. *J. Phys. Chem. C* **2014**, *118*, 14595−14605.

43. Kawasaki, H.; Yamamoto, H.; Fujimori, H.; Arakawa,R.; Iwasaki**,**Y**.;** Inada**,** M. Stability of the DMF-Protected Au Nanoclusters: Photochemical, Dispersion, and Thermal Properties. *Langmuir*, **2010**, *26*, 5926–5933.

44. Pastoriza-Santos, I.; Liz-Marza´n, L.M. Formation of PVP-Protected Metal Nanoparticles in DMF. *Langmuir* **2002**, *18*, 2888-2894.

45. Chen,Y.; Gu, X.; Nie, C-G.; Jiang, Z-Y.; Xie, Z-X.; Lin, C-J. Shape Controlled Growth of Gold Nanoparticles by a Solution Synthesis. *Chem. Commun.* **2005**, 4181–4183.

46. Liu, X.; Li, C.; Xu, J.; Lv, J.; Zhu, M.; Guo, Y.; Cui, S.; Liu, H.; Wang, S.; Li, Y. Surfactant-Free Synthesis and Functionalization of Highly Fluorescent Gold Quantum Dots. *J. Phys. Chem. C* **2008**, *112*, 10778–10783.

47. Pastoriza-Santos, I.; Liz-Marza´n, L.M. Formation and Stabilization of Silver Nanoparticles through Reduction by *N*,*N*-Dimethylformamide. *Langmuir*, **1999**, *15*, 948–951.

48. Little, B. K.; Li, Y.; Cammarata, V.; Broughton, R. Mills, G. Metallization of Kevlar Fibers with Gold. *ACS Appl. Mater. Interfaces* **2011**, *3*, 1965–1973.

49. Hall, B. D.; Zanchetb, D.; Ugarte. D. Estimating Nanoparticle Size from Diffraction Measurements. *J. Appl. Cryst.* **2000**, *33*, 1335-1341.

50. Young, J. T.; Boerio, F. J. Molecular Structure of Monolayers from Thiol-Terminated Polyimide Model Compounds on Gold. 1. A Spectroscopic Investigation. *Langmuir* **1996**, *12*, 1219-1226.

51. Lin-Vien, D.; Colthup, N.B.; Fatley, W.G.; Grasselli, J.G. The Hand book of Infrared and Raman Characteristic Frequencies of Organic Molecules. *Academic Press Inc.***1991**.

52. Angayarkanni, S. A.; Philip, J. Role of Adsorbing Moieties on Thermal Conductivity and Associated Properties of Nanofluids. *J. Phys. Chem. C* **2013**, *117*, 9009−9019.

53. Labande, A.; Ruiz, Astruc, D. Supramolecular Gold Nanoparticles for the Redox Recognition of Oxoanions: Syntheses, Titrations, Stereoelectronic Effects, and Selectivity. *J. Am. Chem. Soc*.**2002**, 124, 1782–1789.

Chapter Three

CORONENE DIIMIDE CONTAINING REDOX ACTIVE ELECTROCHROMIC POLYMER FILM VIA ELECTROPOLYMERIZATION OF DIPHENYLAMINE END GROUPS

3.1 Introduction

Research in the field of organic semiconducting polymers and their possible uses in electronics has been growing rapidly in recent decades. Numerous scientists have put considerable effort to developing new polymers and investigate of their properties. Our research group has synthesized new monomers containing a central redox active moiety flanked by two polymerizable functional groups and subsequently, electropolymerized and studied the mechanism of this process as well as their optical and electronic properties.

Some coronene derivatives have shown columnar discotic liquid-crystalline (LC) mesophases which makes them important candidates for organic electron transport materials.[1-2] Perylene diimides have been reported as electron-transport materials with very high electron mobility as well as having high chemical, thermal and photochemical stability.[3-9] Coronene has an extended core size over perylene, therefore it might have stronger intermolecular interactions leading to better charge-carrier mobility.

Different polymers based on perylene and naphthalene diimides have been synthesized and used as n-type semiconducting polymers for organic field effect transistors.[10-18] Thiophene,[10] thienothiophene,[12] thienopyrrole,[12] and phenothiazine[13] have been incorporated in the bay position of perylene diimide and copolymers have beenchemically synthesized. Usta et al. prepared a donor–acceptor pi conjugated polymer of dithiencoronene diimide with electron and hole mobilities of up to 0.30 $cm^2/V.s$ and 0.04 $cm^2/V.s$ respectively.[19]

Recent theoretical studies of coronene imides showed that functionalization in the imide position also controlled the electronic properties.[20] Wang et al. synthesized perylene containing polyimides from diamine derivatives of perylene.[21]

Electropolymerization is a very exciting route for producing new functional materials. The major application of this process is to make conducting polymers. Conducting polymers have been prepared via electropolymerization of a wide variety of organic molecules, pyrrole,[22] aniline,[23] thiophene,[24] furan,[25] indole ,[26] thianaphthene,[27] and carbazole.[28] P-phenoxyphenylamine and diphenylamine also can be electropolymerized at a moderate oxidation potential, i.e. these groups are excellent end group for electroactive monomers. In our lab diphenylamine functionalized at the imide position of perylene and naphthalene have been synthesized and polymer films were made on the surface of Au, glassy carbon (GC), Pt and indium tin oxide (ITO) electrodes via electropolymerization.[29-35] Spectroscopic and electrochemistry of these polymer films were also extensively studied. Spectroelectrochemistry studies of naphthalene diimide polymers show a solvent-dependent absorption energy band.[34] The electrochemical quartz crystal nanobalance (EQCN) technique have been used to explore the mechanism of film formation and kinetics of ion incorporation into polymer films in case of perylene and naphthalene diimide polymer.[33,35-36] Also these polymers exhibit different color in different redox states which makes them promising candidate for electrochromic materials.[34-35]

Spin coating is the most used method to make thin films for fabricating optoelectronic devices. However, in the spin coating process, a polymer has to be well soluble in a solvent. Semiconducting polymers with low solubility are difficult to fabricate into organic field effect transistor (OFET). Processes that result in highly self organized thin films are desirable for better interchain pi-pi stacking.[37] It has been reported that electropolymerized 3-hexylthiophene thin

films show a broader optical absorbance range than spin-coated samples but also comparable pi-pi stacking.[38] Manipulation of film thickness is easy using electropolymerization techniques by controlling the time of reaction and the number of scans.

Here we synthesized new a coronene diimide monomer containing a diphenylamine end group, N,N′-di-(phenylamino(phenyl)-5,11-dialkyl coronene tetracarboxylic diimide (DCTD)

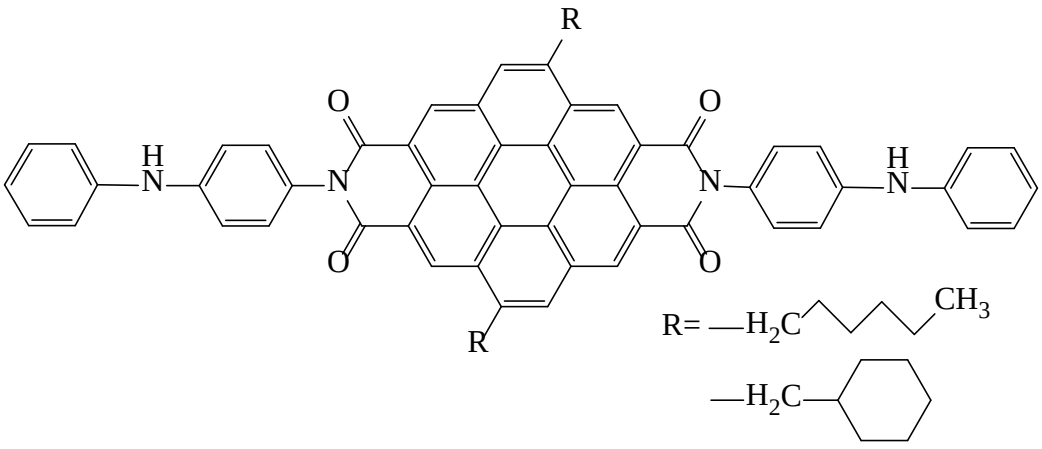

Scheme 3.1: Chemical structure of DCTD monomer.

(Scheme 3.1). DCTD was electropolymerized onto different conducting surfaces, such as Au, GC, and ITO glass slides. Electrochemistry, potential dependent UV-Vis-near IR as well as electrochromic properties and polymer microstructures are also discussed.

3.2 Experimental

3.2.1 Reagents and Materials:

CH_2Cl_2, hexane, $CHCl_3$ were purchased from BDH Chemicals. Dimethylformamide (DMF), dimethyl sulfoxide (DMSO) and methanol were obtanined from EMD Millipore Corporation. Trifluoroacetic acid (TFA) (Aldrich) and tert-butyl hydroxide (Alfa Aesar) were used as received. CH_2Cl_2, CH_3CN and dichloroethane were freshly distilled from calcium

hydride (Alfa Inorganics Inc.). DMSO, DMF and quinoline (Aldrich) were distilled under vacuum before use. Anhydrous toluene and THF were obtained from a solvent purification system (Pure Process Technology). Perylene tetracarboxylic dianhydride, bromine, cyclohexylamine, copper iodide, $Pd(PPh_3)_4$, triethylamine (anhydrious), 1,8-diazabicyclo[5.4.0]undec-7-ene (DBU) were obtained from Sigma -Aldrich. 4-amino-diphenylamine was purchased from Acros Organics, used after recrystallization from ethanol. The ionic liquid, 1-butyl-3-methylimidazolium bis(trifluoromethylsulfonyl)imide (BMIM TFSI) was purchased from Ionic Liquid Technologies, USA. ^{1}H and ^{13}C NMR spectra were obtained from either Bruker 600 or 400 MHz NMR instruments. Mass spectrometry data were collected from Waters Quadrapole Time of Flight (Q-TOF), Electron Spray Ionization (ESI) and Bruker MALDI-Q-TOF instruments. Sinapic acid (Sigma-Aldrich) was used as a matrix. An Agilent 8453 UV-Visible spectrophotometer, a Shimadzu IR Prestige -21 FTIR spectrometer and a Shimadzu RF-6000 Spectrofluorometer were used to characterize the product of the monomer synthesis.

3.2.2 Synthesis of N,N-Di-[p-phenylamino(phenyl)-5,11-di-dialkyl Coronene Tetracarboxylic Diimide(DCTD):

The entire synthetic process (scheme 3.2) was performed by modifying similar literature procedures.[1,39-41]

N,N'-dicyclohexyl perylene-3,4,9,10-tetracarboxylic diimide (2):

5 g of perylene-3,4,9,10-tetracarcrboxylic dianhydride were placed in round bottom flask with 86 g cyclohexylamine and refluxed at 145^{o} C for 15 h. The reaction mixture was cooled to

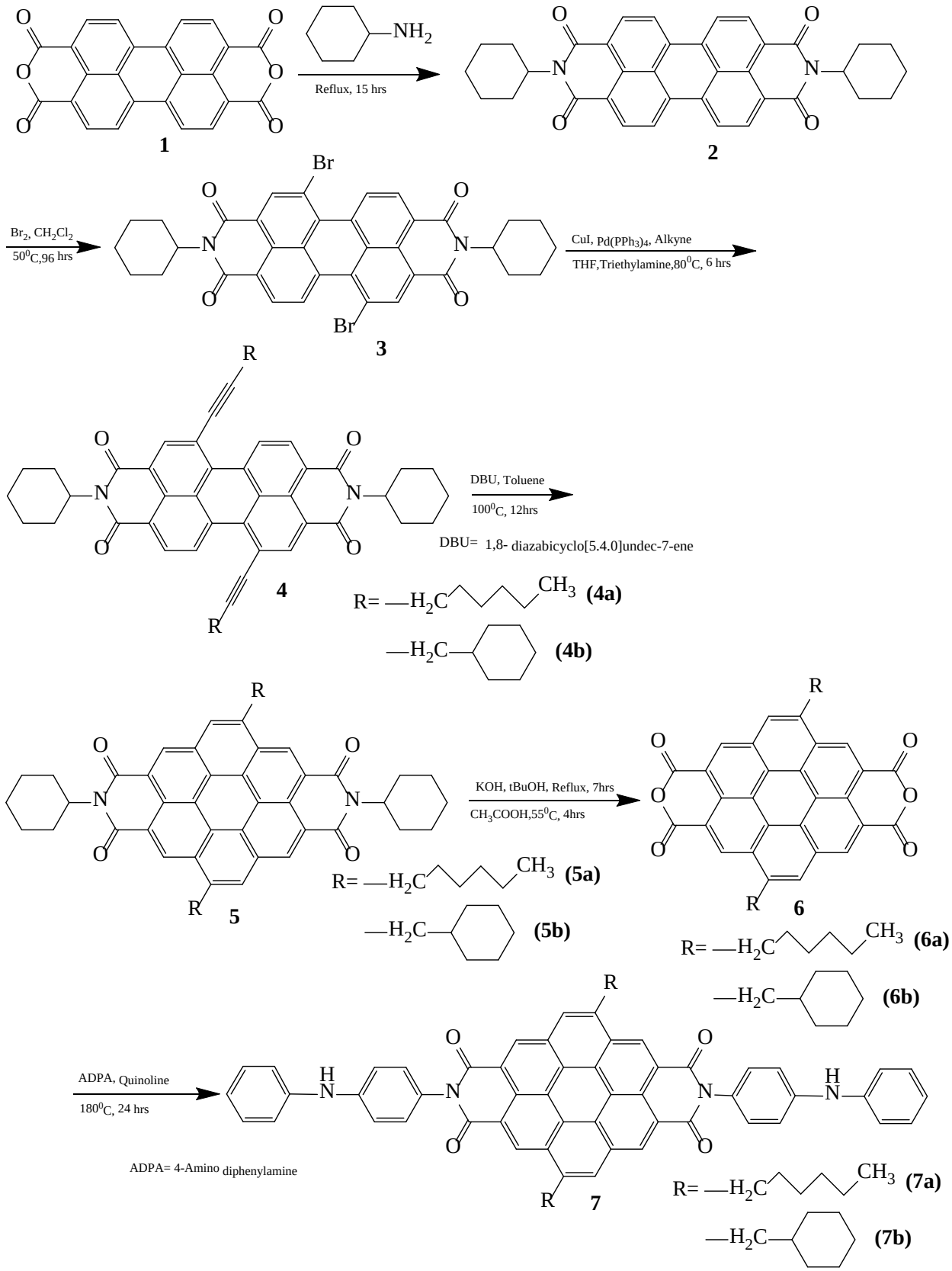

Scheme 3.2: Synthesis of DCTD monomers

room temperature; 100 mL of a 5% NaOH solution was added and the precipitate filtered. Finally the precipitate was washed with ethanol (300 mL) and the product was dried at 100^{o} C in a vacuum oven at 30 mm Hg. The yield of this product was 63%. ^{1}H NMR (600 MHz, $CDCl_3$): δ=8.69(d, 4H), 8.64(d, 4H), 5.07(m, 2H), 2.60(m, 4H), 1.94(m, 4H), 1.78(m, 6H), 1.39(m, 4H), 1.34(m, 2H); ^{13}C NMR(600 MHz, $CDCl_3$):δ = 163.92, 134.51, 131.42, 129.45, 126.45, 123.09, 50.02, 29.12, 26.55, 25.45; UV-Vis (CH_2Cl_2): λ_{max} (ε, $Lmol^{-1}cm^{-1}$) = 524 (120600), 487 (74400), 457 (28400), 430(9400); Fluorescence (CH_2Cl_2, λ_{ex}=524 nm): λ_{em}= 533; FT-IR (KBr):(cm^{-1}) = 2930, 2853, 1696, 1657, 1595, 1575, 1405, 1354, 1340, 1263, 1247, 1181, 1119, 810, 744, 653; MS (ESI): m/z = 554.20(M^-)(calculated 554.63)

***N,N'-dicyclohexyl-1,7-dibromo perylene-3,4,9,10-tetracarboxylic diimide (3)**:*

1.0 g of **2** and 18.7 g of bromine in 60 mL CH_2Cl_2 were heated at 50^{o} C for 96 h. The excess bromine was removed using N_2 and the product was dried under vacuum. **3** was purified through silica gel column chromatography with the CH_2Cl_2: hexane (85:15) eluent. 1.18 g of pure red solid compound 3 was separated (yield 92%). ^{1}H NMR(600 MHz, $CDCl_3$): δ= 9.49(d, 2H), 8.90(s, 2H), 8.69(d, 2H), 5.03(m, 2H), 2.58(m, 4H), 1.94(m, 4H), 1.78(m, 6H), 1.50(m, 4H), 1.38(m, 2H); ^{13}C NMR(600 MHz, $CDCl_3$):δ= 163.33,1.62.78, 137.94, 132.81, 132.65, 129.97, 129.22, 128.45, 127.02, 123.70, 123.29, 120.71, 54.25, 29.09, 26.50, 25.39; UV-Vis (CH_2Cl_2): λ_{max},nm (ε, $Lmol^{-1}cm^{-1}$) = 524 (69200), 488(47800), 457(18900), 390(8610), 273(35600), 263(35200); Fluorescence (CH_2Cl_2, λ_{ex}= 526nm): λ_{em}= 544nm; FT-IR(KBr):(cm^{-1}) = 2930, 2922, 2852, 1699, 1660, 1588, 1451, 1418, 1397, 1382, 1326, 1301, 1256, 1236, 1187, 1157, 1115, 984, 825, 808, 745, 687; MS(ESI): m/z = 710.04(M^-)(calculated 710.04).

***N,N'-dicyclohexyl-1,7-di(oct-1-ynyl) perylene-3,4,9,10-tetracarboxylic diimide (4a)**:*

N,N-dicyclohexyl-1,7-dibromo perylene-3,4,9,10-tetracarcrboxylic diimide, **3** (500 mg), CuI(10.8mg) and $Pd(PPh_3)_4$ (81.4 mg) were placed in a three neck flask under an Ar atmosphere and a mixture of dry THF (60 mL) and dry triethylamine (60 mL) were added to the flask under Ar through a double tipped transfer needle. 1-octyne (311.2 mg, 4 equiv.) was added to the reaction mixture through a septum using a syringe and heated at 80^o C for 6 h. The reaction was monitored by TLC. After completion of the reaction, 200 mL of cold, dilute HCl (HCl: ice water = 1:3) were added, the solution was stirred and the organic phase was separated through extraction with CH_2Cl_2. Extraction continued until the aqueous layer was neutral. The pure product was purified using silica gel column chromatography (solvent: CH_2Cl_2: hexane=1:1). 430 mg of pure product were isolated (yield 80%). ^{1}H NMR(600 MHz, $CDCl_3$): δ = 10.1(d,2H), 8.65(s,2H), 8.53(d,2H), 5.03(m,2H), 2.64(m,4H), 2.55(m,4H), 1.94-0.94(m,40H); UV-Vis(CH_2Cl_2): λ_{max} (ε, $Lmol^{-1}cm^{-1}$) = 549(48400), 510(31100), 476(12700), 296(37800); Fluorescence (CH_2Cl_2, λ_{ex}= 548nm) : λ_{em}= 564nm; FT-IR(KBr): (cm^{-1}) = 2929, 2855, 2208, 1701, 1657, 1602, 1590, 1458, 1409, 1342, 1328, 1245, 811; MS(MALDI): m/z = 771.53 ($M+H^+$)(calculated 770.41).

N,N'-dicyclohexyl-1,7-di(3-cyclohexylprop-1-ynyl) perylene-3,4,9,10-tetracarboxylic diimide (4b):

Synthesis and purification of **4b** is similar to the proceduce used to obtanin **4a**. N,N-dicyclohexyl-1,7-dibromo perylene-3,4,9,10-tetracarcrboxylic diimide, **3** (250 mg), CuI(5.4 mg) and $Pd(PPh_3)_4$ (40.7 mg) were placed in a three neck flask in under argon atmosphere and a mixture of dry THF (30 mL) and dry triethylamine (30 mL) were added to the flask under Ar through a double tipped transfer needle. 3-cyclohexyl-1-propyne (172.1 mg, 4 equiv.) was added to the reaction mixture through a septum by a syringe and heated at 80^o C for 6 h. The reaction

was monitored by TLC. After 6 h, 200 mL of cold dilute HCl (HCl: ice water= 1:3) were added under stirring and the organic phase was separated through extraction with CH_2Cl_2. Extraction continued until the aqueous layer was neutral. 215 mg pure product was separated by silica gel column chromatography (solvent: CH_2Cl_2: hexane = 1:1) (yield 77%). ^{1}H NMR(600 MHz, $CDCl_3$): δ = 10.05(d, 2H), 8.65(s, 2H), 8.50(d, 2H), 5.03(m, 2H), 2.54-1.14(m, 46H); FT-IR(KBr) :(cm^{-1}) = 2925, 2852, 2206, 1701, 1657, 1601, 1589, 1450, 1409, 1342, 1328, 1260,1243, 811. UV-Vis (CH_2Cl_2): λ_{max} (ε, $Lmol^{-1}cm^{-1}$) = 550(72900), 511(44400), 478(17300), 297(67500); Fluorescence (CH_2Cl_2, λ_{ex}= 550nm) : λ_{em} = 567nm.

N,N'-dicyclohexyl-5,11-dihexyl coronene-2,3,8,9-tetracarboxylic diimide (5a):

200 mg of **4a** were dissolved in toluene, which was deoxygenated using argon gas for one hour, then 0.2 mL DBU were added through a septum into the reaction mixture. The reaction mixture was stirred at 100-110^o C for 12 h. After 12 h, 200 mL of cold, dilute HCl (HCl: ice water= 1:3) were added under stirring and the organic phase was separated through extraction with CH_2Cl_2. Extraction continued until the aqueous layer was neutral. The product was dried over $MgSO_4$ and 100 mL of methanol were added and the precipitate was collected through filtration. 150 mg of pure product was obtained (yield 75%). ^{1}H NMR(600 MHz, $CDCl_3$):9.46(s,2H), 9.20(s,2H), 8.28(s,2H), 5.38(m,2H), 3.54(m,4H), 2.89(m,4H), 2.15(m, 8H), 2.01(m, 6H), 1.70(m, 10H), 1.43(m, 8H), 0.98(m, 6H); UV-Vis($CHCl_3$): λ_{max} (ε, $Lmol^{-1}cm^{-1}$) = 512(17500), 478(11400), 429(62800), 404(29200), 382(7200), 338(77200), 334(75600); Fluorescence ($CHCl_3$, λ_{ex} = 478nm):λ_{em}= 516nm; FT-IR(KBr)(cm^{-1}) = 2928, 2855, 1704, 1660, 1606, 1509, 1468, 1406, 1330,1301, 1258, 1191, 1147, 925, 810; MS(MALDI):m/z = 771.20 ($M+H^+$) (calculated 770.41).

N,N'-dicyclohexyl-5,11-di(1-cyclohexyl ethane) coronene-2,3,8,9-tetracarboxylic diimide (5b):

Synthesis of **5b** is similar as **5a**. 120 mg of co **4b** were dissolved in 50 mL toluene, which was deoxygenated with Ar for one hour, then 116 μL DBU were added through a septum into the reaction mixture. The reaction mixture was stirred at 100-110^{o} C for 12h. After that, 100mL cold dilute HCl (HCl: ice water= 1:3) were added under stirring and the organic phase was separated through extraction with CH_2Cl_2. Extraction continued until the aqueous layer was neutral. The product was dried over $MgSO_4$ and 70 mL of methanol added and the precipitate was collected through filtration. 85 mg of pure product was obtained (yield 71%). ^{1}H NMR(600 MHz, $CDCl_3$+d-TFA): δ = 9.9 (s, 2H), 9.64(s, 2H), 8.67(s, 2H), 5.37(m, 2H), 3.64-108 (m, 46H); FT-IR(KBr) :(cm^{-1}) = 2923, 2853, 1704, 1660, 1606, 1459, 1451, 1405, 1340, 1302, 1258,1243, 1148. UV-Vis ($CHCl_3$): λ_{max} (ε, $Lmol^{-1}cm^{-1}$) = 509(16300), 475(11700), 427(52700), 403(24300), 379(7300), 337(69600), 331(67600); Fluorescence (CH_2Cl_2, λ_{ex} = 478nm) :λ_{em} = 515nm.

N,N'-dicyclohexyl-5,11-dihexyl coronene-2,3,8,9-tetracarboxylic dianhydride (6a)*:*

140 mg of **5a** were added to 8 mL *tert*-butyl alcohol containing 1.06 g KOH and the reaction mixture was refluxed (~95-100^{o} C) for 7 h.Then the reaction was cooled to 50^{o} C and 24.0 mL of acetic acid were added keeping the temperature at 50^{o} C for 4 h. The products were filtered, washed with water until neutral, washed with methanol and dried in a vacuum oven at 100^{o} C at 30mm Hg. 106 mg of product were obtained (yield 96%). UV-Vis ($CHCl_3$+TFA):526(12400), 511(10700), 492(7200), 477(5600), 422(30500), 399(16700), 333(47800), 327(46400) ; Fluorescence ($CHCl_3$, λ_{ex}= 422nm): λ_{em}= 516 nm; FT-IR(KBr): 2956,

2928, 2856, 1776, 1738, 1606, 1507, 1465, 1295, 1286, 1247, 1236, 1219, 1210, 1143, 1107, 1013, 999, 807, 764, 748; MS(MALDI):m/z=609.07 ($M+H^+$)(calculated 608.68).

N,N'-dicyclohexyl-5,11-di-(1-cyclohexyl ethane) coronene-2,3,8,9-tetracarboxylic dianhydride (6b):

78 mg of **5b** were added to 3.5 mL *tert*-butyl alcohol containing 0.55 g KOH and the reaction mixture was refluxed (~95-100^o C) for 12 h and then cooled to 70^o C. Then 11.0 mL of acetic acid were added and the temperature was kept at 70^o C for 5 h. The products were filtered, washed with water until neutral, washed with methanol and then dried in a vacuum oven at 100^o C at 30mm Hg for overnight. 63 mg product were obtained (98%). UV-Vis (CH_2Cl_2+TFA):527(32300), 492(18600), 422(53600), 401(36000), 334(88000), 327(86600); Fluorescence (CH_2Cl_2, λ_{ex}= 422nm): λ_{em}= 521 nm; FT-IR (KBr):(cm^{-1}) = 2924, 2852, 1775, 1750, 1609, 1507, 1469, 1450, 1246, 1116, 807.

Synthesis of N,N-di-[p-phenylamino(phenyl)-5,11-di-dihexyl coronene tetracarboxylic diimide (7a) :

80 mg of **6** were dissolved in 6.20 mL of quinoline containing 96.9 mg N-phenyl-p-phenylenediamine (4 equiv.) and 8.8 mg of zinc acetate. The temperature of the reaction mixture was held at 180^o C for 24 h under Ar. After cooling to room temperature, 20 mL diethyl ether were added to the reaction flask, the precipitate filtered and washed with water and then diethyl ether. The product was dried under vacuum (30 mm Hg) overnight and 102 mg pure product were isolated (yield 82%). ^{1}H NMR(600 MHz, $CDCl_3$+d-TFA):δ =10.08(s, 2H), 9.91(s, 2H), 8.88(s, 2H), 7.88-7.61(m,18H), 3.71-0.90(m, 26H); UV-Vis($CHCl_3$+TFA): λ_{max} (ε, $Lmol^{-1}cm^{-1}$) = 521(24000), 486(16000), 434(101400), 409(52000), 386(18200), 333(132800); Fluorescence ($CHCl_3$, λ_{ex}= 478nm):λ_{em} = 523; FT-IR(KBr): (cm^{-1}) = 3384, 2956, 2927, 2856, 1710, 1665,

1604, 1595, 1518, 1495, 1467, 1401, 1343, 1320, 1305, 1244, 926, 810, 796, 754, 584; MS(MALDI):m/z =942.04($M+H^+$)(Calculated 941.12).

Synthesis of N,N-di-[p-phenylamino(phenyl)-5,11-di-(1-cyclohexyl ethane) coronene tetracarboxylic diimide (7b):

60 mg of **6b** were dissolved in 4.6 mL of quinoline containing 69.9 mg of N-phenyl-p-phenylenediamine (4 equiv.) and 6.3 mg of zinc acetate The temperature of the reaction mixture was held at 180^o C for 24 h under argon gas. After cooling to room temperature, 15 mL diethyl ether were added to the reaction flask, the precipitate filtered, then washed with water and then diethyl ether. The product was dried at 100^0 C under vacuum (30 mm Hg) overnight and 86 mg pure product were isolated (yield 93%). UV-Vis(CH_2Cl_2+TFA): λ_{max} (ε, $Lmol^{-1}cm^{-1}$) = 525(20100), 490(13900), 435(62500), 410(35400), 335(91700); Fluorescence (CH_2Cl_2, λ_{ex}= 478nm):λ_{em} = 524; ^{1}H NMR(600 MHz, $CDCl_3$+d-TFA):δ = 10.20(s, 2H), 10.01(s, 2H), 9.00(s, 2H), 7.41-7.67(m, 18H), 3.76-0.89(m, 26H); FT-IR(KBr) :(cm^{-1}) = 2919, 2852, 1711, 1663, 1606, 1595, 1512, 1496, 1339, 1314, 1253, 1202.

3.2.3 Electrochemistry:

Cyclic Voltammetry was performed on a modified AFRDE4 Bi-Potentiostat (Pine Instrument Co.) electrochemistry workstation. The measurements were done using a three electrode electrochemical cell equipped with spiral Pt wire counter electrode and Ag/AgCl reference electrode saturated with KCl. The working electrodes were glassy carbon disks (3mm diameter), Au disk (1.5mm diameter) and Indium Tin Oxide (ITO) coated glass (variable dimension) electrodes. The Au and GC disk electrodes were polished using alumina powder sonicated for one minute in water, cleaned with hydrogen peroxide and finally rinsed with

CH_2Cl_2. The ITO electrodes were cleaned using soap water (Alconox liquid) in an ultrasonic bath followed by cleansing with acetone and ethanol for 20 minutes each and finally rinsed with CH_2Cl_2. The solutions were purged with argon gas before the measurements which were done at room temperature.

3.2.4 Visible-NIR spectroelectrochemistry:

The electropolymerization was performed in the long path length homemade spectroelectrochemical cell that employed ITO glass slides (75 X 25 X 1.1mm, 70-100 Ω.□, Delta Technology Ltd) as working electrodes. This cell has two windows, the front window consisted of an ITO electrode and the rear one was microscope glass slide. Three holes have been drilled for degassing the solution, and to position the counter and reference electrodes. The Ag/AgCl saturated with KCl was used as reference and a Pt mesh served as counter electrode. The electrode potential was controlled by a modified AFRDE4 Bi-Potentiostat (Pine Instrument Co.) electrochemistry workstation while UV-Vis measurements were performed with an Agilent 8453 UV-Visible spectrophotometer. Solutions in the electrochemical cell were bubbled with Ar for at least 10 mins. The electrochemical potential was stepped to the appropriate value and each spectrum was taken when the cell current decayed to zero.

3.2.5 Atomic Force Microscopy (AFM):

The morphological analysis of polymer films deposited on ITO were performed using a Bruker AFM system (multimode 8). The Scan-Asyst-Air mode was used for imaging the samples. AFM imaging in the Scan-Asyst-Air mode is very similar to the peak force tapping mode in where the operation is a non-rosonant procedure. However, in the Scan-Asyst-Air mode, all the imaging parameters are automatically adjusted. The Scan-Asyst algorithm can optimize

the minimum force required to track sample surfaces and to control the scan rate and the z limit. All images were generated by the Bruker NanoScope Analysis 1.5 software.

3.3 Results and Discussions

3.3.1. Electropolymerization of monomers:

The monomer, N,N-di-[p-phenylamino(phenyl)-5,11-di-alkyl coronene tetracarboxylic diimide (DCTD) has low solubility in many organic solvents such as CH_2Cl_2, CH_3CN, THF, dichloroethane, dichlorobenzene. For these solvents, addition of TFA increased the solubility. Given that, CH_2Cl_2 is a convenient solvent due to high dielectric constant, easy purification, this liquid was used as the solvent for the electropolymerization. The cyclic voltammogram of the electropolymerization of the DCTD monomer is shown in Figure 3.1. The ionic liquid, BMIM TFSI (0.1 M) and TFA (~0.8-2.4% v/v) were used as supporting electrolytes. In this electro-oxidation process, the first scan shows a large oxidation peak current at 1.05 V and the corresponding reduction shows two peaks at 0.87 and 0.62 V. During the second and subsequent scan, two oxidation peaks occurred at 0.92 and 0.74 V and the corresponding reduction peaks were observed upon reversing the scan direction (Figure 3.1.A). The oxidation and reduction peak currents gradually increases as the number of scan increased in the same potential window but the intensity of the first peak at 1.05 V decreased. This peak represents the irreversible oxidation of the diphenylamine group. Similar results have been reported in case of electropolymerization of the diphenylamine end group in monomers containing naphthalene diimide, ferrocene, perylene diimide.[29-35] As the first reverse scan (negative direction) of DCTD exhibits no reduction peak corresponding to 1.05 V oxidation peaks, the two new reduction peak were assigned for the reduction of newly formed diphenylbenzidine (DPB) cations (one is for

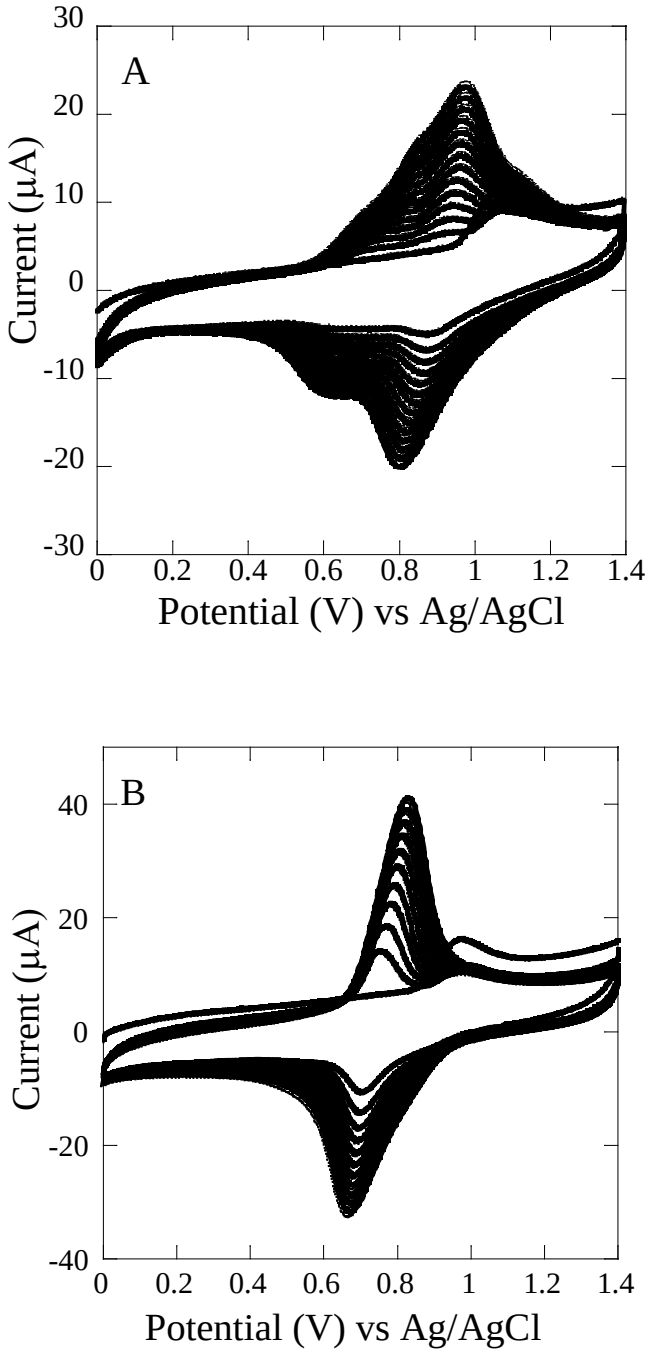

Figure 3.1: Polymerization of 0.1mM DCTD in CH_2Cl_2 containing 0.1M BMIM TFSI and TFA (0.8% and 2.4 % v/v for **7a** and **7b** respectively) at a GC disk electrode (area 0.071 cm^2). Scan rate 200 mV/s. A. monomer **7a**; B. monomer **7b**.

DPB^{+} and other is for DPB^{2+}). According toYang and Bard, DPB formed by the inter ring carbon-carbon coupling of either two diphenylamine radicals of two monomers (the EECC mechanism), or one diphenylamine radical from one monomer and one neutral diphenylamine from other monomer (ECEC mechanism) (scheme 3.3.).[42] However, Hao showed that the DPB formed by oxidation of the naphthalene diimide monomer (DNTD) took place via ECEC mechanism.[36] Figure 3.1 B shows the oxidative polymerization of monomer **7b**. The first oxidation potential occurred at 0.97V, with the reverse scan showing only one reduction peak at 0.70V instead of two reduction peaks noticed during the polymerization of monomer **7a**. On the second positive scan in the potential range of 0 to 1.40V, only one oxidation peak was observed. Monomer **7b** is less soluble than the monomer **7a**, so three times more TFA (~2.4% v/v) was needed to solubilize. We suggest the two oxidation and reduction peaks were merged as has been seen in other highly acidic solvents.[30] From the difference of voltammetric response of both monomers, it was observed that in more acidic media, diphenylamine will oxidize at lower potentials i.e., electrooxidation is preferable in acidic media. Formation of the diphenylamine radical cations in acidic and neutral conditions are different (Scheme 3.4).[42-43] Diphenylamine is protonated in acidic media. The protonated diphenylamine is more susceptible to oxidation than the neutral diphenylamine. Therefore acid catalyzed diphenylamine oxidation is more preferable. Previously it has been reported that electropolymerization of aniline and pyrrole were also favorable to acidic media.[44-45]

3.3.2 Electrochemistry of Polymer film in different solvents:

After preparing polymer films on different conducting surfaces, such as Au, GC and ITO, we have studied the electrochemistry of these polymer films in different solvents. Figure 3.2(A) shows the cyclic voltammogram of DCTD polymer on a GC electrode surface in the 0.1M

EECC process:

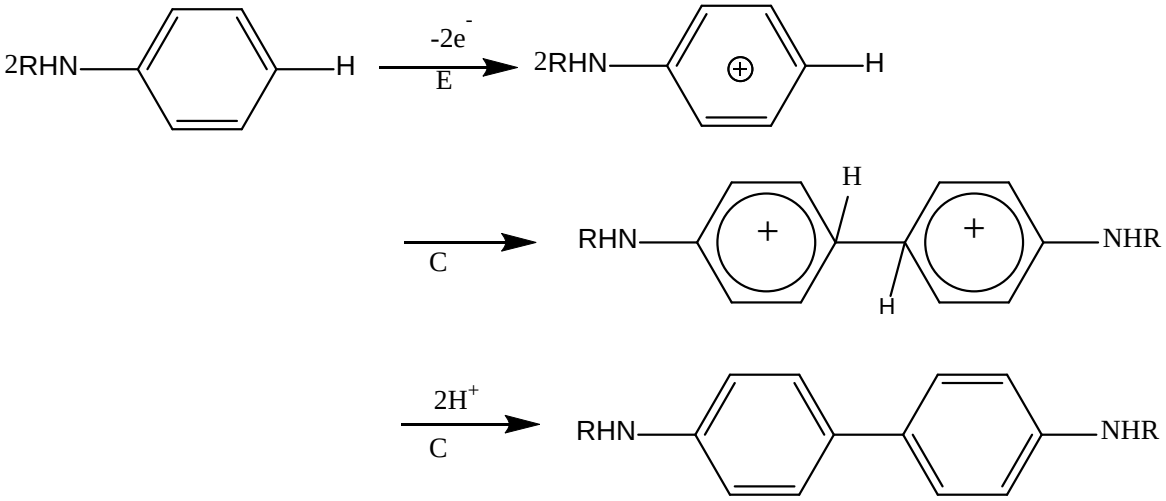

ECEC process:

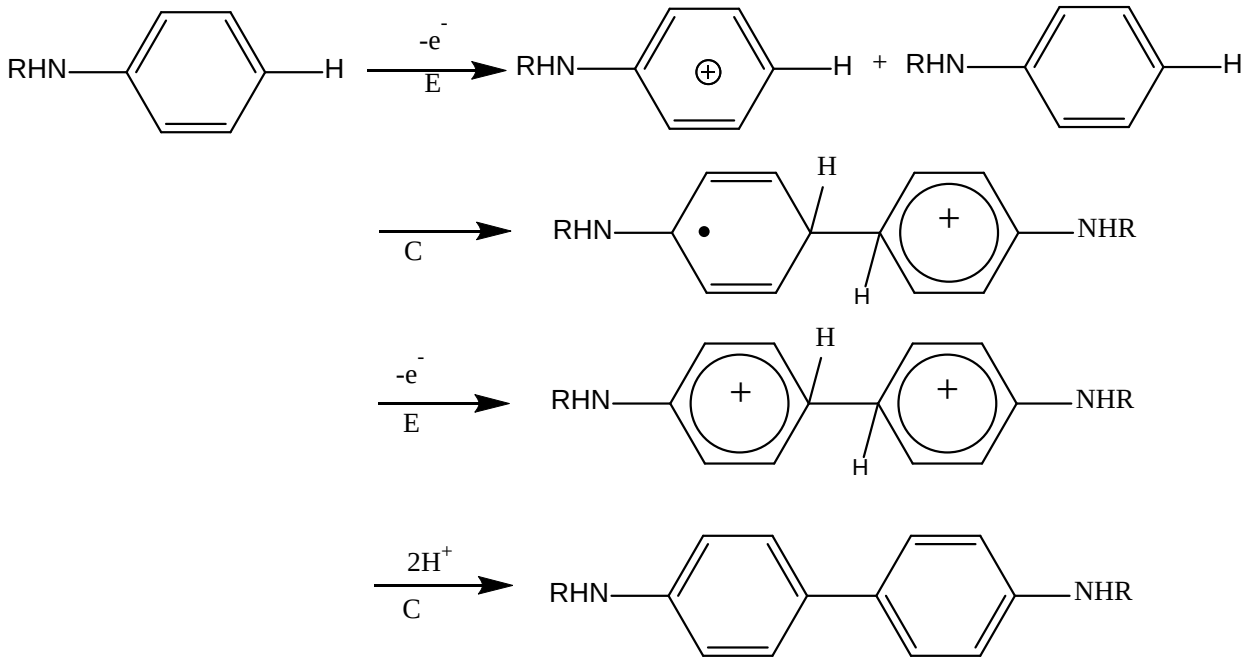

Scheme 3.3: EECC and ECEC mechanism.[42]

A. with acid[43]

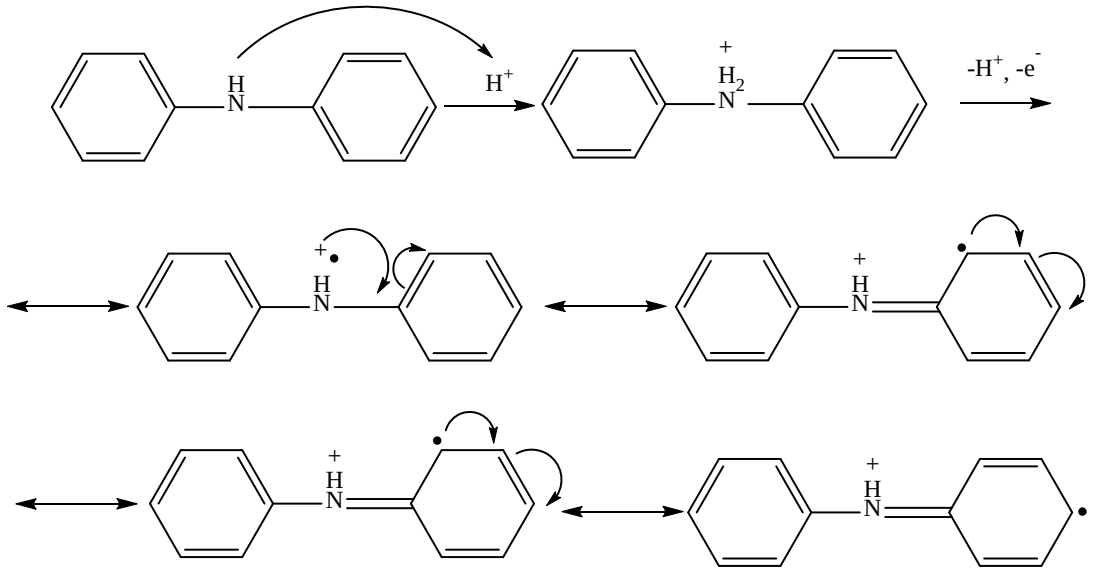

B. without acid[42]

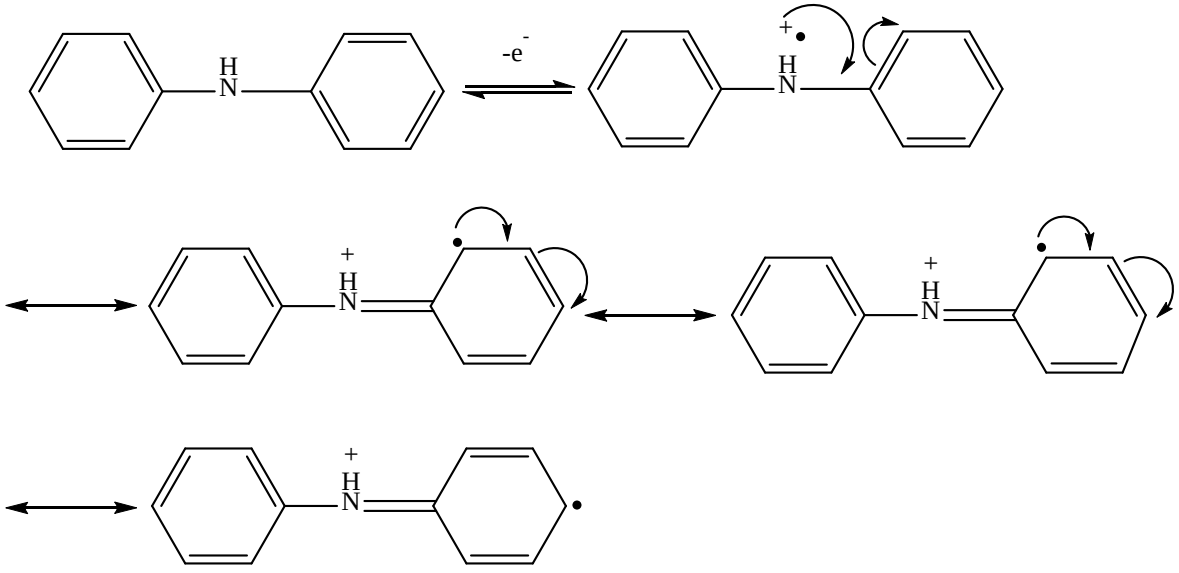

Scheme 3.4: Diphenylamine cation formation A. with acid, B. without acid.

BMIM TFSI solution of CH_2Cl_2. The thickness of the film was $4.0x10^{-9}$ mol/cm^2 which was estimated by integrating the DPB oxidation peaks. In the positive potential scan, two sets of redox peaks were noticed; these redox couples corresponded to the presence of electroactive DPB in the polymer chain. In the positive potential range DPB produces two radical cation, DPB^+ and DPB^{2+}.This is consistent with previous work done in our group with other diphenylamine end group containing polymer films.[29-35]Also linear dependence the peak current dependence on the scan rate confirmed that the polymer film was surface confined (Figure 3.3). The electrochemical behaviors of DPB group in the other solvents, is different except in dichloroethane. In DMSO and DMF, the redox behavior of DPB is ill defined, so that this group is not electroactive under those conditions. In the negative scan range up to 0.0 V vs Ag/AgCl, the reversible reduction peaks occur at -0.97 and -1.22V vs Ag/AgCl (sat. KCl) in CH_2Cl_2. The reduction peaks are consistent with the presence of a redox active coronene tetracarboxylic diimide group. The peak potentials in different solvents are summarized in Tables 3.1 and 3.2. For solvents with low donor number, i.e. with high Lewis acidity, DPB shows good

Table 3.1: Effect of solvent on the electrochemistry of DCTD polymer in oxidation potential (positive scan) (0.1M BMIM TBSI).

Solvent	DN[a]	AN[b]	Ep_{a1}/Ep_{c1}(V)	ΔEp_1(mV)	Ep_{a2}/Ep_{c2}(V)	ΔEp_2(V)
CH_2Cl_2	0	20.4	0.75/0.65	100	0.98/0.87	110
$C_2H_4Cl_2$	0	16.7	0.50/0.53	30	0.84/0.73	110
THF	20.0	8.0	-	-	0.92/0.82	100
CH_3CN	14.1	18.9	-	-	1.04/0.87	170
DMF	26.6	16.0	-	-	-	-
DMSO	29.8	19.3	-	-	-	-

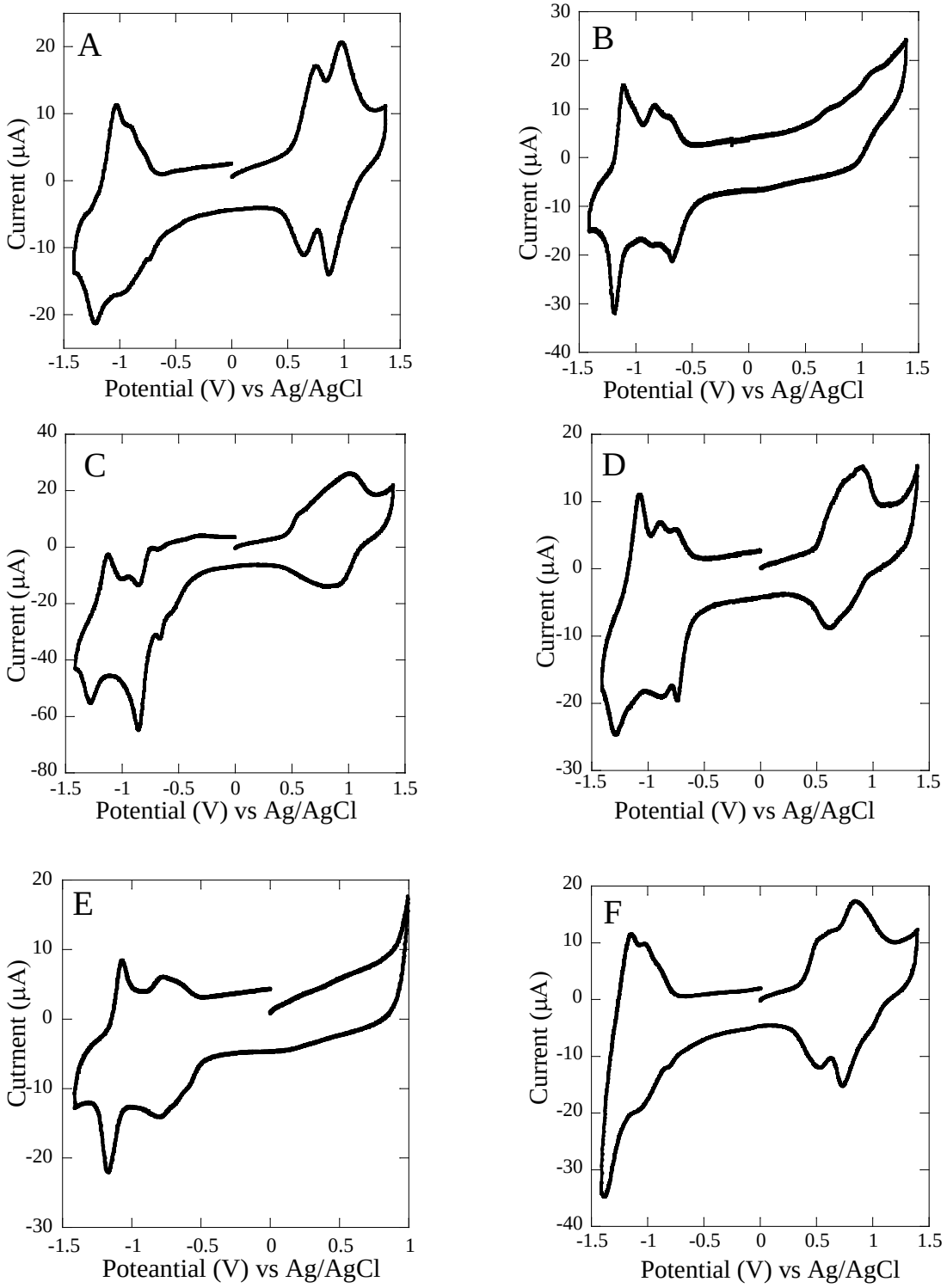

Figure 3.2: Cyclic voltammograms of poly(DCTD) film on GC electrode surfaces in different solvent containing 0.1 M BMIM TFSI electrolyte . GC electrode area=0.071 cm^2. Scan rate 200 mV/s. A. CH_2Cl_2; B. DMF; C. CH_3CN; D. THF; E. DMSO; F. Dichloroethane.

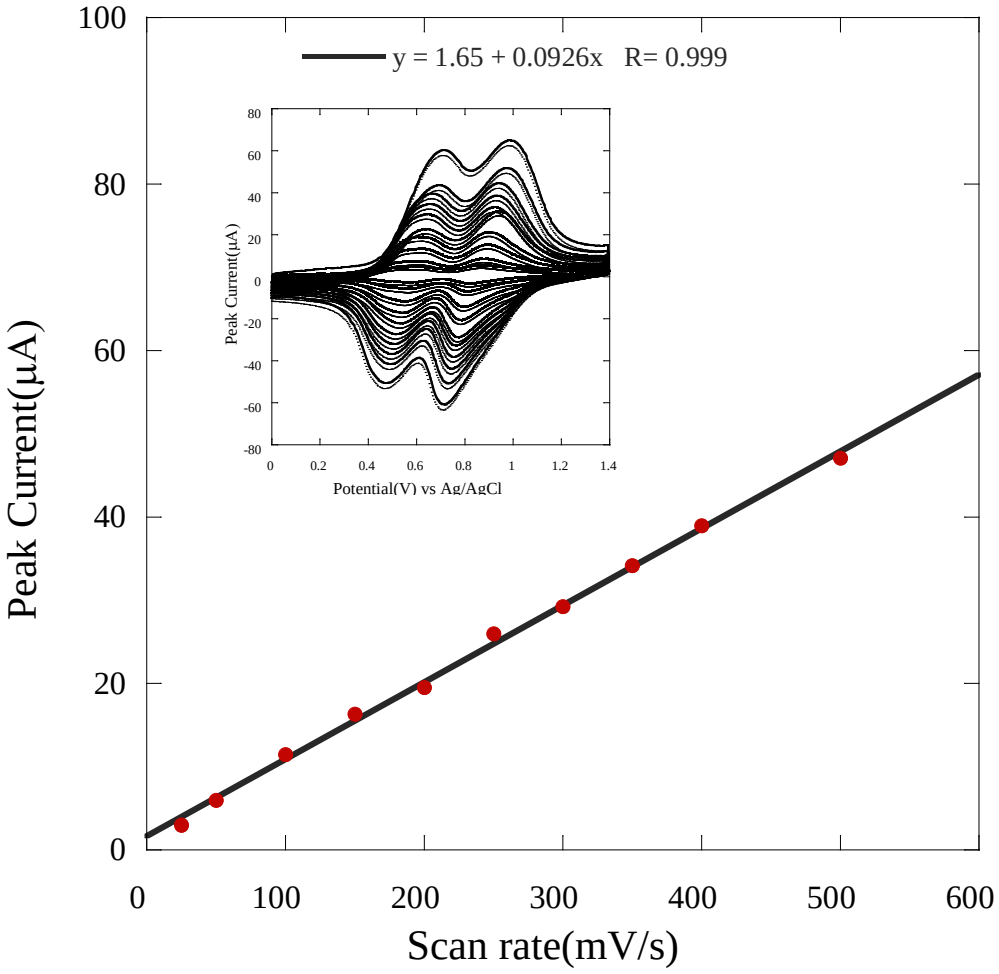

Figure 3.3: Scan rate dependence on DPB oxidation peak of DCTD film on GC electrode surface in the 0.1M BMIM TFSI solution of CH_2Cl_2 (GC electrode area = 0.071 cm^2). The inset shows CV's of a this poly(DCTD) film, scan rate 25(smallest current) and 500(largest current)mV/s.

Table 3.2: Effect of solvent on the electrochemistry of polymer in reduction potential (negative scan) (0.1M BIBM TBSI).

Solvent	DN[a]	AN[b]	Ep_{c1}/Ep_{a1}(V)	ΔEp_1(V)	Ep_{c2}/Ep_{a2}(V)	ΔEp_2(V)
CH_2Cl_2	0	20.4	-0.97/-0.90	70	-1.22/-1.03	190
$C_2H_4Cl_2$	0	16.7	-1.06/-1.02	40	-1.38/-1.14	240
THF	20.0	8.0	-0.89/-0.88	10	-1.29/-1.07	220
CH_3CN	14.1	18.9	-0.86/0.93	70	-1.28/-1.12	160
DMF	26.6	16.0	-0.87/-0.83	40	-1.19/-1.11	80
DMSO	29.8	19.3	-0.80/-0.76	40	-1.17/-1.07	100

[a]DN= Gutmann donor number, [b]AN=Gutmann acceptor number[46]

electrochemical reversibility upon oxidation. In the solvents THF, CH_3CN, DMF and DMSO with high donor number, the first reduction potentials are more positive than those for solvents with low donor number because the tetracarboxylic diimide anions are more stable in solvents with high donor number.

3.3.3 Effect of electrolyte on the electrochemistry of poly(DCTD):

The previous section shows that poly(DCTD) is electroactive in 0.1 M 0.1M BMIM TFSI solution of CH_2Cl_2. Here the effect of the electrolyte on the electrochemistry of poly(DCTD) was studied. The Figure 3.4 shows the electrochemistry of poly(DCTD) on a GC electrode in acetonitrile containing 0.1M electrolyte. Prior to performing the electrochemistry, the polymer was grown on the surface of the GC electrode from a solution of 0.1mM DCTD in CH_2CH_2 containing 0.1M BMIM TFSI. The estimated film thickness was 2.77×10^{-9} mol/cm^2. At potentials positive of 0.0V, the voltammetric peaks were not well-defined for the $2e^-$ oxidation of DPB in solutions containing several electrolytes such as BMIM TFSI, $TEABF_4$, $LiClO_4$. However, the electrochemistry was well-defined when the in the electrolyte contained the anions BF_4^-, and ClO_4^-($TBABF_4$ and $TBAClO_4$). Moreover in CH_2Cl_2 containing BMIM TFSI (Figure

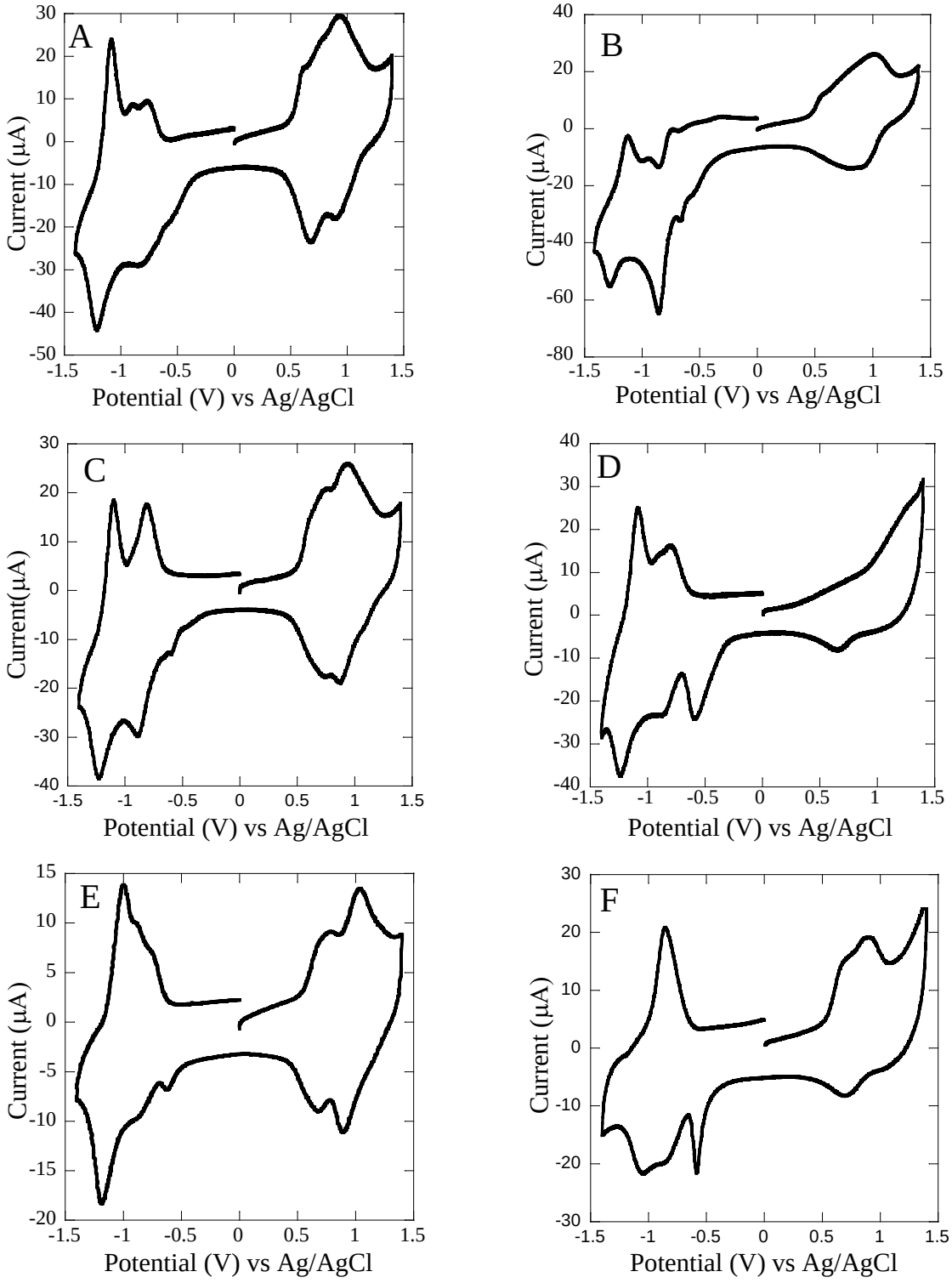

Figure 3.4: Cyclic voltammograms of poly(DCTD) film on GC electrode surfaces in CH_3CN solvent containing 0.1M electrolyte . GC electrode area=0.071 cm^2. Scan rate 200 mV/s. A. $TBABF_4$; B. BMIM TFSI; C. $TBAClO_4$; D. $TEABF_4$; E. $TBAPF_6$; F. $LiClO_4$

3.3), well separated $2e^-$ oxidation and reduction signals of DPB were obtained. Therefore in the positive potential range, the electrochemistry of poly(DCTD) was affected by both the cation and anion of the supporting electrolyte. On the other hand, in the negative scan, all the voltammograms show at least two pairs of redox peaks except for $LiClO_4$. In the $LiClO_4$ case the electrochemistry was not reversible indicating that the interaction of a smaller inorganic cation and the tetracarboxylic diimide anion was not favorable. Similar behavior for the diimide anion in naphthalene and perylene diimide were reported previously.[35-36,46]

3.3.4 Spectroelectrochemistry of DCTD polymer:

The DCTD polymer was made on a ITO with a thickness of 9.63×10^{-9} mol/cm^2 and then studied by UV-Visible-near IR spectroscopy at the different potentials in a 0.1M BMIM TFSI solution of CH_2Cl_2. Figure 3.5 depicts the spectrum of the neutral state of poly(DCTD) showing absorption maxima at 513, 480, 430, 408 and 333 nm. At the oxidation potential of 800 mV vs Ag/AgCl, a broad absorption band centered at 900nm was detected, presumably due to the formation of π-stacking of the DPB^+ unit of poly(DCTD).[29-35] The absorption for π-stacking in the polymer containing perylene , naphthalene and ferrocene exhibits a peak at around 1100 nm.[29-32,34-35] The absorption band shifting toshorter wavelengths in the case of poly (DCTD), which might be due to increased steric hindrance between chains as compared to the other polymers. The absorption bands between 400 to 513 nm dramatically increased in intensity, at the same time that the intensity of the band at 333 nm decreased. Upon further oxidation, an intense absorption band appeared at 602 nm which indicates oxidation of the DPB group to DPB^{2+} and also decreases the intensity for the absorption band at 900 nm, indicating that the dication formation in the polymer chain reduces the π-stacking interaction. [29-32,34-35] Upon reduction of the polymer films at -1000 mV vs Ag/AgCl, i a radical anion is formed with new

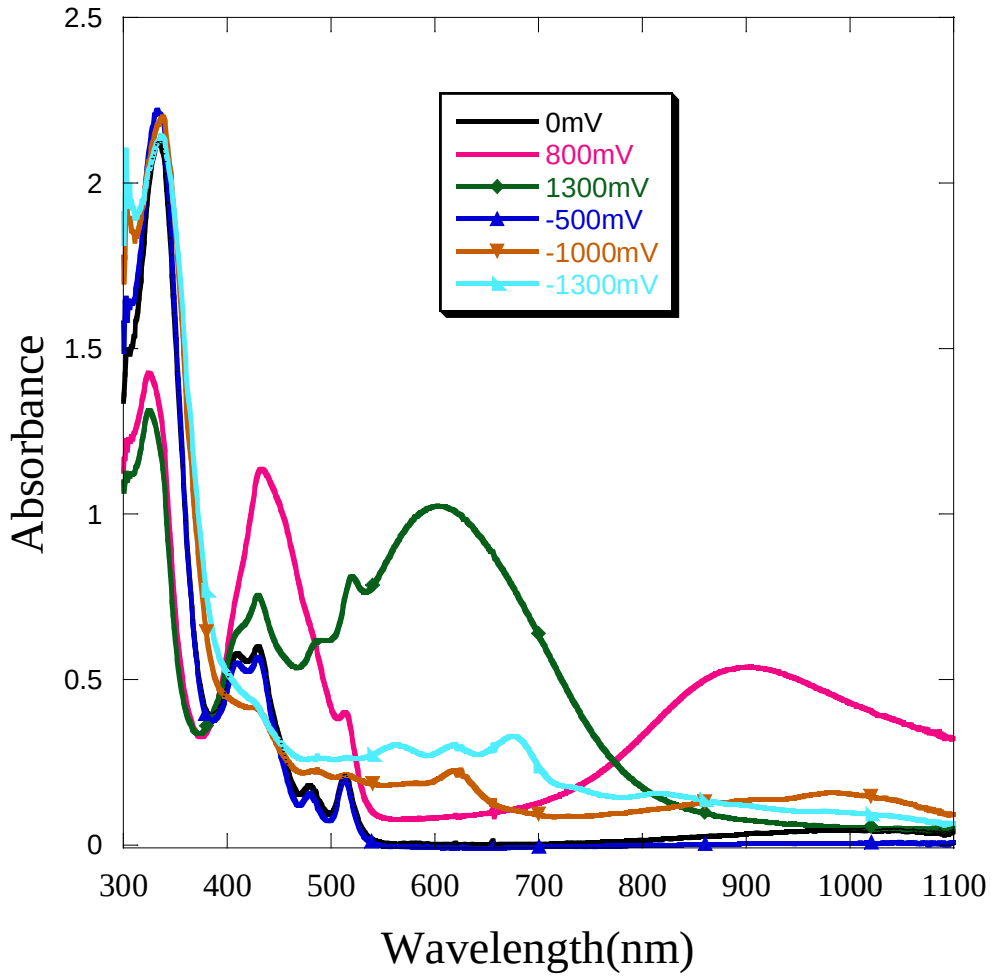

Figure 3.5: Visible-near IR spectroelctrochemistry poly(DCTD) film on the surfaces of ITO electrode at different potentials (vs Ag/AgCl) in 0.1 M BMIM TFSI solution of CH_2Cl_2.

absorption bands at 620 and 982 nm appearing in the spectrum. Also the absorption bands between 400 to 513 nm dramatically decrease in intensity. When applying a very negative potential of -1.3V, the tetracarboxylic diimide reduces to a dianion, and the spectrum showed additional peaks at 562, 676 and 824 nm together with a decay of the peak at 982nm.

3.3.5 Electrochromic Behavior:

Poly(DCTD) displays reversible changes of color upon containing the potential. In Figure 3.6 shows photographs of the polymer film in a 0.1M BMIM TFSI solution of CH_2Cl_2 at different potentials. The color of the polymer film color was yellow similar to the color of the DCTD monomer in solution. With an anodic change of potential, the color of the polymer film changes to greenish yellow and blue.[29,31,34] With a cathodic change the potential the color changes to violet and green.

3.3.6 Morphology of the Polymer film:

To investigate the microstructure and morphology of the poly(DCTD) film on ITO surfaces AFM analysis was performed. Polymers were made using the same method employed for other characterizations. The surface coverage of the ITO was 6.22 $x10^{-9}$mol/cm^2, which was measured by integrating the voltammetric peak. Figure 3.7 shows both phase and height images of the polymer film, where we found very small grain sizes indicating that the large continuous domain has not been grown the polymer bed. This might be due to the side chain at the 5 and 11 positions of the coronene core structure or because the film is too thin to be grown for the large domain. However, the grain growths were very uniform and smooth reflecting a self-organizing behavior that enabled better $\pi - \pi$ stacking formation.

0mV

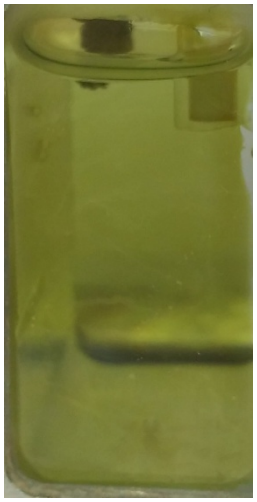

+900mV

+1200mV

-1100mV

-1300mV

Figure 3.6: Photograph of poly(DCTD) thin film on ITO surface in 0.1M BMIM TFSI solution of CH_2Cl_2 at different potentials.

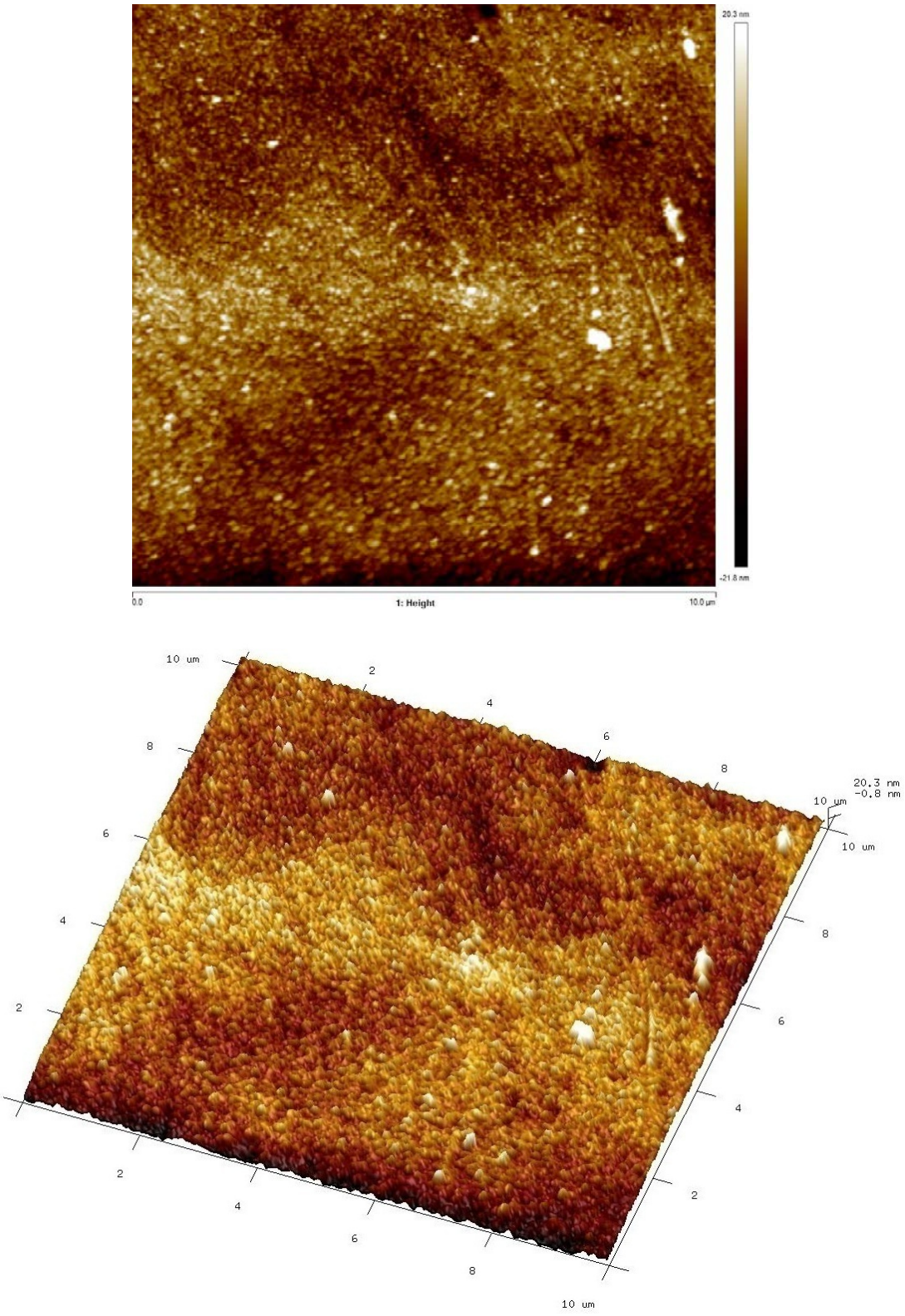

Figure 3.7: AFM images on poly(DCTD) on ITO electrode surface : Phase image (top) and height image (bottom).

3.4 Conclusions

A novel coronene containing diphenylamine end group monomer has been successfully synthesized and polymers have been made on different conductive surfaces via electropolymerization. The synthesized polymer is electroactive and in 0.1M BMIM TFSI solution of CH_2Cl_2, the film shows multi step reversible redox reactions in both anodic and cathodic directions. Solvents with high Lewis acidity show more feasible DPB oxidation. In contrast solvents with high Lewis basicity, imide reduction appeared at more positive potential values. The larger electrolyte cations, BMIM or TBA were more efficient for both oxidation and reduction of DPB and tetracarboxylic diimide group respectively. Spectroelectrochemistry experiments show a strong absorption at near IR region arises upon further oxidation after the first oxidation step of DPB due to π-stacking on the polymer film. Electrochromic behaviors have been observed in both positive and negative direction potential changes which in a rare in phenomenon organic polymers.

3.5 References

1. Rohr, U.; Kohl, C.; Mühllen, K.; van de Craats, A.; Warman, J. Liquid Crystalline Coronene Derivatives .*J. Mater. Chem.* **2001**, *11*, 1789-1799.

2. An, Z.; Yu, J.; Domercq, B.; Jones, S. C.; Barlow, S.; Kippelen, B.; Marder, S. R.; Room-Temperature Discotic Liquid-Crystalline Coronene Diimides Exhibiting high Charge-Carrier Mobility in Air. *J. Mater. Chem.* **2009**, *19*, 6688–6698.

3. Huang, C.; Barlow, S.; Marder, S. R.; Perylene-3,4,9,10-tetracarboxylic Acid Diimides: Synthesis, Physical Properties, and Use in Organic Electronics. *Org. Chem.* **2011**, *76*, 2386–2407.

4. Breeze, A. J.; Salomon, A.; Ginley, D. S.; Gregg, B. A.; Tillmann, H.; Ho¨rhold, H.-H. Polymer—Perylene Diimide Heterojunction Solar Cells. *Appl. Phys. Lett*. **2002**, *81*, 3085-3087.

5. Yakimov, A.; Forrest, S. R. High Photovoltage Multiple-Heterojunction Organic Solar Cells Incorporating Interfacial Metallic Nanoclusters. *Appl. Phys. Lett.* **2002**, *80*, 1667-1669.

6. Schmidt-Mende, L.; Fechtenkötter, A.; Müllen, K.; Moons, E.; Friend, R. H.; MacKenzie, J. D. Self-organized Discotic Liquid Crystals for High-Efficiency Organic Photovoltaics. *Science* **2001**, *293*, 1119- 1122.

7. Graser, F.; Hädike, E.; Kristallstruktur und Farbe bei Perylen-3,4:9,10-bis(dicarboximid)-Pigmenten. *Liebigs Ann. Chem.***1980**, 1994-2011

8. Nagao, Y.; Misono, T. Synthesis and Properties of *N*-alkyl-*N′*-aryl-3,4:9,10-Perylenebis(dicarboximide). *Dyes Pigm.* **1984**, *5*, 171-188.

9. Rademacher, A.; Märkle, S.; Langhals, H.; Lösliche Perylen-Fluoreszenzfarbstoffe mit hoher Photostabilität. *Eur. J. Inorg. Chem.***1982**, *115*, 2927-2934.

10. Chen, Z.; Zheng, Y.; Yan, H.; Facchetti, A. Naphthalene dicarboximide- vs Perylenedicarboximide-Based Copolymers. Synthesis and Semiconducting Properties in Bottom-Gate N-Channel Organic Transistors. *J. Am. Chem. Soc.* **2009**, *131*, 8-9.

11. Zhan, X.; Tan, Z. A.; Domercq, B.; An, Z.; Zhang, X.; Barlow, S.; Li, Y.; Zhu, D.; Kippelen, B.; Marder, S. R. A High-Mobility Electron-Transport Polymer with Broad Absorption and Its Use in Field-Effect Transistors and All-Polymer Solar Cells. *J. Am. Chem. Soc.* **2007**, *129*, 7246-7247.

12. Zhan, X. W.; Tan, Z. A.; Zhou, E. J.; Li, Y. F.; Misra, R.; Grant, A.; Domercq, B.; Zhang, X. H.; An, Z. S.; Zhang, X.; Barlow, S.; Kippelen, B.; Marder, S. R. Copolymers of Perylene Diimide with Dithienothiophene and Dithienopyrrole as Electron-Transport Materials for All-Polymer Solar Cells and Field-Effect Transistors. *J. Mater. Chem.* **2009**, *19*, 5794-5803.

13. Zhou, W. Y.; Wen, Y. G.; Ma, L. C.; Liu, Y. Q.; Zhan, X. W. Conjugated Polymers of Rylene Diimide and Phenothiazine for n-Channel Organic Field-Effect Transistors. *Macromolecules* **2012**, *45*, 4115-4121.

14. Yan, H.; Chen, Z.; Zheng, Y.; Newman, C.; Quinn, J. R.; Dotz, F.; Kastler, M.; Facchetti, A. A High-Mobility Electron-Transporting Polymer for Printed Transistors .*Nature* **2009**, *457*, 679-686.

15. Guo, X.; Watson, M. D. Conjugated Polymers from Naphthalene Bisimide. *Org. Lett.* **2008**, *10*, 5333-5336.

16. Durban, M. M.; Kazarinoff, P. D.; Luscombe, C. K. Synthesis and Characterization of Thiophene-Containing Naphthalene Diimide n-Type Copolymers for OFET Applications. *Macromolecules* **2010**, *43*, 6348-6352.

17. Huang, H.; Youn, J.; Ponce Ortiz, R.; Zheng, Y.; Facchetti, A.; Marks, T. Very Large Silacylic Substituent Effects on Response in Silole-Based Polymer Transistors *Chem. Mater.* **2011**, *23*, 2185-2200.

18. Durban, M. M.; Kazarinoff, P. D.; Segawa, Y.; Luscombe, C. K. Synthesis and Characterization of Solution-Processable Ladderized n-Type Naphthalene Bisimide Copolymers for OFET Applications. *Macromolecules* **2011**, *44*, 4721-4728.

19. Usta, H.; Newman, C.; Chen, Z.; Facchetti, A. Dithienocoronenediimide-Based Copolymers as Novel Ambipolar Semiconductors for Organic Thin-Film Transistors. *Advan. Mater.* **2012**, *24*, 3678–3684.

20. Sanyal, S. Manna, A. K.; Pati, S. K.; Effect of Imide Functionalization on the Electronic, Optical, and Charge Transport Properties of Coronene: A Theoretical Study *J. Phys. Chem. C* **2013**, *117*, 825–836

21. Wang, Z. Y.; Qi, Y.; Gao, J.P. Sacripante,G.G.; Sundararajan, P. R.; Duff. J. D. Synthesis, Characterization, and Xerographic Electrical Characteristics of Perylene-Containing Polyimides. *Macromolecules* **1998**, *31*, 2075–2079.

22. Zhou, M.; Heinze. J. Electropolymerization of Pyrrole and Electrochemical Study of Polypyrrole: 1. Evidence for Structural Diversity of Polypyrrole. *Electrochim Acta*. **1999**, *44*, 1733–1748.

23. Camalet, J.-L.; Lacroix , J.-C.; Nguyen, T.D.; Aeiyach, S.; Pham, M.C.; Petitjean, J.; Lacaze, P.-C. Aniline Electropolymerization on Platinum and Mild Steel from Neutral Aqueous Media. *J. Electroanal. Chem.* **2000**, *485*, 13–20.

24. Wei, Y.; Chan, C.C.; Tian, J.; Jang, G. W.; Hsueh. K.F. Electrochemical Polymerization of Thiophenes in the Presence of Bithiophene or Terthiophene: Kinetics and Mechanism of the Polymerization. *Chem. Mater.***1991**, *3*, 888–897.

25. Demirboğa, B.; Önal, A. M. Electrochemical Polymerization of Furan and 2-Methylfuran. *Synthetic Met*.**1999**, *99*, 237–242.

26. Saraji, M.; Bagheri, A. Electropolymerization of Indole and Study of Electrochemical Behavior of the Polymer in Aqueous Solutions. *Synthetic Met.* **1998**, *98*, 57–63.

27. Wang, F.; Shi, G.; Chen, F.; Xu, J.; Zhang, J. Electrochemical Polymerization of Thianaphthene. *J. Electroanal. Chem.* **2001**, *510*, 29–34.

28. Wei, Z.; Xu, J.; Nie, G.; Du, Y.; Pu, S. Low-potential electrochemical Polymerization of Carbazole and its Alkyl Derivatives. *J. Electroanal. Chem.* **2006**, *589*,112–119.

29. Wang, L.; Goodloe, W. G.; Stallman, B. J.; Cammarata, V. Synthesis, Electrooxidation, and Characterization of Bis(diphenylamine)naphthalene Diimide. *Chem Mate*r. **1996**, *8*, 1175-1181.

30. Wang, Q. Q. Copolymerization and Characterization of Novel Bis(Diphenylamine) Monomers. M S Thesis. Auburn University.**1999**.

31. Wang, L.; Wang, Q.Q.; Cammarata, V. Electro-oxidative Polymerization and Spectroscopic Characterization of Novel Amide Polymers Using Diphenylamine Coupling. *J. Electrochem. Soc.* **1998**, *145*, 2648-2654.

32. Wang, L.; Cammarata, V. Electropolymers based on diphenylamine II-Stacking in cationic Benzidine Units. *Thin Solid Films* **1996**, *284-285*, 297-300.

33. Cammarata, V.; Hao, N.; Metz, J.; Liang, J. Electrochemical Quartz Crystal Microbalance Studies of the Growth of Perylene-Containing Films. *ACS Symposium Series 832. Conducting Polymers and Polymer Electrolytes* **2009**, *5*, 59–74.

34. Wang, L. Synthesis, polymerization and Langmuir-Schaefer films of Novel Electroactive Compounds with Diphenylamine End Groups. PhD dissertation. Auburn University **1997**.

35. Liang, J. Preparation, Characterization and Applications of Electroactive Polymers in Electrochrmism and Sensors. PhD dissertation. Auburn University **2003**.

36. Hao, N. Electrochemistry and Electrochemical Quartz Crystal Microbalance (EQCM) Studied of Novel Conducting Polymers films. M.S. Thesis .Auburn University **2001.**

37. H. Sirringhaus, H.; Brown,P.J.; Friend, R. H.; Nielsen,M.M.; Bechgaard, K.; Langeveld-Voss, B. M. W.; Spiering, A. J. H.; Janssen, R. A. J.; Meijer, E. W.; Herwig, P.; de Leeuw, D. M. Two-Dimensional Charge Transport in Self-Organized, High-Mobility Conjugated Polymers. *Nature* **1999**, *401*, 685-688.

38. Patel, R. J.; Tighe, T. B.; Ivanov, I. N.; Hickner, M.A. Electro-optical Properties of Electropolymerized Poly(3-hexylthiophene)/Carbon Nanotube Composite Thin Films. *J. Polym. Sci. Pol. Phys.* **2011**, *49*, 1269–1275.

39. Rajasingh, P.; Cohen, R.; Shirman, E.; Shimon, L.J.W.; Rybtchinski, B. Selective Bromination of Perylene Diimides under Mild Conditions. *J. Org. Chem.* **2007**, *72*, 5973–5979.

40. Chen, Z. J.; Wang, L. M.; Zou, G.; Zhang, L.; Zhang, G. J.; Cai,X. F.; Teng, M. S. Colorimetric and Ratiometric Fluorescent Chemosensor for Fluoride ion Based on Perylene Diimide Derivatives. *Dyes and Pigm* **2012**, *94*, 410–415.

41. Würthner, F.; Stepanenko, V.; Chen, Z.; Saha-Möller, C. R.; Kocher, N.; Stalke, D. Preparation and Characterization of Regioisomerically Pure 1,7-Disubstituted Perylene Bisimide Dyes. *J. Org. Chem.* **2004**, *69,* 7933–7939.

42. Yang, H.; Bard, A. J. The application of Rapid Scan Cyclic Voltammetry and Digital Simulation to the Study of the Mechanism of Diphenylamine Oxidation, Radical Cation Dimerization, and Polymerization in Acetonitrile. *J. Electroanal. Chem.***1991**, 306, 87-109.

43. Pankratov, A. N.; Morozov, V. I.; Mushtakova, S. P.; II'yasov, A. V. Mechanism of Oxidation of Diphenylamine in an Acidic Medium. *Russ. Chem. Bull.* **1984**, 33, 1363-1367

44. Obaid, A.Y.; El-Mossalamy, S. A.;El-Hallag, I. S.; Hermas, A. A.; Al-Thabaiti, S. A.; A. M. Asiri, A. M. Electrodeposition and Characterization of Polyaniline on Stainless Steel Surface via Cyclic, Convolutive Voltammetry and SEM in Aqueous Acidic Solutions. *Int. J. Electrochem. Sci.* **2014**, 9, 1003-1015.

45. Zhou, M.; Heinze. J. Electropolymerization of Pyrrole and Electrochemical Study of Polypyrrole. 2. Influence of Acidity on the Formation of Polypyrrole and the Multipathaway Mechanism. *J. Phys. Chem. B* **1999**, 103, 8443-8450.

46. Lu, W.; Gao, J. P.;Wang, Z. Y.;Qi, Y.; Sacripante, G. G.; Duff, J. D.; Sundararajan, P. R. Electrochemical Characterization, Electrochroism, and Voltage-Dependent Fluorescence of Novel Perylene-Containing Polyimides. *Macromolecules* **1999**, *32,* 8880-8885.

Chapter Four

DIPHENYLAMINE END GROUP BILAYER POLYMER FILM: ELECTROCHEMICAL AND I-V CHARACTERIZATION

4.1 Introduction

Organic electronics have shown potential because of their low-cost, low temperature synthesis and fast manufacturability.[1-2] Organic heterojunctions including p-n junctions are the fundamental elements of organic electronic devices, organic photovoltaics (OPV) and Organic light emitting diodes (OLED).[1,3] So it is necessary to understand the electron transport behavior at the junction for better device fabrication. In the junction, net electron flow occures only in one direction, and is called rectification.

Despite much substantial progress in the area of inorganic p-n junctions, over the years scientists have been trying to build organic junctions. Use of conducting polymer in the device has a challenge because of their bipolar nature.[4-5] To overcome this problem, several doping methods are used such as chemical doping and mechanical press contracting,[6] photochemical doping,[7-8] ion implantation,[9-10] and internal ion compensation.[11-12]

There are two common types of rectifying devices based on organic molecules that have been developed. These are single molecule layer and bilayer devices. Organic diodes consisting of single molecule architecture were proposed by Aviram and Ratner in 1974.[1] Many more unimolecular rectifying devices have developed by other investigators since their revolutionary work.[14-15] The donor-acceptor groups in the molecule are typically bridged by a sigma bond. Molecules are attached on the metal surfaces for single layer diodes via self assembly[16-17]or Langmuir-Blodgett methods.[18-19]

Recently Luo and co-workers observed rectifying behavior in long donor–acceptor molecular wires.[20] The donor block was first synthesized from the Au surface via a stepwise

imine condensation reaction between 4,4′(5′)-diformyltetrathiafulvalene and 1,4-diaminobenzene linkers. Then the acceptor, N,N′-di(4-anilino)-1,2,4,5-benzenebis(dicarboximide) was attached to it through terephthaldehyde linkers.[20]

Besides the single molecule diodes, several Schottky diode junctions with conducting polymer films deposited on metal surfaces have been demonstrated.[21-24] Moreover, inorganic-organic hybrid diodes using a monolayer of ferrocene thiol molecules in contact with Ga_2O_3 have shown high rectification ratio (RR).[25-30]

Bilayer polymeric films from conducting and redox polymers also showed current rectification. Murray and others have reported thatcharge trapping occures on the polymer/polymer interface.[30-32] Sequentially deposited polymers containing Ru and Fe complexes: Pt/poly-$[Ru(4\text{-vinylpyridine})_3]^{3+}$/poly-$[Fe(\text{vinylpyridine})_3]^{2+}$ in solution showed electron transfer and charge trapping.[32] P-N junctions from common conducting polymers such as polyacetylene, polyaniline and polypyrrole have also been reported.[6,33-34] Polyacetylene doped with Na and AsF_5 have been made into a p-n junction diode.[6] Aizawa and Shirakawa have electropolymerized polypyrrole (n doped) and polythiophene (p doped) layers on a Pt electrode and measured rectification behavior.[33] Similar methods have been used by Torres and Fox to study bilayer rectification from three different polymers, poly(2,2-bithiophene), poly(Pyrrole), and poly(3-bromothiophene).[34]

Bilayer rectification has been characterized by both electrochemical and spectroscopic methods. Upon an applied voltage, rectification depends on the charge state of the material in the junction area of the diode. So the electrical properties and doping/undoping process play an important role in the diode performance. The electrochemical properties of conducting polymer can explore the charge trapping and blocking in the bilayer.[31,34,35]

In solid-state diode fabrication, the common anode materials are Au,[35] Ag[25-30] and ITO.[36] The conducting polymer layers are deposited on the surface of these materials. The top contact (cathode) construction in the bilayer diode is critical because top contact can control the performance of the device. There are three different techniques used over the years for top contact fabrication:[37] 1) electron beam or thermal evaporation of metals such as Al, Au, Ti etc.; 2) deposition of metal, chemically or electrochemically; and 3) drop deposition at room temperature of a liquid metal or alloy, such as Hg and GaIn. Electron beam or thermal evaporation methods create atomic level contact. However, for organic p-n junctions, a hot metal vapor destroys the deposited layer, so that defects on the deposited layer make connection between top and bottom contacts possible that shorts the junctions.[38] One study has shown that ~50-90% of devices generate short circuit situations when the top contact was made via metal evaporation.[39] Electrochemical and electroless deposition on the polymer surface using redox reactions to reduce the selected metal ions often involves pinholes on the polymer surfaces. Metal deposition into these pinholes also can short circuit on the device, consequently creating an imperfect rectification behavior of the organic polymer diodes.[35] Thick polymer films usually preventdevice damage but this decreases rectification efficiency by decreasing the rate of electron hopping between the redox layers of the polymers. Liquid metals, like Hg form good top contacts in the organic based diodes because they forms conformal contacts.[40-41] But Hg is not environmental friendly, so researchers avoid using Hg as an electrical contact. The other room temperature liquid metal is an alloy of Ga and In (75% Ga and 25% In by weight). Whitesides and his research group have extensively studied the GaIn liquid alloy as top contact in SAM based molecular diodes.[25-30] GaIn electrodes exhibit several advantages: 1) this material is conductive (resistivity ~29.4×10^{-6} Ω.□), so it is good for electrical contact; 2) The alloy is a

room temperature liquid (melting point =15.5^{o} C) and can form metastable and nonspherical structures; 3) it is a low viscosity fluid that is moldable and can be shaped like any free standing materials; 4) it is relatively non-toxic; and 5) the work function value (4.1-4.2 eV) is close to that of Hg (4.5 eV). In this chapter, we have used a GaIn eutectic for the fabrication of the top contact of the device.

Li has studied the electrochemical behavior of bilayers from different polymer films such as poly(DNTD), poly(DPTD), poly(Cl_4DPTD), and poly(FD).[35] These polymer films were grown on an Au surface via electropolymerization. All these polymer bilayer systems such as poly(DNTD)/poly(FD) ; poly(DPTD)/poly(FD), poly(Cl_4DPTD)/poly(FD) showed current rectification in solution containing a supporting electrolyte and also in the solid-state because poly(FD) is unipolar material. The highest rectification ratio (RR) was found to be 650.

In chapter Three, we have demonstrated the electropolymerization of a new monomer DCTD. The potential dependent UV-visible-NIR, electrochromism and morphology have also been discussed. Here we present a study on the bilayer, poly(DCTD)/poly(FD) electrochemistry and rectification in solution with supporting electrolyte and also the I-V characterization of solid-state bilayer diodes.

4.2 Experimental

4.2.1 Reagents and Materials:

FD was synthesized as previously reported.[42] Dichloromethane was freshly distilled from calcium hydride (Aldrich) before use. Tetrabutylammonium hexafluorophosphate, ($TBAPF_6$) was obtained from Aldrich and tetrabutylammonuim tetrafluoroborate ($TBABF_4$) was synthesized as described in the literature.[43] The ionic liquid,1-butyl-3-methylimidazolium bis(trifluoromethylsulfonyl)imide (BMIM TFSI) (Figure 4.1) was purchased from Ionic liquid

technologies, USA. Microscope gold slides (Deposition Research Laboratory Inc., MO, USA) were cut into ~10 X 25 mm. Ga and In samples to be used as a for top contact were also obtained from Aldrich.

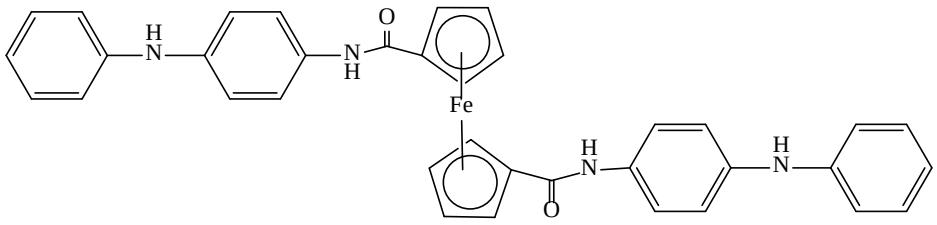

FD

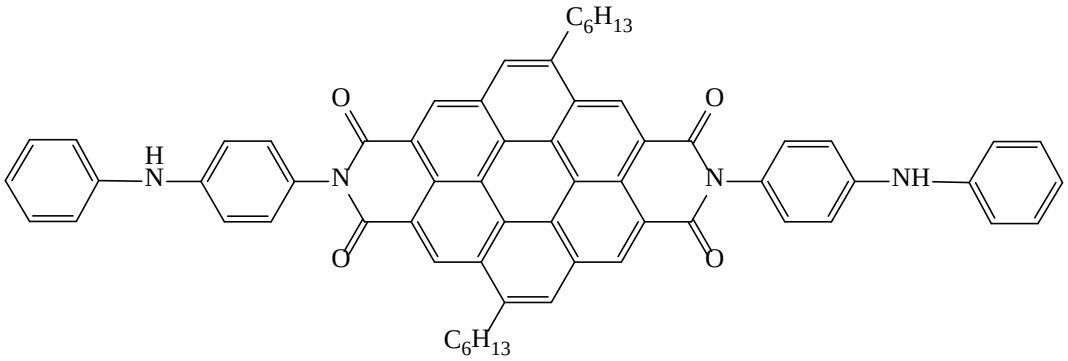

DCTD

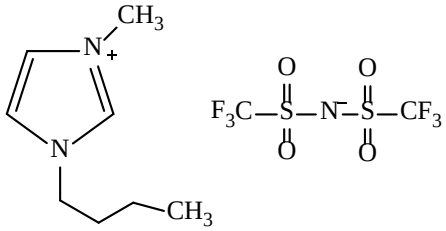

BMIM TFSI

Figure 4.1: Structure of the monomers with diphenylamine end group and supporting electrolyte.

4.2.2 Polymer bilayers and their electrochemical study:

Sequential layers of polymers were made by cyclic voltammetry was performed on a modified AFRDE4 Bi-Potentiostat (Pine Instrument Co.) electrochemistry workstation. The experiments were done using a three electrode electrochemical cell with a spiral Pt wire counter electrode and a Ag/AgCl saturated with KCl reference electrode. The working electrodes were Au disk (2mm diameter) and gold coated glass electrodes. Au disks were polished with alumina powder, sonicated for one minute in water, then cleaned with hydrogen peroxide and finally rinsed with CH_2Cl_2. Gold slides were cleaned in soap water (Alconox liquid) in an ultrasonic bath for 5min followed by 3min in DI water. They were then dipped into piranha solution (H_2SO_4: H_2O_2=3:1) *(Caution! Piranha reacts violently with organic compounds. Extreme care should be applied in handling the piranha solution.)* for 10min, rinsed with DI water and dried using N_2. Finally the slides were cleaned using aplasma (Harrick Plasma Cleaner-PDC-32G) created from air for 5 minutes and rinsed with CH_2Cl_2 before use. The electropolymerization of FD was done in 0.3 mM FD solution of CH_2Cl_2 containing 0.1M $TBAPF_6$ and the polymerization of DCTD was performed as described in Chapter Three.

4.2.3 Fabrication of top contact:

To perform characterizations of the solid state diodes, the top electrical contact employed was GaIn as described in the Introduction. A droplet of GaIn eutectic with an approximate diameter of 1.0 mm was applied to the surface of the top polymer layers. Non-conducting Epoxy glue (Bob Smith Industries Inc.) was used to circle the eutectic to fix it in the desired position. The diode arrangement is shown on the Figure 4.2.

4.2.4 I-V measurements:

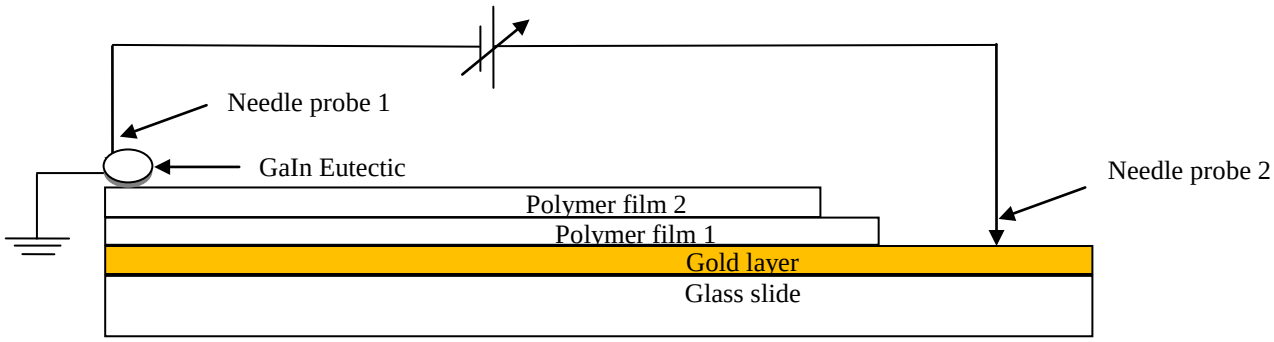

Figure 4.2: Schematic diagram of bilayer diode for I-V measurements.

I-V characterization was performed in a two point probe system connected to either a Keithley 2400 source meter or a Keithley 7002 switch system. The potential was stepped in either 0.05 or 0.1 V for all measurements. I-V data was recorded by the computer equipped with Labview program.

4.3 Results and Discussion

4.3.1 Single layer polymer modified electrode:

Single layers of poly(FD) and poly(DCTD) were made on an Au electrode (area=0.0314 cm^2) via electropolymerization. The detail of the electropolymerization of FD monomer was described by Wang, L.[42] Poly(FD) was grown from the 0.3 mM FD solution in CH_2Cl_2 containing 0.1M $TBAPF_6$. However, the DCTD monomer is not very soluble in CH_2Cl_2, so ~0.8% v/v TFA was added to increase the solubility, and then the electropolymerization was performed in the 0.1 mM DCTD solution in CH_2Cl_2 containing 0.1 M BMIM TFSI ionic liquid. The cyclic voltammograms of FD and DCTD show a reversible electrooxidation of the diphenylamine end group of the monomers (Figure 4.3 and 4.4). The electroactive diphenylbenzidine (DBP) formed by the inter ring carbon-carbon coupling of diphenylamine radicals from two monomers.[42] The cathodic and anodic charge was estimated by integrating the respective regions of the voltammograms. For both polymers, the charging rates of oxidation are slightly higher than the corresponding reductions. Faster rates of charging via oxidation have also been observed in common conducting polymers, polypyrrole and polythiophene.[33,44] For monomers, five cyclic voltammetry experiments were performed and the average of the integrated anodic and cathodic peaks was plotted against the number of voltammetric cycles (Figure 4.3 and 4.4). From the plots, a linear relationship of the film growth with voltammetric cycle was determined. The plot shows that the average 3.4 μC charge passed during each cycles

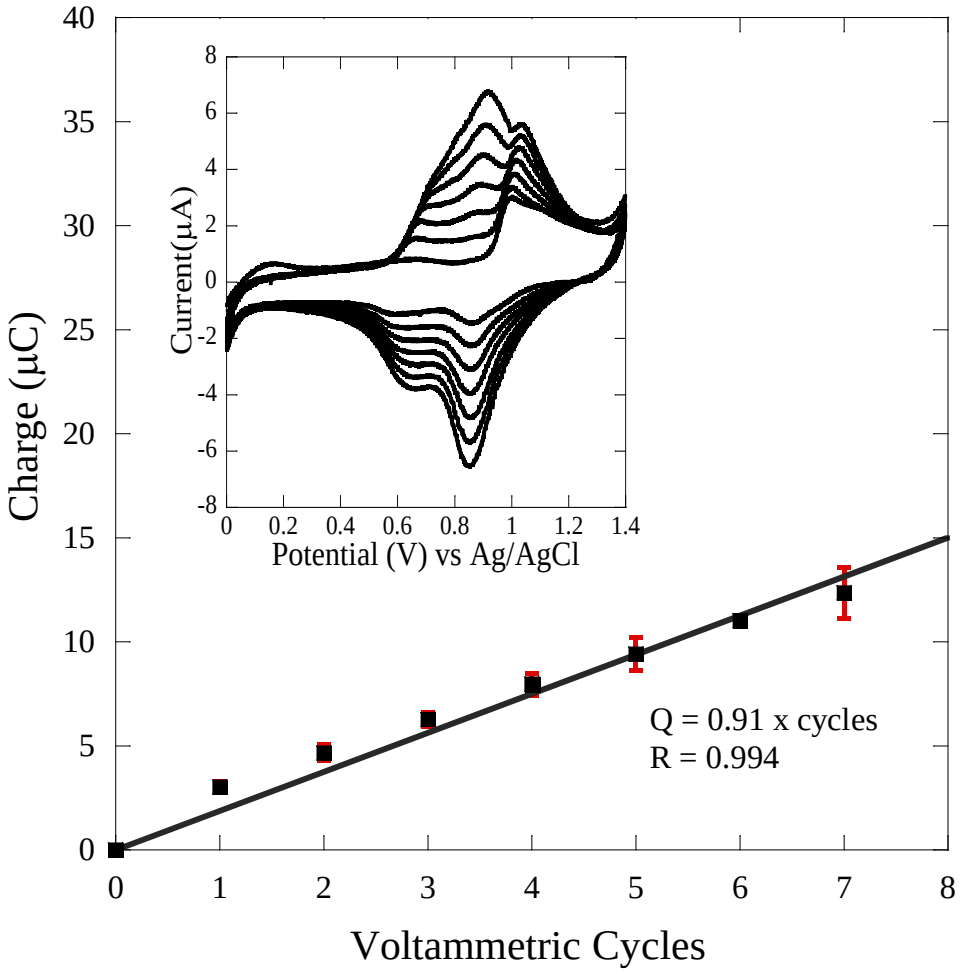

Figure 4.3: Charge vs voltammetric cycles for the electropolymerization of 0.1 mM DCTD in a CH_2Cl_2 solution containing 0.1 M BMIM TFSI ionic liquid on Au electrode (area = 0.0314 cm^2)(scan rate 200 mV/s, charge was integrated from 0.5 to 1.2 V (± 0.05V).

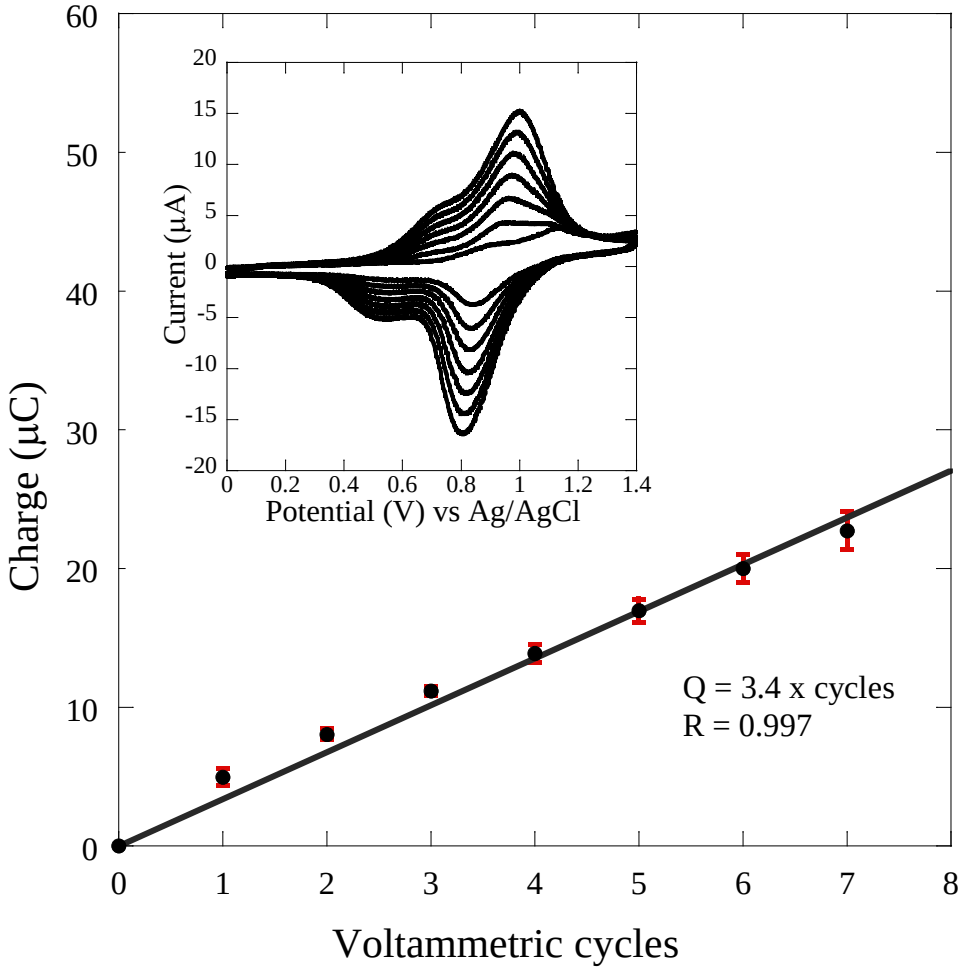

Figure 4.4: Charge vs voltammetric cycles for the electropolymerization of 0.3 mM FD in a CH_2Cl_2 solution containing 0.1 M $TBAPF_6$ on Au electrode (area = 0.0314 cm^2) (scan rate 200 mV/s, charge was integrated from 0.5 V to 1.2 V (± 0.05V).

for 0.3 mM FD. So, $5.6x10^{-10}$ mol/cm^2 FD was grown on the Au surface for each voltammetric cycle. For 0.1 mM DCTD the charge and corresponding surface coverage during each cycle were 0.91 μC and $1.5x10^{-10}$ mol/cm^2 respectively.

4.3.2 Bilayer polymer modified electrode:

Two bilayers were made for the current rectification study. The poly(DCTD) film was grown on a poly(FD) modified Au electrode, defined as Au|poly(FD)|poly(DCTD). The other film consisted of an inverted arrangement of the bilayer, Au|poly(FD)|poly(DCTD), defined as Au|poly(DCTD) |poly(FD). Data on the bilayer formation via electropolymerization are shown in the Figure 4.5 and 4.6. For the Au|poly(FD)|poly(DCTD) bilayer film, two redox peaks of diphenylbenzidine (DPB) were detected in the first scan. The current increases upon the number of scans, indicating that poly(DCTD) was grown on the poly(FD) modified electrode. Similar voltammetric features were observed during the bilayer, Au|poly(DCTD) |poly(FD) formation (Figure 4.5). Also the average charge calculated from the voltammetric response varieslinear with the number of voltammetric cycles (Figure 4.5 and 4.6). On average $1.3x10^{-10}$ mol/cm^2 poly(DCTD) was grown on the Au|poly(FD) electrode during each scan of cyclic voltammetry in 0.1 mM DCTD solution. However, $1.5x10^{-9}$ mol/cm^2 poly(FD) was grown on the Au|poly(DCTD) electrode on each voltammetric cycle in 0.3 mM FD solution.

4.3.3 Electrochemistry of the bilayer polymers:

After electrodeposition of a single layer and also of a second layer on the top of the first polymer layer , the cyclic voltammetry of the films in CH_2Cl_2 containing 0.1 M $TBAPF_6$ was performed to investigate the rectification behavior of the junction built in between the polymeric layers. Figure 4.7 shows the voltammograms of the the single layer, Au|poly(DCTD) and the bilayer , Au|poly(DCTD)|poly(FD) in CH_2Cl_2 containing 0.1M $TBAPF_6$. Both the single and

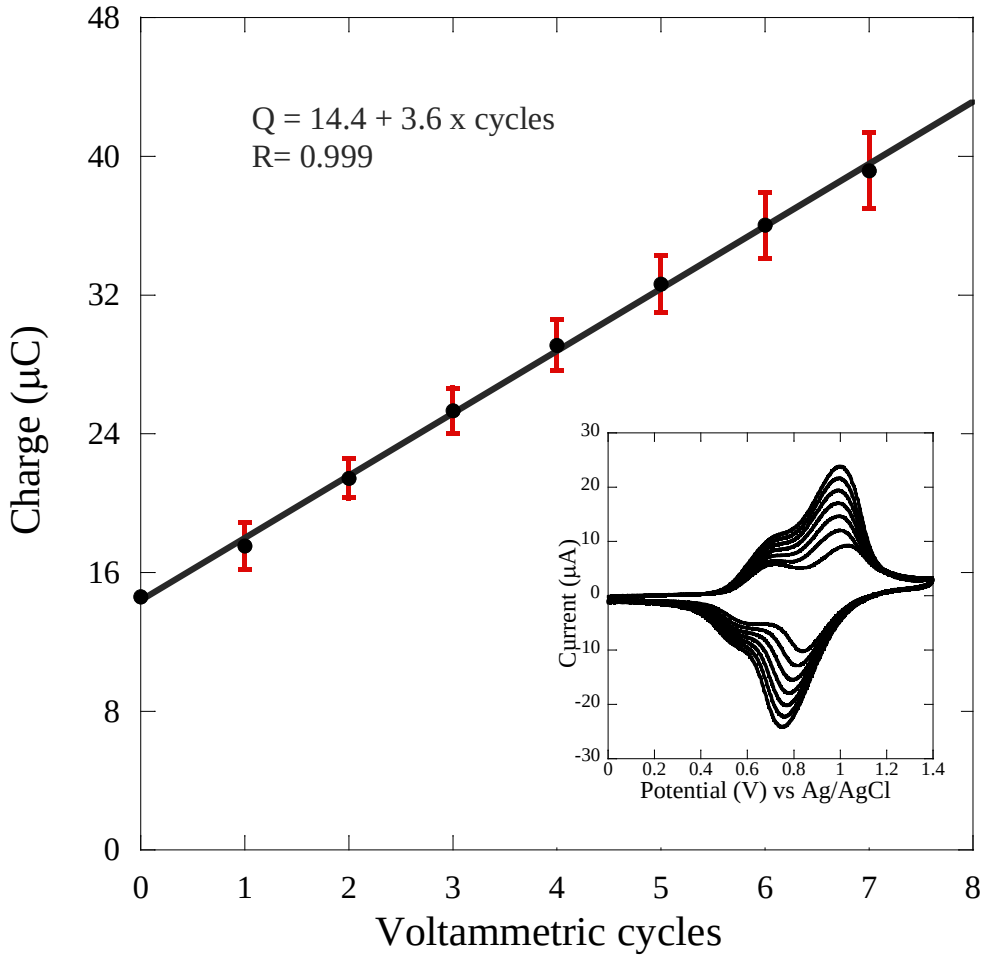

Figure 4.5: Charge vs. voltammetric cycles for the electropolymerization of 0.3 mM FD in a CH_2Cl_2 solution containing 0.1 M $TBAPF_6$ on poly(DCTD) modified Au electrode (area = 0.0314 cm^2) (scan rate 200 mV/s, charge was integrates from 0.5 to 1.2 V(± 0.05 V).

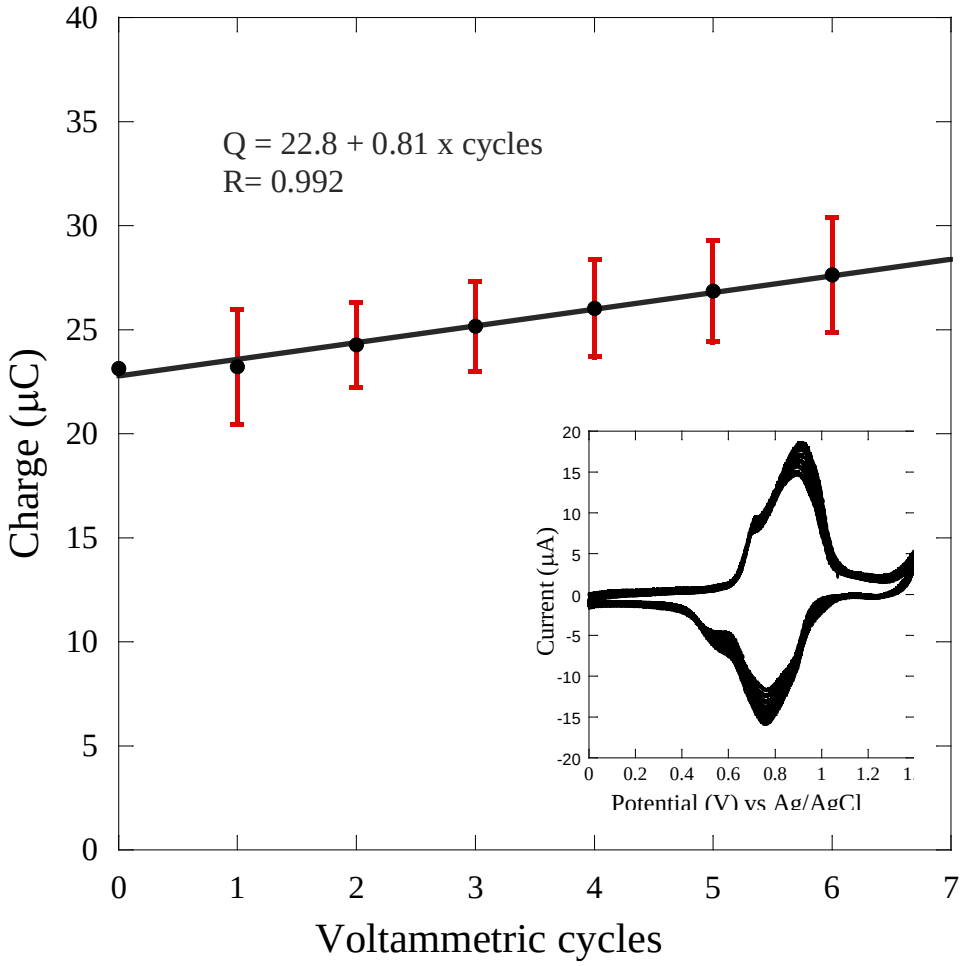

Figure 4.6: Charge vs. voltammetric cycles for the electropolymerization of 0.1 mM DCTD in a CH_2Cl_2 solution containing 0.1 M BMIM TFSI ionic liquid on poly(FD) modified Au electrode (scan rate 200 mV/s, charge was integrates from 0.5 to 1.2 V (± 0.05 V).

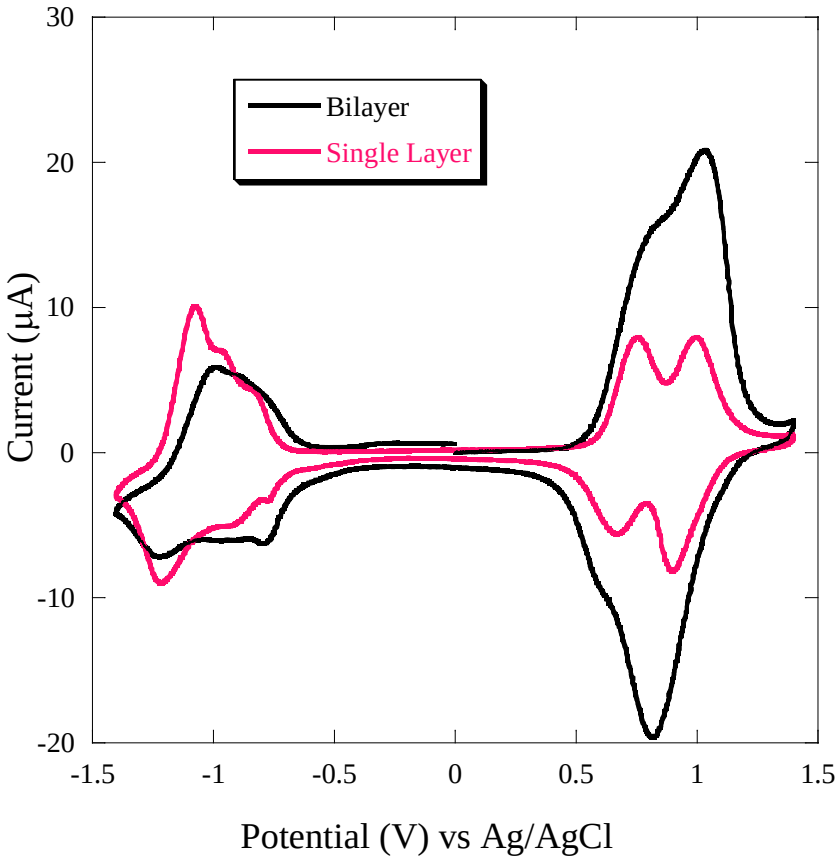

Figure 4.7: Electrochemistry of bilayer, Au|poly(DCTD)|poly(FD)(black) and single layer, Au|poly(DCTD) (red) scanned in a 0.1 M $TBABF_6$ solution at scan rate 200 mV/s.

bilayer exhibit two redox peaks at positive and negative potentials respectively. In the positive direction, there is a substantial increase of the DPB oxidation and reduction signals indicating the poly(FD) layer is located on the top of the poly(DCTD) layer. The linear dependence peak current vs scan rate indicates that the bilayers are surface immobilized.(Figure 4.8).The estimated film thickness in these layers is about 2.8 $x10^{-9}$ mol/cm^2 for poly(DCTD) and 4.4 $x10^{-9}$ mol/cm^2 for poly(FD). In the negative potential range, the diimide reduction current is almost equal in both single and bilayer. The average charge of cathodic and anodic peaks of the diimide is ~16 μC, although the peak potentials are a little different for single and bilayer films. This might be due to the change of conductivity of the polymer films. However, we can conclude that that there is no significant disturbance of the inner layer redox behavior induced by the outer layer. Electrochemistry of the inverted bilayer was also studied. Figure 4.9 shows the cyclic voltammogram of the single layer, Au|poly(FD) and bilayer Au|poly(FD)|poly(DCTD). The electrochemical response in the positive direction of the Au|poly(FD)|poly(DCTD) was similar to that of the bilayer Au|poly(DCTD)|poly(FD). In the positive potential region, the anodic and cathodic current of bilayer polymer is higher than the single layer polymer, implying that poly(DCTD) is electrodeposited on the top of the single layer, Au|poly(FD). Figure 4.10 describes the linear relationship of peak current and scan rate indicating that the bilayer was surface-confined. The reversible two waves for bilayer films are similar to the two waves of the single layer film, although the single layer Au|Poly(FD) exhibits three redox species: DPB^0/DPB^+, DPB^+/DPB^{2+}, Fc^0/Fc^+. The ferrocene oxidation and reduction peaks overlap with the peak for the redox couple DPB^+/DPB^{2+}. However, in the negative scan direction, the voltammetric feature is ill-defined as the FD is not electroactive in the negative direction for single layer films. Moreover, no diimide redox peak was observed when the bilayer modified

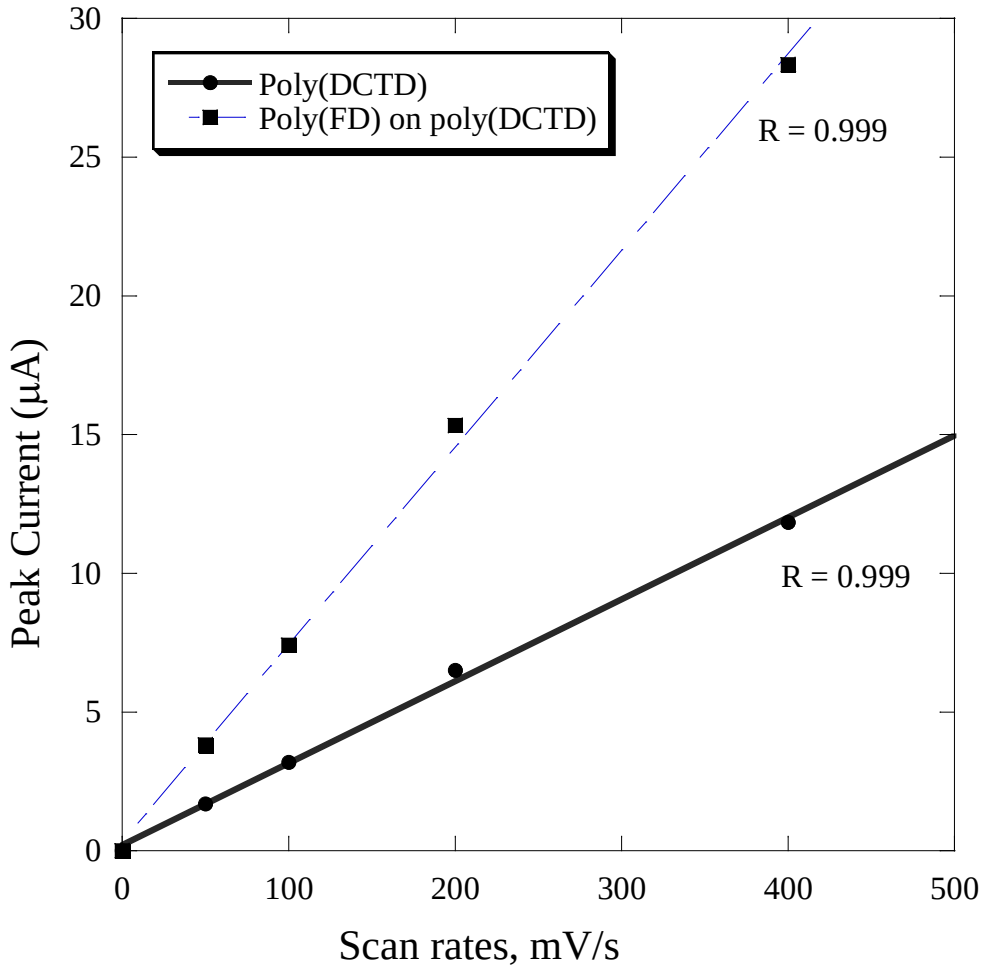

Figure 4.8 : Linear relationship between peak current vs scan rates for Au|poly(DCTD) and Au|poly(DCTD)|poly(FD) in CH_2Cl_2 containing 0.1 M $TBAPF_6$. Peak current evaluated based on first oxidation of DBP.

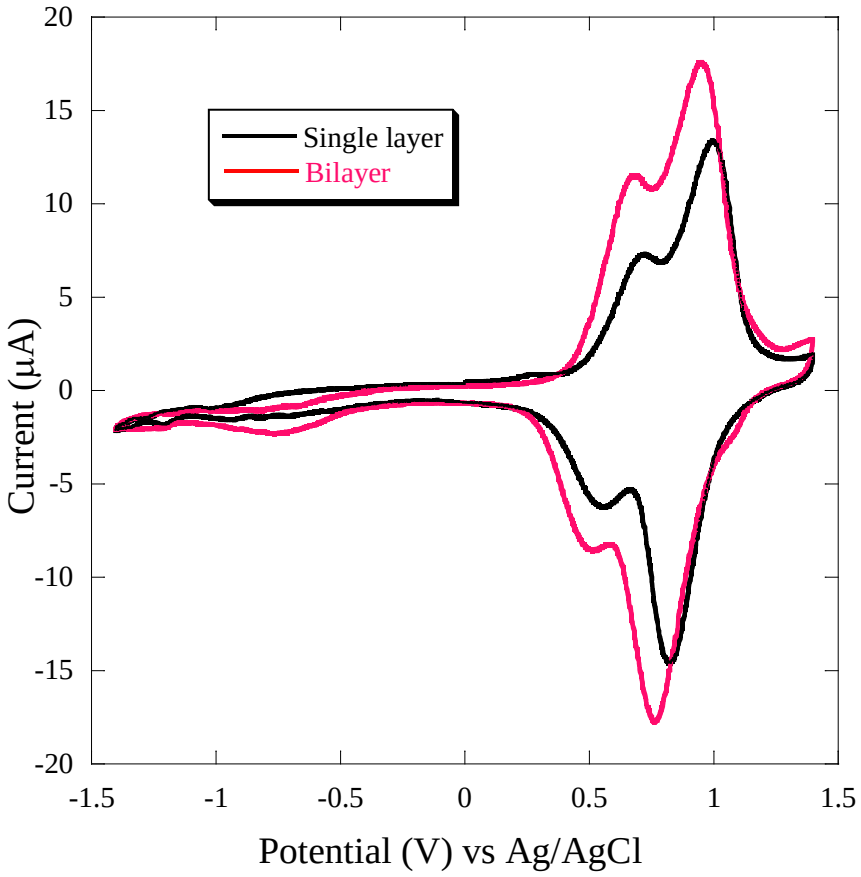

Figure 4.9: Electrochemistry of bilayer, Au|poly(FD)|poly(DCTD)(red) and single layer, Au|poly(FD) (black) scanned in a 0.1 M $TBABF_6$ solution at scan rate 200 mV/s.

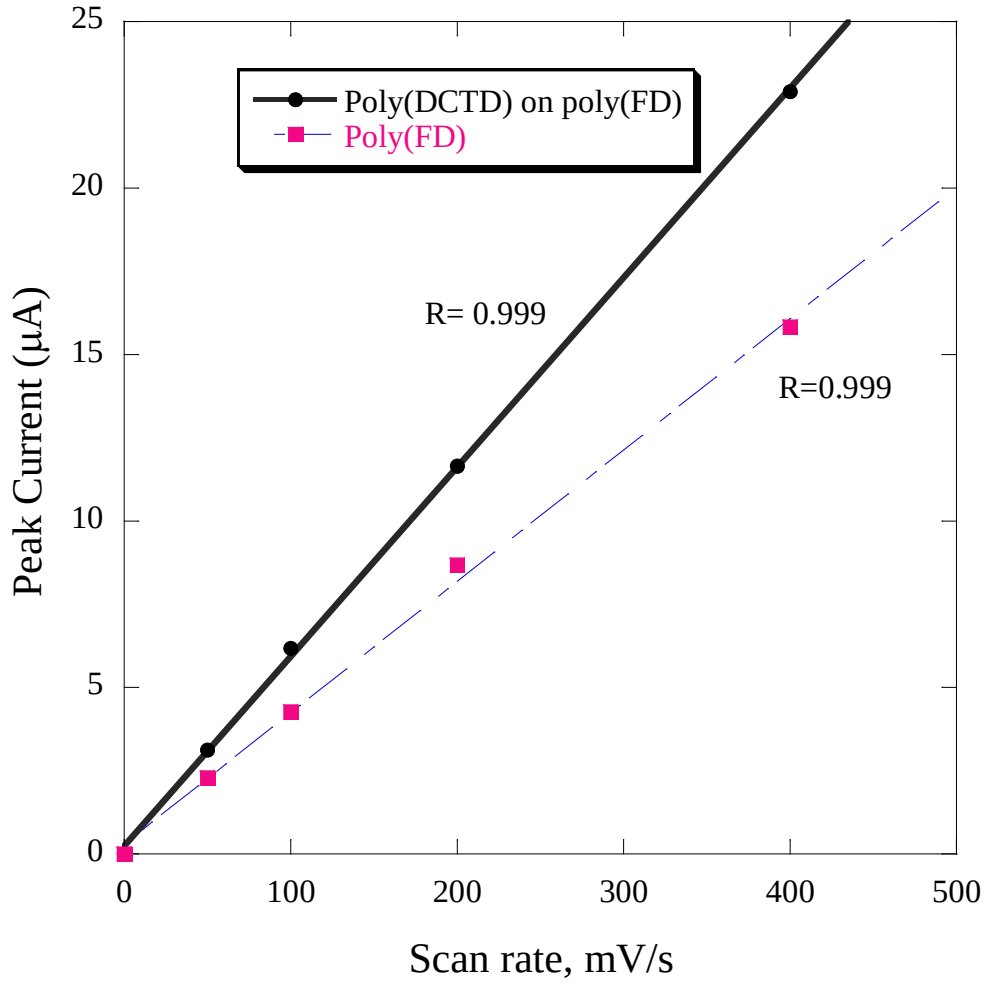

Figure 4.10: Linear relationship between peak current vs scan rates for Au|poly(FD) and Au|poly(FD)|poly(DCTD) in CH_2Cl_2 containing 0.1 M $TBAPF_6$. Peak current evaluated based on first oxidation of DBP.

electrode was scanned in the potential range of potential 0 to -1.4V vs Ag/AgCl. This indicates that the electron transport was blocked by the inner layer, poly(FD) film.

From the above electrochemical study, it was observed that unidirectional electron transportoccured at in the interface of the bilayer polymer films. This observation can be explained using the following schematic diagrams (Scheme 4.1 and 4.2). Scheme 4.1 depicts the charge transfer behavior of the bilayer Au|poly(DCTD)|poly(FD). When a positive potential is applied, both layers are oxidized as both polymer chains contain DPB units. When the potential is close to that of the DPB oxidation, The DPB donates an electron to the Au electrode, but this is then reduced by the the poly(FD) layer. So the flow of electrochemical charge through the bilayer is the combined total of both layers. However, when a potential is applied negative of 0.0 V vs Ag/AgCl, the diimide of the inner layer was reduced to its anion (DCTD $+e^- \longrightarrow$ $DCTD^-$). As there was no easily reducible moiety in the poly(FD) film, no electron was transferred to the outer layer, so the charge transferred in the negative direction is confined to the inner layer. Scheme 4.2 displays the electron transfer behavior of the bilayer, Au|poly(FD)|poly(DCTD). Upon application of an anodic potential, the electron transfer from both layers is similar to the bilayer Au|poly(DCTD)|poly(FD). So, in the positive potential direction transfer of the charge is independent of the sequence of the polymer layer. However, when the bilayer was scanned in the negative direction there was no electron transfer between these two interfaces, electrode/inner layer and inner layer/outer layer. The inner layer, poly(FD) was not reduced at -1.4V because it has no reducible unit and also the diimide unit of the outer layer is not reduced as the inner layer hindered the electron transfer from the electrode.

4.3.4 Diode characterization:

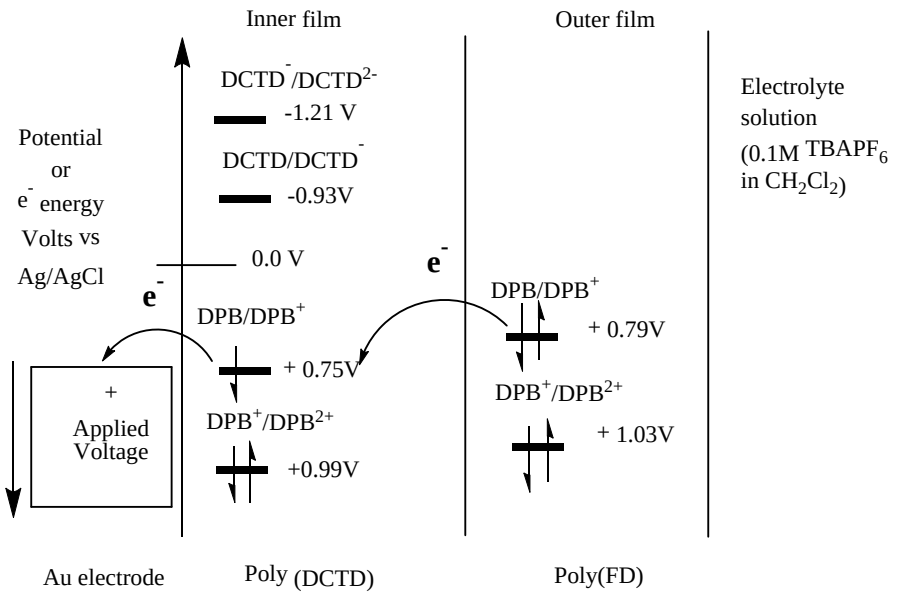

A: Positive potential Applied

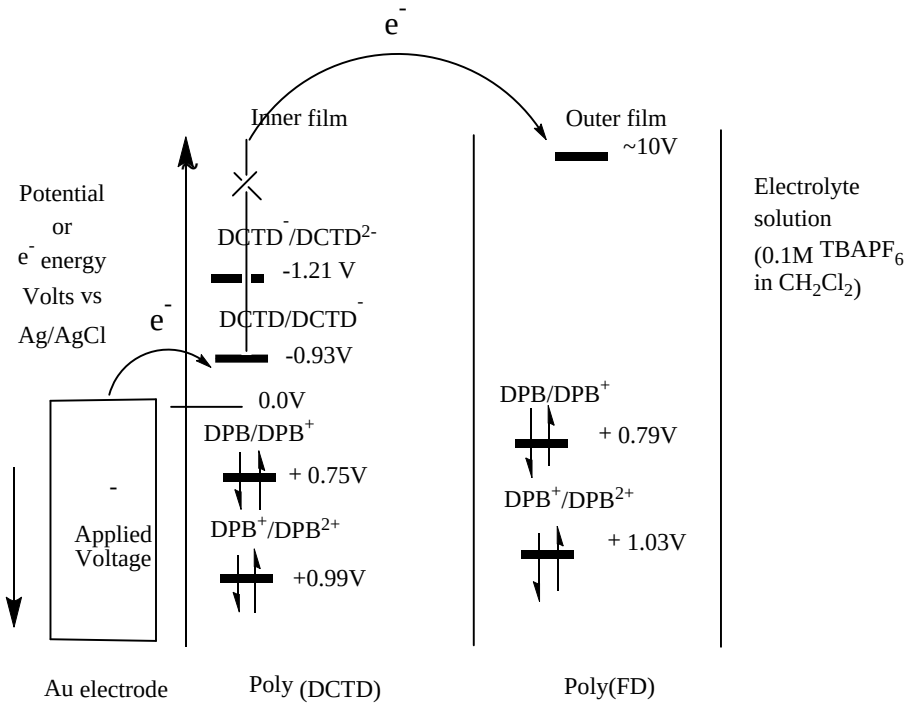

B: Negative potential Applied

Scheme 4.1: Electron transfer in bilayer, Au|poly(DCTD)|poly(FD) in 0.1 M $TBAPF_6$.

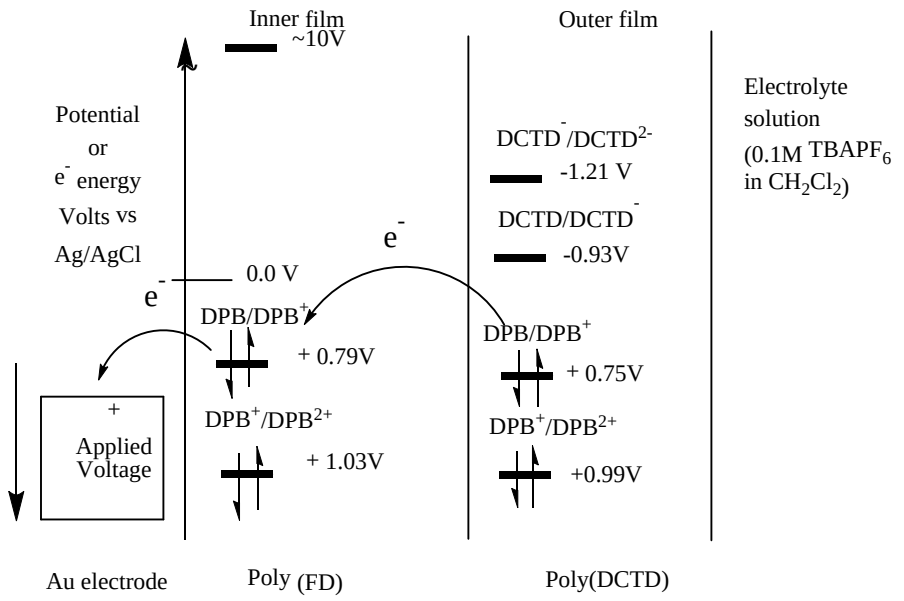

A: Positive Potential Applied

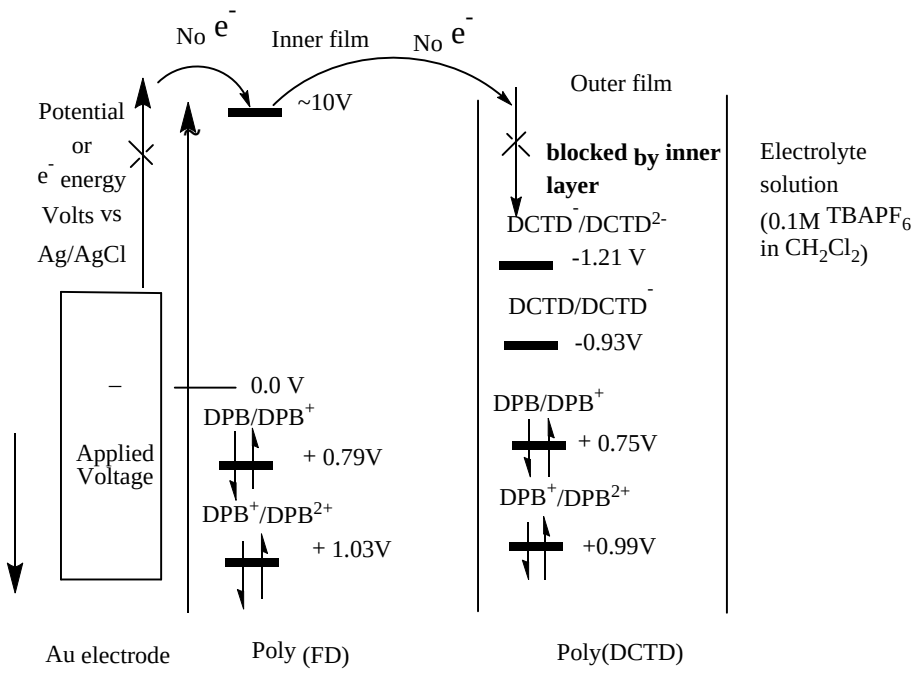

B: Negative Potential Applied

Scheme 4.2: Electron transfer and blocking in bilayer, Aupoly|(FD)|poly(DCTD) in a 0.1 M $TBAPF_6$.

To investigate the rectification behavior of the bilayers in solid state, a bilayer diode was fabricated with a droplet of GaIn eutectic. The current -voltage characterization was carried out by connecting an Au electrode on the positive probe and GaIn on the negative probe. The current -voltage curve of the bilayers Au|poly(FD)|poly(DCTD)|GaIn and Au| poly(DCTD)| poly(FD)|GaIn are shown in Figure 4.11 and 4.12 respectively. For the bilayer, Au|poly(FD)|poly(DCTD)|GaIn, a positive turn on voltage and a reversed bias break down appeared at ~ +1.9 and -9.6 V respectively. It has been reported that poly(FD) is a p-type material.[35] As the positive voltage applied to p-type material, the diode is considered as in the forward bias condition. The knee voltage of the forward bias is ~ +1.2 V. When the applied voltage passed the knee voltage of +1.2 V, it crosses the potential barrier of the diode and then current starts to flow. The bilayer diode, Au|poly(DCTD)| poly(FD)|GaIn was connected in reversed bias condition where a positive voltage was applied to the n-type material, poly(DCTD). In this arrangement of the diode, a negative turn on voltage was observed at -7.0V. The rectification ratio ($RR=I_{forward}/I_{reverse}$) for both devices was plotted against applied voltage (Figure 4.13). The highest rectification ratios of the device, Au|poly(FD)|poly(DCTD)|GaIn is 98 at ± 4.5 V. The rectification ratio of p-n junction ranges from 80 to 600.[35] However, the RR value of the bilayer device with poly(DNTD) and poly(DPTD) studied in our group is much higher than the device with DCTD.[35] Also here we have evaluated the ideality factor (n) and saturation current (I_s) shown in Table 4.1 according to the Shockley diode equation:[45]

$$I = I_s \left[exp\left(\frac{qV}{nkT}\right) - 1 \right] \qquad (4.1)$$

Here Is, the saturation current, is the current flowing in reverse bias, V, is the applied voltage (positive value of V, forward voltage), q is the electric charge, n is the ideality factor and kT is the thermal energy, k is the Boltzmann constant and T is the temperature. By plotting ln I vs V,

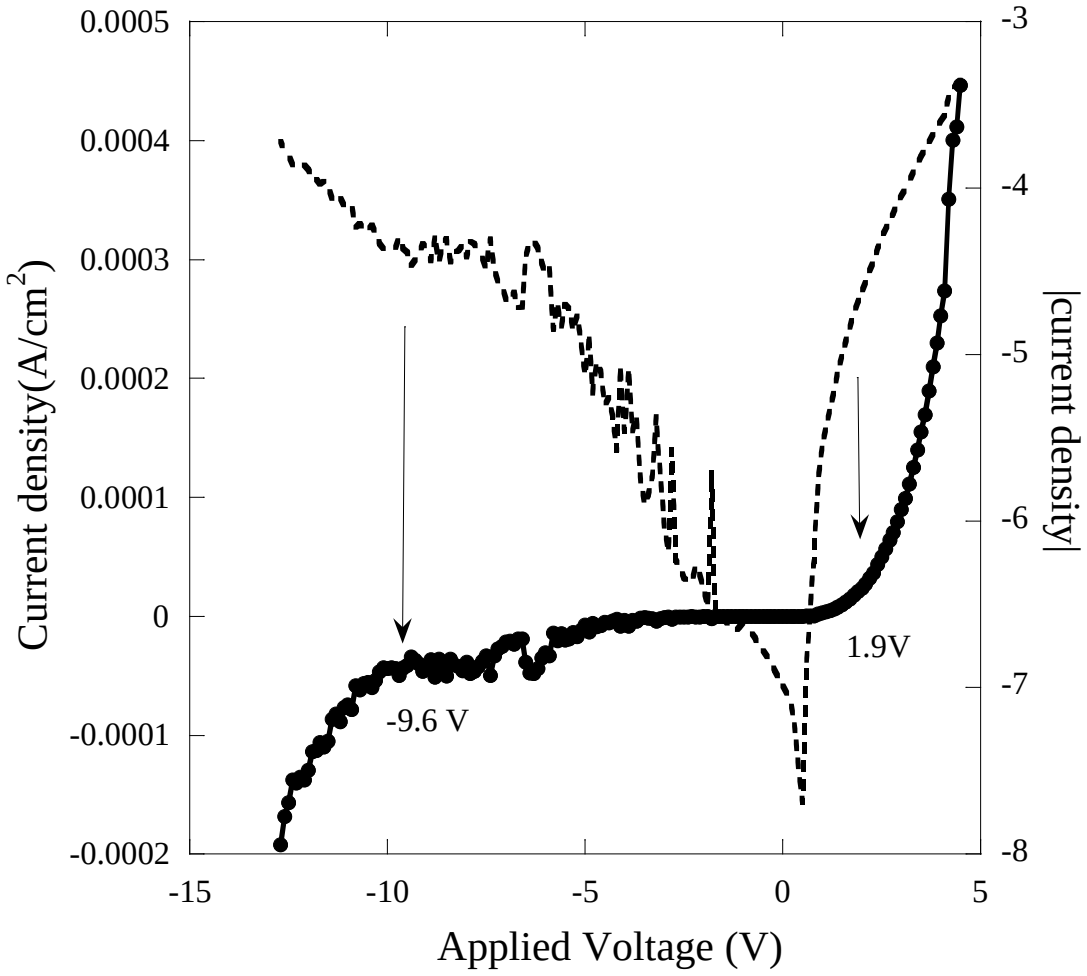

Figure 4.11: I-V characteristics of a an Au|poly(FD)|poly(DCTD)|GaIn with $\Gamma_{poly(FD)}$=5.6x10^{-9} mol/cm^2 and $\Gamma_{poly(DCTD)}$ = 5.1x10^{-9} mol/cm^2.

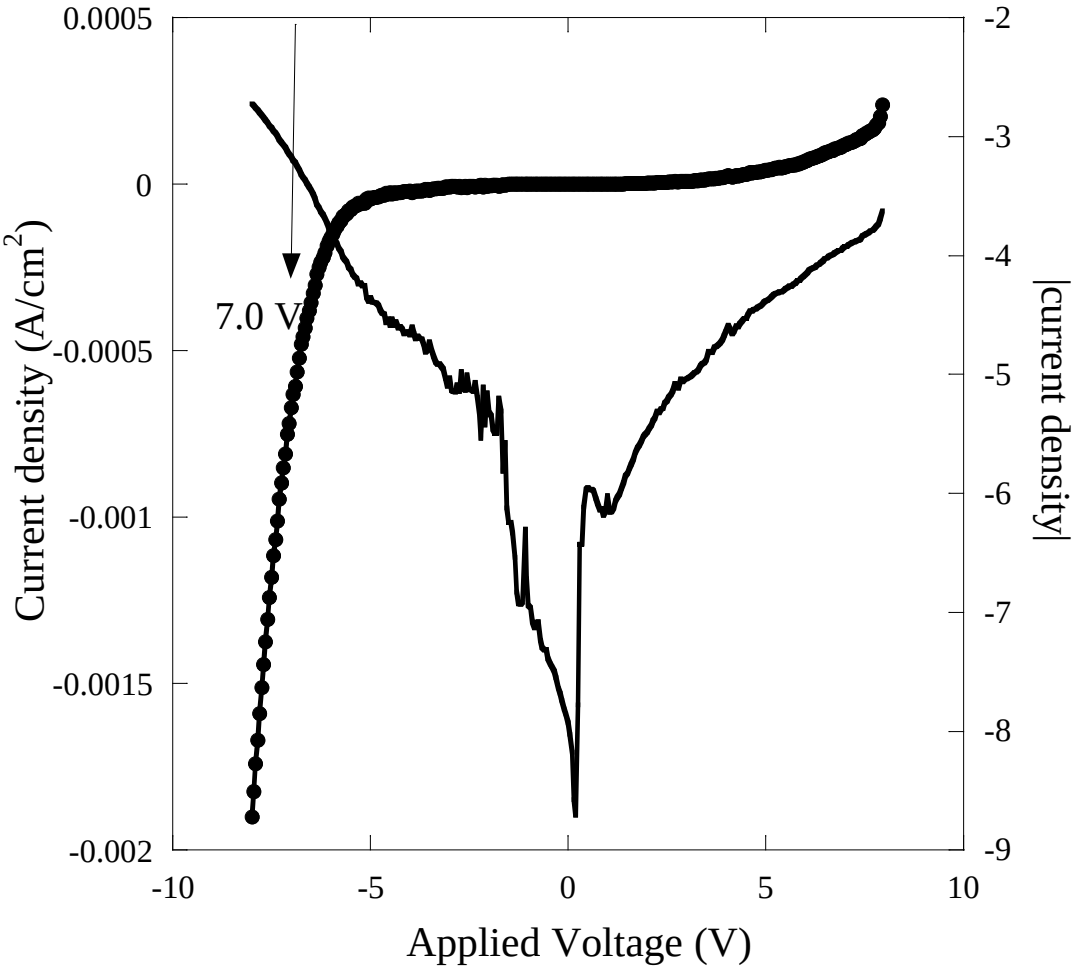

Figure 4.12: I-V characteristics of a an Au|poly(DCTD)|poly(FD)|GaIn with $\Gamma_{poly(DCTD)}$= 4.9x 10^{-9}mol/cm^2 and $\Gamma_{poly(FD)}$= 5.0 x10^{-9} mol/cm^2.

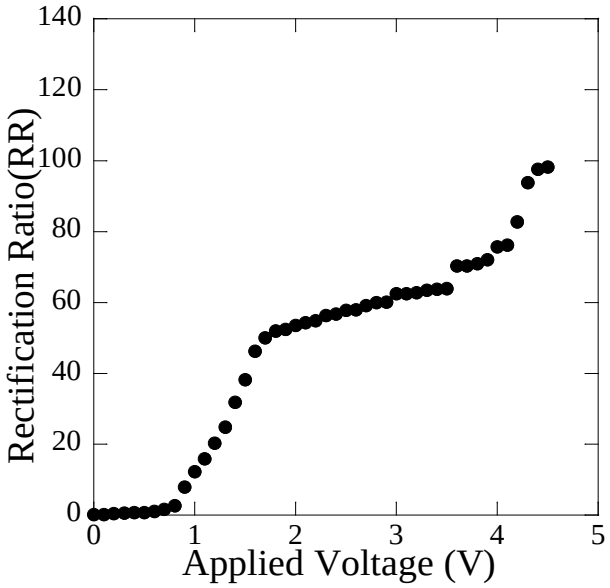

A: Au|poly(FD)|poly(DCTD)|GaIn

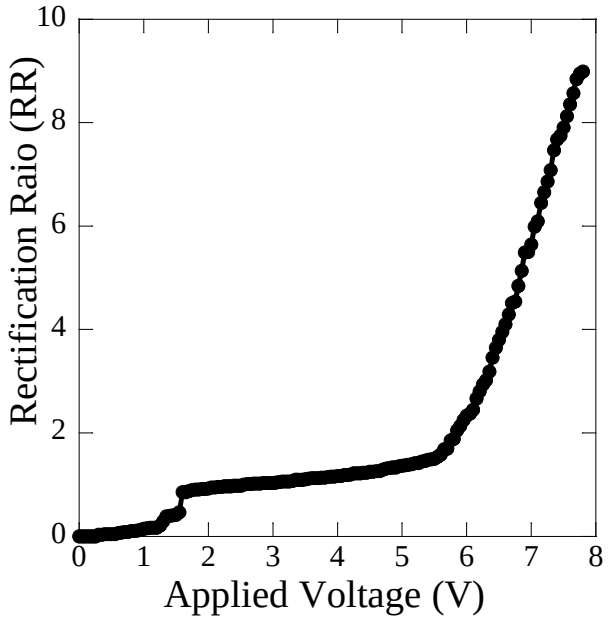

B: Au|poly(DCTD)|poly(FD)|GaIn

Figure 4.13: Rectification ratios at different applied voltages.

n and I_s can be calculated from the slope and intercept, where n is equal to $\frac{kT}{q}\frac{\partial lnI}{\partial V}$ for *qV>> nkT* and lnI_s is the intercept. The ideality factor of the devices is much higher than that of the inorganic silicon based diode(*n* = 1-2) [45] as well as other doped organic p-n junction diodes.[36] This ideality factor for the forward bias diode is close to the previously studied diode from DNTD and DPTD with FD (n = 10-16). Also the saturation current of the devices is much larger

Table 4.1: Characteristic parameters for the bilayer diodes

Device	$\Gamma_{n\text{-type}}$ mol/cm^2	$\Gamma_{p\text{-type}}$ mol/cm^2	Ideality factor(*n*)	Saturation Current (A/cm^2)	Rectification Ratio(RR)
Au|(FD)|(DCTD|GaIn	5.1x10^{-9}	5.6x10^{-9}	16.7	2.7x10^{-7}	98
Au|(DCTD|(FD)|GaIn	4.9x10^{-9}	5.0x10^{-9}	30.7	6.8x10^{-8}	9

than that of doped p-n junction diodes.[36]

4. 4 Conclusions

A polymer bilayer was electrodeposited on the metal electrode surface sequentially. From the electrochemical study, it was observed that a unidirectional charge transport occurred between the polymer layers. Also in the solid state diode, we have demonstrated that a current rectification behavior take place with these bilayers. However, the characteristic parameters of diode junction are not comparable with the other organic p-n junctions. These deviations from other organic diode might be either due to material performance or improper device fabrication method. Here we used bipolar DCTD as n-type material. This might result in a large forward bias due to the high resistivity of the material. Also during the polymer fabrication, some pin holes may exist in the film which induces electrical shunt that prevents reverse current

saturation. Moreover, it has been reported that when a GaIn eutectic comes contact with air, a thin layer of gallium oxide (Ga_2O_3) in generated.[37] Ga_2O_3 is a n-type semiconductor material that can produce a Schottky junction via interaction with the outer layer of the polymer, causing improper ohmic contact resulting in poor device performance.

4. 5 References

1. Matyba, P.; Maturova, K.; Kemerink, M.; Robinson, N. D.; Edman, L. The Dynamic Organic p–n Junction. *Nat. Mat.* **2009**, *8*, 672 – 676.

2. Dhara, B. M.; Kinib, G. S.; Xiab, G.; Junga, B. J.; Markovicb, N.; Katz, H. E. Field-Effect-Tuned Lateral Organic Diodes. *Proceedings of the National Academy of Sciences* **2010**, *107*, 3972-3976.

3. Tang, C. W. 2-Layer Organic Photovoltaic Cell. *Appl. Phys. Lett.* **1986**, *48*, 183–185.

4. Reynolds, J.; Skoheim, T. A. Handbook of Conducting Polymers, 2 Vol. Set; 3rd ed.; CRC Press, **2007**.

5. Kudo, T.; Kimura, M.; Hanabusa, K.; Shirai, H. Fabrication of p–n Junction Diodes from Phthalocyanine and Electropolymerized Perylene Derivatives. *J. Porphyrins Phthalocyanines* **1998**, *2*, 231-235.

6.Chiang, C. K.; Gau, S. C.; Fincher, C. R., Jr.; Park, Y. W.; MacDiarmid, A. G.; Heeger, A. Polyacetylene, $(CH)_x$: n-type and p-type Doping and Compensation. *J. Appl. Phys. Lett.* **1978**, *33*, 18-20.

7. Yamashita, K.; Kunugi, Y.; Harima, Y.; Chowdhury, A.-N. Fabrication of an Organic p-n Homojunction Diode Using Electrochemically Cation- and Photochemically Anion-Doped Polymer. *Jpn. J. Appl. Phys., Part 1* **1995**, *34*, 3794-3797.

8. Lin, F.; Walker, E. M.; Lonergan, M. C. Photochemical Doping of an Adaptive Mix-Conducting p−n Junction. *J. Phys. Chem. Lett.* **2010**, *1*, 720-723.

9. Koshida, N.; Wachi, Y. Application of Ion Implantation for Doping of Polyacetylene Films. *Appl. Phys. Lett.* **1984**, *45*, 436-437.

10. Wang, W. M.; Wan, H. H.; Rong, T. W.; Bao, J. R.; Lin, S. H. Diode Characteristics and Degradation Mechanism of Ion Implanted Polyacetylene Films. *Nucl. Instrum. Methods Phys. Res., Sect. B* **1991**, *B61*, 466-471.

11. Cheng, C. H. W.; Lonergan, M. C. A Conjugated Polymer p-n Junction. *J. Am. Chem. Soc.* **2004**, *126*, 10536-10537.

12. Cheng, C. H. W.; Boettcher, S. W.; Johnston, D. H.; Lonergan, M. C. J. Unidirectional Current in a Polyacetylene Hetero-ionic Junction. *Am. Chem. Soc.* **2004**, *126*, 8666-8667.

13. Aviram, A.; Ratner, M. A. Molecular Rectifiers. *Chem. Phys. Let.* **1974**, *29*, 277-283.

14. Metzger, R. M. Unimolecular Electrical Rectifiers. *Chem. Rev.* **2003**, *103*, 3803-3834.

15. Ashwell, G. J.; Chwialkowskaa, A.; Hermann High, L. R. Au-S-CnH2n-Q3CNQ: self-Assembled Monolayers for Molecular Rectification. *J. Mater. Chem.* **2004,** *14*, 2389–2394.

16. Oh, S.-K.; Baker, L. A.; Crooks, R. M. Electrochemical Rectification Using Mixed Monolayers of Redox-Active Ferrocenyl Dendrimers and n-Alkanethiols. *Langmuir* **2002**, *18*, 6981-6987.

17. Liu, Y.; Offenhäusser, A.; Mayer, D. Electrochemical Current Rectification at Bio-Functionalized Electrodes. *Bioelectrochem.* **2010**, *77*, 89-93.

18. Martin, A. S.; Sambles, J. R.; Ashwell, G. J. Identification of the Process Producing Observed Rectifying Characteristics of Metal/Langmuir-Blodgett Film/Metal Structures. *Thin Solid Films* **1992**, *210-211*, 313-316.

19. Martin, A. S.; Sambles, J. R.; Ashwell, G. Molecular Rectifier. *J. Phys. Rev. Lett.* **1993**, *70*, 218-221.

20. Luo, L.; Balhorn, L.; Vlaisavljevich, B.; Ma, D.; Gagliardi, L.; Frisbie, C. D. Hopping Transport and Rectifying Behavior in Long Donor–Acceptor Molecular Wires. *J. Phys. Chem. C* **2014**, *118*, 26485–26497.

21. Shi, G.; Yu, B.; Xue, G.; Jin, S.; Li, C. Electrochemical Fabrication of a P-type Silicon–Polythiophene p–n Junction Diode. *J. Chem. Soc. Chem. Commun.* **1994**, 2549-2550.

22. Renkuan, Y.; Hong, Y.; Zheng, Z.; Youdou, Z.; Yongan, W. Polyaniline / Silicon Heterojunctions. *Synth. Met.* **1991**, *41*, 731-734.

23. Miyauchi, S.; Goto, Y.; Tsubata, I.; Sorimachi, Y. Heterojunction Devices Consisting of Conducting Polymers. *Synth. Met.* **1991**, *41*, 1051-1056.

24. Narasimhan, M.; Hagler, M.; Cammarata, V.; Thakur, M. Junction Devices Based on Sulfonated Polyaniline. *Appl. Phys. Lett.* **1998**, *72*, 1063-1065.

25. Reus, W. F.; Thuo, M. M.; Shapiro, N. D.; Nijhuis, C. A.; Whitesides, G. M. The SAM, Not the Electrodes, Dominates Charge Transport in Metal-Monolayer//Ga_2O_3/Gallium–Indium Eutectic Junctions. *ACSnano* **2012**, *6*, 4806–4822.

26. Nijhuis, C. A.; Reus, W. F.; Barber, J. R.; Whitesides, G. M. Comparison of SAM-Based Junctions with Ga_2O_3/EGaIn Top Electrodes to Other Large-Area Tunneling Junctions. *J. Phys. Chem. C* **2012**, *116*, 14139−14150.

27. Yuan, L.; Thompson, D.; Cao, L.; Nerngchangnong, N.; Nijhuis, C. A. One Carbon Matters: The Origin and Reversal of Odd–Even Effects in Molecular Diodes with Self-Assembled Monolayers of Ferrocenyl-Alkanethiolates. *J. Phys. Chem. C* **2015,** *119*, 17910−17919.

28. Song, P.; Yuan, L.; Roemer, M.; Jiang, L.; Nijhuis, C. A. Supramolecular vs Electronic Structure: The Effect of the Tilt Angle of the Active Group in the Performance of a Molecular Diode. *J. Am. Chem. Soc*. **2016**, *138*, 5769-5772.

29. Yuan, L.; Nerngchamnong, N.; Cao, L.; Hamoudi, H.; Barco, E.; Roemer, M.; Sriramula, R. K.; Thompson, D.; Nijhuis, C. A. Controlling the direction of rectification in a molecular diode. *Nat. commun.* **2015**, *6*, 6324.

30. Abruna, H. D.; Denisevich, P.; Umana, M.; Meyer, T. J.; Murray, R. W. Rectifying Interfaces using Two-Layer Films of Electrochemically Polymerized Vinylpyridine and Vinylbipyridine Complexes of Ruthenium and Iron on Electrodes. *J. Am. Chem. Soc.* **1981**, *103*, 1-5.

31. Denisevich, P.; Willman, K. W.; Murray, R. W. Unidirectional Current Flow and Charge State Trapping at Redox Polymer Interfaces on Bilayer Electrodes:Principles, Experimental Demonstration, and Theory. *J. Am. Chem. Soc.* **1981**, *103*, 4727-4737.

32. Pickup, P. G.; Murray, R. W. Bilayer Electrodes: Theory and Experiment for Electron trapping Reactions at the Interface between two Redox polymer Films. *J. Electroanal. Chem.* **1984**, *164*, 39-46.

33. Aizawa, M.; Shinohara, H.; Yamada, T.; Akagi, K.; Shirakawa, H. Electrochemical Fabrication of a Polypyrrole/Polythiophene p-n Junction Diode. *Synth. Met*. **1987**, *18*, 711-714.

34. Torres, W.; Fox, M. N. Rectifying Bilayer Electrodes: Layered Conducting Polymers on Platinum. *Chem. Mater* **1990**, *2*, 306-311.

35. Li, Y. Organic Electronic and Optoelectronic Devices Based on Diphenylamine End-group Polymers. PhD dissertation. Auburn University **2010**.

36. Harada, K.; Werner, A. G.; Pfeiffer, M.; Bloom, C. J.; Elliott, C. M.; Leo, K. Organic Homojunction Diodes with a High Built-in Potential: Interpretation of the Current-Voltage Characteristics by a Generalized Einstein Relation. *Phys. Rev. Lett.* **2005**, *94*, 036601/1-036601/4.

37. Chiechi, R. C.; Weiss, E. A.; Dickey, M. D.;Whitesides, G. M. Eutectic Gallium–Indium (EGaIn): A Moldable Liquid Metal for Electrical Characterization of Self-Assembled Monolayers. *Angrew. Chem. Int. Ed.* **2008**, *47*, 142-144.

38. Beebe, J. M.; Kushmerick, J. G. Nanoscale switch elements from self-assembled monolayers on silver. *Appl. Phys. Lett*. **2007**, *90*, 083117.

39. Haick, H.; Cahen, D. Contacting Organic Molecules by Soft Methods: Towards Molecule-Based Electronic Devices. *Acc. Chem. Res.* **2008**, *41*, 359-66.

40. Weiss, E. A.; Chiechi, R. C.; Kaufman, G. K.; Kriebel, J. K.; Li, Z.; Duati, M.; Rampi, M. A.; Whitesides, G. M. Influence of Defects on the Electrical Characteristics of Mercury-Drop Junctions: Self-Assembled Monolayers of n-Alkanethiolates on Rough and Smooth Silver. *J. Am. Chem. Soc.***2007**, *129*, 4336.

41. Rampi, M. A.; Whitesides, G. M. A Versatile Experimental Approach for Understanding Electron Transport through Organic Materials. *Chem. Phys.* **2002**, *281*, 373-391.

42. Wang, L. Synthesis, polymerization and Langmuir-Schaefer films of novel electroactive compounds with diphenylamine end groups. PhD dissertation. Auburn University. **1997**.

43. Sawyer, D. T.; Roberts Jr., J. L. Experimental Electrochemistry for Chemist. *John Wiley & Sons.* **1974.**

44. Pickup, P. G.; Osteryoung, R. A. Charing and Discharging Rate Studies of Polypyrrole Films in $AlCl_3$,:1-Methyl-(3-ethyl)-Imidiazolium Chloride Molten Salts and in CH_3CN. *J. Electroanal. Chem.* **1985**, *195*, 271-288.

45. Shockley, W. Electronics and Holes in Semiconductors; Van Nostrand: New York, **1950**.

Chapter Five

NAPHTHALENE DIIMIDE FUNCTIONALIZED CdS NANOCRYSTALS

5.1 Introduction

Semiconductor nanocrystals are a very promising class of material for biological imaging, optoelectronic and photovoltaic applications.[1–4] These nanocrystals show tunable optical and electronic properties as a function of size.[5–7]Their chemical stability, high photobleaching threshold, and narrow emission signals make them better fluorophores over organic molecules.[8] Among all Cd chalcogens nanoparticles, CdS is the most basic and most studied semiconductor quantum dot because of its easy processibility.[9]

Different synthetic approaches such as physical,[10,11] chemical[12–14] and biological[15,16] for CdS nanocrystals have been developed. As CdS nanocrystals provide size dependent properties, the control of particle size is a major issue. Therefore methods have been developed for capping the particle surfaces with organic molecules to prevent further growth and agglomeration.[17,18] Polymer[13,19] and thiol containing molecules[20,21] are commonly used as capping agents. Moreover, surface functionalization is usally necessary to achieve the certain applications. For example, the biocompatibility of CdS nanoparticles is a prerequisite for biological and medical uses.[22] Preparation of CdS in biological systems such as tobacco mosaic virus,[16] and engineered *E. coli*,[23] makes it biocompatible. Furthermore, semiconductor nanocrystals can form hybrid donor-acceptor system when these particles are capped with organic molecules.[24] Fullerene (C_{60}) functionalized quantum dots have been reported as donor-acceptor systems where the quantum dots serve as electron donors and light absorbers and C_{60} act as an electron acceptor.[24–30] Kamat, et al. demonstrated that electron transfer occurs from CdSe quantum dot to the thiolated C_{60}. They showed that the electron transfer is an ultrafast process taking place in the picosecond to

nanosecond timescale. Consequently this hybrid nanocomposite constitutes a light harvesting system.[26]

Naphthalene diimide is a n-type semiconductor. [31] Our research group has synthesized different monomers containing redox active ferrocene, naphthalene, and perylene diimide with diphenylamine end group and electropolymerized them.[32–35] Wang synthesized a thiol functionalized naphthalene diimide(DPA-NDI-SH)(Scheme 5.1) and made self-assembled monolayers of this molecule on Au surfaces.[36] In Chapter Two, we have demonstrated naphthalene diimide functionalized Au and Ag nanoparticles synthesized in DMF and DMSO, respectively. CdS nanoparticles hav been synthesized also in DMSO both with ligands (ethylhexanoate)[37] and without ligands in which the particles are stabilized by DMSO.[14]

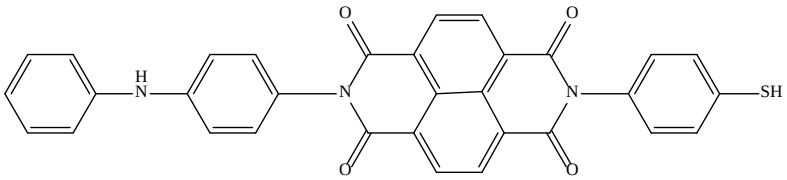

Scheme 5.1: Chemical structure of DPA-NDI-SH

In this chapter, we report the preparation of naphthalene diimide functionalized CdS nanocrystals in DMSO. Additionally, we have characterized the synthesized CdS nanocrystal by UV-visible, Fluorescence, FT-IR and XRD.

5.2 Experimental

5.2.1 Materials:

Cadmium acetate dihydrate and sodium sulfide nonahydrate were purchased from Fisher Scientific and Sigma-Aldrich, respectively. Dimethyl sulfoxide (DMSO) was obtained from Macron Fine Chemicals. All chemicals were used as received.

5.2.2 Synthesis of DPA-NDI-SH:

DPA-NDI-SH has been synthesized according to process described earlier,[36] which was discussed in Chapter Two. Briefly the synthetic procedure for DPA-NDI-SH is as follows: 0.30 g of 1,4,5,8-naphthalene tetracarboxylic dianhydride were placed in a flask, 10 mL of DMA were added and heated to 90^{o} C to dissolve the dianhydride. Then a solution of 4-aminothiophenol (0.14 g in 6 mL of DMA) was added dropwise over 10 min and the resulting solution was heated at 135^{o} C for 20 h. The product was precipitated out with diethyl ether, filtered and washed with copius amounts of acetone and diethyl ether. 0.24 g of the intermediate product, N-(p-aminothiophenyl)-1,4,5,8-naphthalene tetracarboxylic imide were obtained. Yield = 56%.

FT-IR (KBr): (cm^{-1}) = 1786, 1746, 1715, 1673, 1587, 1490, 1447, 1346, 1247, 1195, 854, 766, 744.

0.24 g N-(p-aminothiophenyl)-1,4,5,8-naphthalene tetracarboxylic imide was dissolved in 10 mL of DMA and the temperature is raised to 135^{o} C. Then 0.26 g of N-phenyl-1,4 phenylenediamine were added portion wise over 10 min. The temperature of the reaction mixture was held at 135^{o} C for 24 h. The product was precipitated out with diethyl ether, filtered and washed with copious amounts of acetone and diethyl ether. 0.23 g of final product was obtained. Yield = 68%.

FT-IR (KBr): (cm^{-1}) = 1714, 1671, 1591, 1511, 1493, 1345, 1248, 1191, 767, 746.

5.2.3 CdS Nanoparticles synthesis:

First, 0.0266 g of $Cd(OAc)_2.2H_2O$ and 0.0014 g of DPA-NDI-SH were dissolved in 49.5 mL of DMSO and purged with N_2 for 30 min. Sodium sulfide solution was prepared by dissolving 0.12 g of $Na_2S.9H_2O$ in 2.5 mL of water. This solution was also purged with N_2 for 30 min. Then 0.5 mL of the freshly prepared sodium sulfide solution were added dropwise to the cadmium acetate solution with vigorous stirring. The dark blue solution was turned yellowish blue within minute. To complete the reaction, stirring was continued for 5 h.[14] CdS nanocrystals without naphthalene diimide were also made following the above method as a control to compare the surface properties.

To collect the particles from the reaction mixture, 50 mL acetone were added to the 50 mL of the reaction mixture and then allowed to settle overnight. The mixture was centrifuged at 8000 rpm for 15 minutes and the solution was decanted. After collecting the precipitate, it was washed two times with acetone, centrifuging after every wash and finally dried with N_2 for XRD and FT-IR characterizations.

5.2.4 Nanoparticles Characterization

Spectroscopic:

A UV-Visible spectroscopic measurement for CdS nanoparticles in DMSO was carried out using HP 8453 UV-Visible spectrophotometer. Emission spectra of the CdS nanocrystal were recorded on a Shimadzu- RF-5301PC Spectrofluorophotometer. The slit width and excitation wavelength were 5 and 340 nm respectively. Fourier transform infrared spectroscopic measurements were carried out by FT-IR spectrophotometer (Shimadzu IR Prestige -21) at 2 cm^{-1} resolution. Prior to the measurements, the dried solid nanoparticles were mixed with potassium bromide and compressed into pellets.

TEM:

TEM micrographs were obtained by ZEISS EM10 instrument operating at 80 kV. The prepared nanoparticles were diluted with acetonitrile and drop casted on carbon-coated copper grids (400 mesh) (Electron Microscopy Sciences) and then dried. The particles size distribution was determined by a counting minimum of 200 particles.

***XRD Analysis*:**

X-ray diffraction (XRD) was carried out on a Rigaku D/MAX 2200 X-ray diffractometer with Cu Kα radiation. The wavelength of Cu Kα radiation was 1.54056 A°. The operating conditions of the diffractometer were 40 kV of voltage, 30 mA of current and 1.2 kW of power.

5. 3 Results and Discussion

5.3.1 CdS nanoparticles formation:

The synthesis scheme of the CdS nanoparticles was performed via a modified version of the method reported by Wankhede and Haram.[14] When the precursors of Cd and S were mixed together the reaction mixture become yellow as shown in the Figure 5.1. This yellow color indicates the CdS nanoparticles formation.[14,38] The CdS particles are grown in DMSO according to simple double displacement reaction.[14] UV-visible absorption spectra of the prepared reaction mixture

$$Cd(OAc)_2 + Na_2S \xrightarrow{DMSO} CdS\ (S) + 2Na(OAc) \qquad (5.1)$$

Figure 5.1: CdS nanoparticles (2 mM) in the reaction mixture without DPA-NDI-SH (left) and with DPA-NDI-SH (right).

(A) and the collected CdS nanoparticles (B) are shown the Figure 5.2. An absorption band was observed at 365 nm in the reaction mixture. After collecting the particles they were redispersed in DMSO. The absorption band of the redispersed particles shifted to 376 nm. A red shift of absorption band indicates larger particles formed upon precipitation from the reaction mixture. The fluorescence emission spectrum exhibits a broad band at 515nm (Figure 5.3). The emission band is assigned to recombination of the charge carrier at sulfur vacancies on the surface of the particles.[14] The results indicate that the emission intensity of the particles with naphthalene diimide ligand is much lower than the emission of the particles without naphthalene diimide. The formation of CdS nanoparticles was also confirmed by their X-ray cystallographic pattern shown in Figure 5.4. The diffractogram depicts three broad peaks at $2\theta = 27.70$, 48.30 and 59.19^{o} which are in good agreement with the signals of hexagonal CdS (JCPDS 41-1049).[9] The broadening of the peaks indicates that the particles sizes are small.[9,14] However, in the XRD of CdS nanoparticles with DPA-NDI-SH, the two broad peaks are resolved into narrow peaks which are also assigned for hexagonal CdS.[14] From the Debye- Scherrer formula, the estimated average particle sizes are 3.5 and 2.7 nm for particles with DPA-NDI-SH and without DPA-NDI-SH respectively. A TEM image of CdS on carbon grid is shown in Figure 5.5.. The histogram of particle sizes indicates that the average particle size is 14.7 ± 4.8 nm. This particle size is much

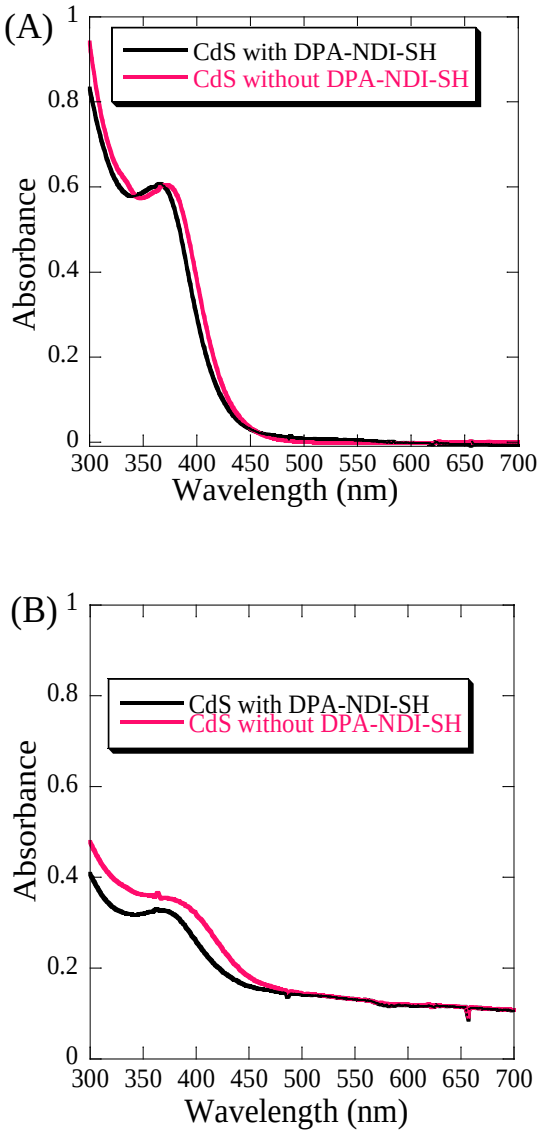

Figure 5.2: UV-visible spectrum of CdS particles (A) in the reaction mixture (0.25 mM) (B) redispersed CdS particles in DMSO after collecting through centrifuge (0.25 mM).

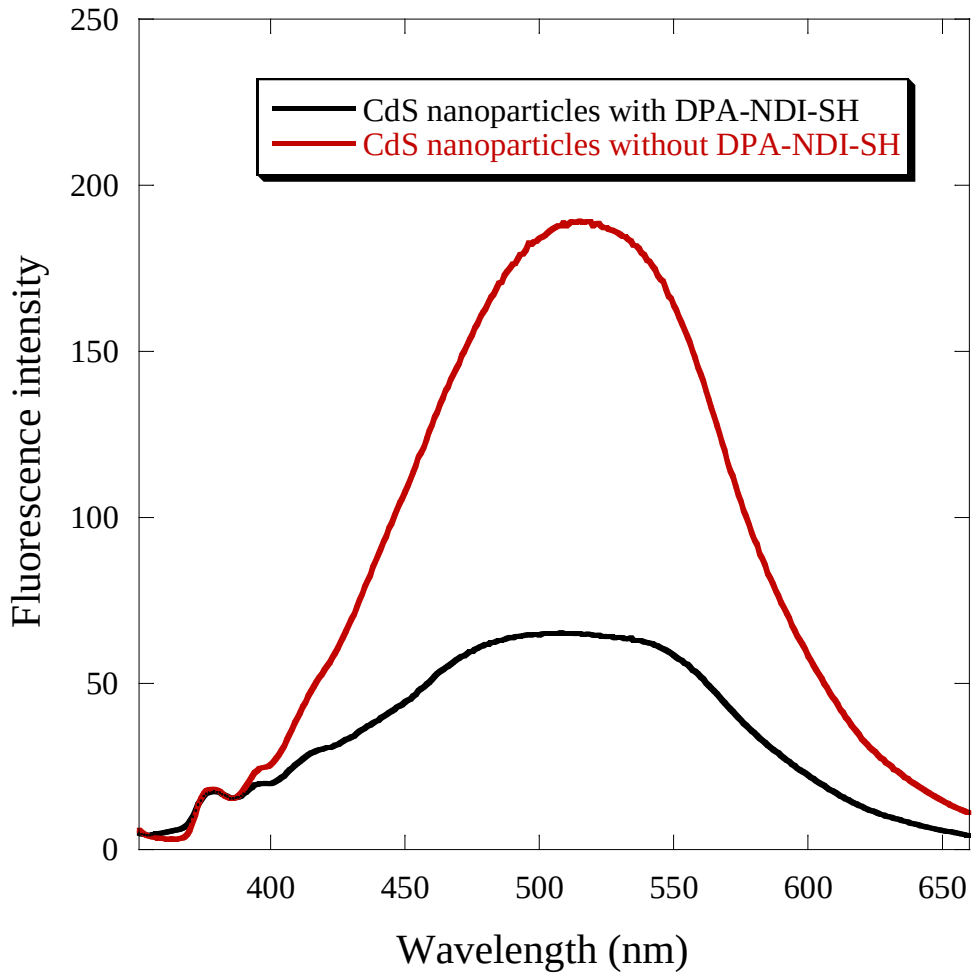

Figure 5.3: Emission spectrum of CdS nanoparticles (0.25 mM) in the reaction mixture with DPA-NDI-SH (black line) and without DPA-NDI-SH (red line).

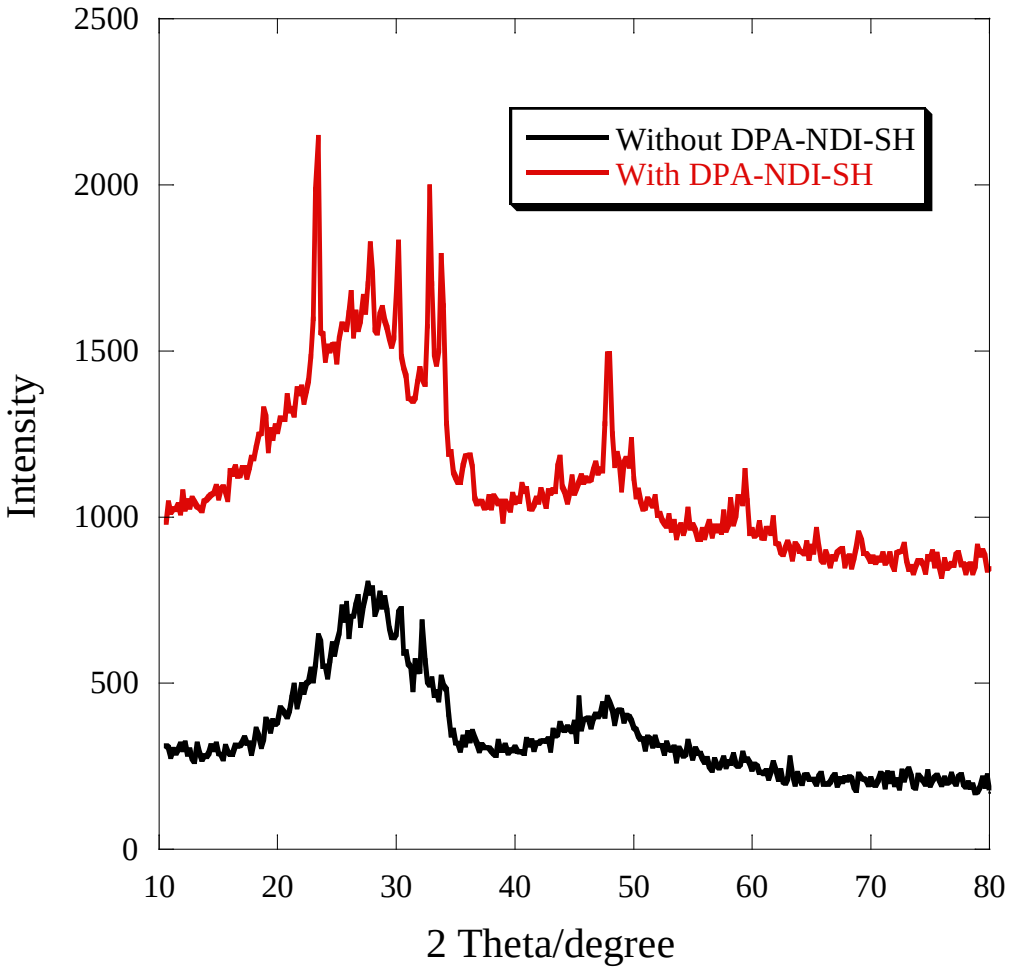

Figure 5.4: X-ray diffractogram of CdS nanoparticles.

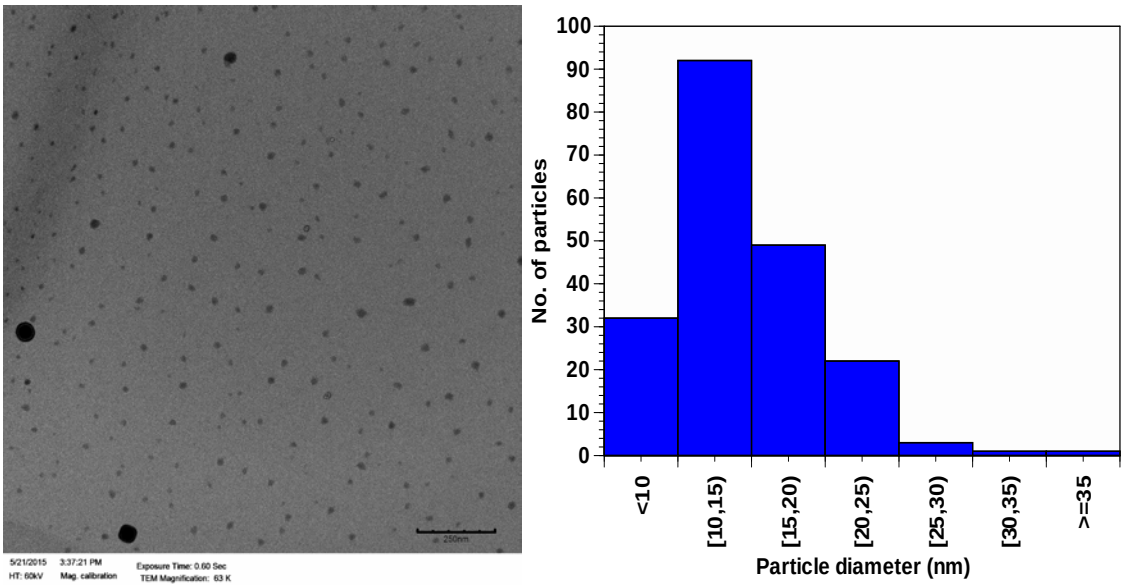

Figure 5.5: TEM image of CdS nanocrystal with histogram for different particles size distribution.

higher than the value obtained from XRD and also as compared with the reported value for CdS particles synthesized in DMSO.[14] The reason for the discrepancy between the two measurements is not known but it is possible that the particles have agglomerated on the TEM grid.

5.3.2 Surface Characterization of the CdS nanoparticles:

The FT-IR spectrum of CdS nanoparticles with DPA-NDI-SH and without DPA-NDI-SH are shown in Figure 5.6. Similar features in the FT-IR spectra were reported in the literature for CdS nanoparticles synthesized in DMSO.[14,39] Elbaum et al. have synthesized CdS nanocrystals from $Cd(OAc)_2$ and elemental S in DMSO,[39] and claim that the peaks at 1575 and 1416 cm^{-1} are for carbonyl symmetric and asymmetric bands of the acetate group respectively. Wankhede and Haram showed that these two peaks disappear when the particles are annealed at 250^o C.[14] The other peaks in the spectrum can be assigned to the Cd-DMSO complex coared on the surface of the particles, the broad peak at 1133 cm^{-1} corresponds to the S=O stretching frequency from DMSO and the peak at 979 cm^{-1} can be assigned to $–CH_3$ groups of both DMSO and acetate.[39] The stretching band of C-S bond was also observed at 629 cm^{-1}.[40] However, the FT-IR spectrum of the particles with DPA-NDI-SH showed additional peaks other than the band from DMSO and acetate group. These bands are attributed to the naphthalene diimide, DPA-NDI-SH. The symmetric and asymmetric stretching bands of the imide group in DPA-NDI-SH located at 1714 and 1672 cm^{-1}, respectively, are present in the nanoparticle vibrational spectrum. The other characteristic bands of DPA-NDI-SH such as the C-N-C symmetric and asymmetric stretching signals at 1345 and 1248 cm^{-1} are also present in the spectrum of the nanoparticles. The weak bands from the benzene ring of the naphthalene diimide are not seen clearly due to the broad and intense band from the DMSO and acetate groups. However, there is no position shift of spectral band of DPA-NDI-SH when the surface of the nanoparticles was coated with this molecule. A

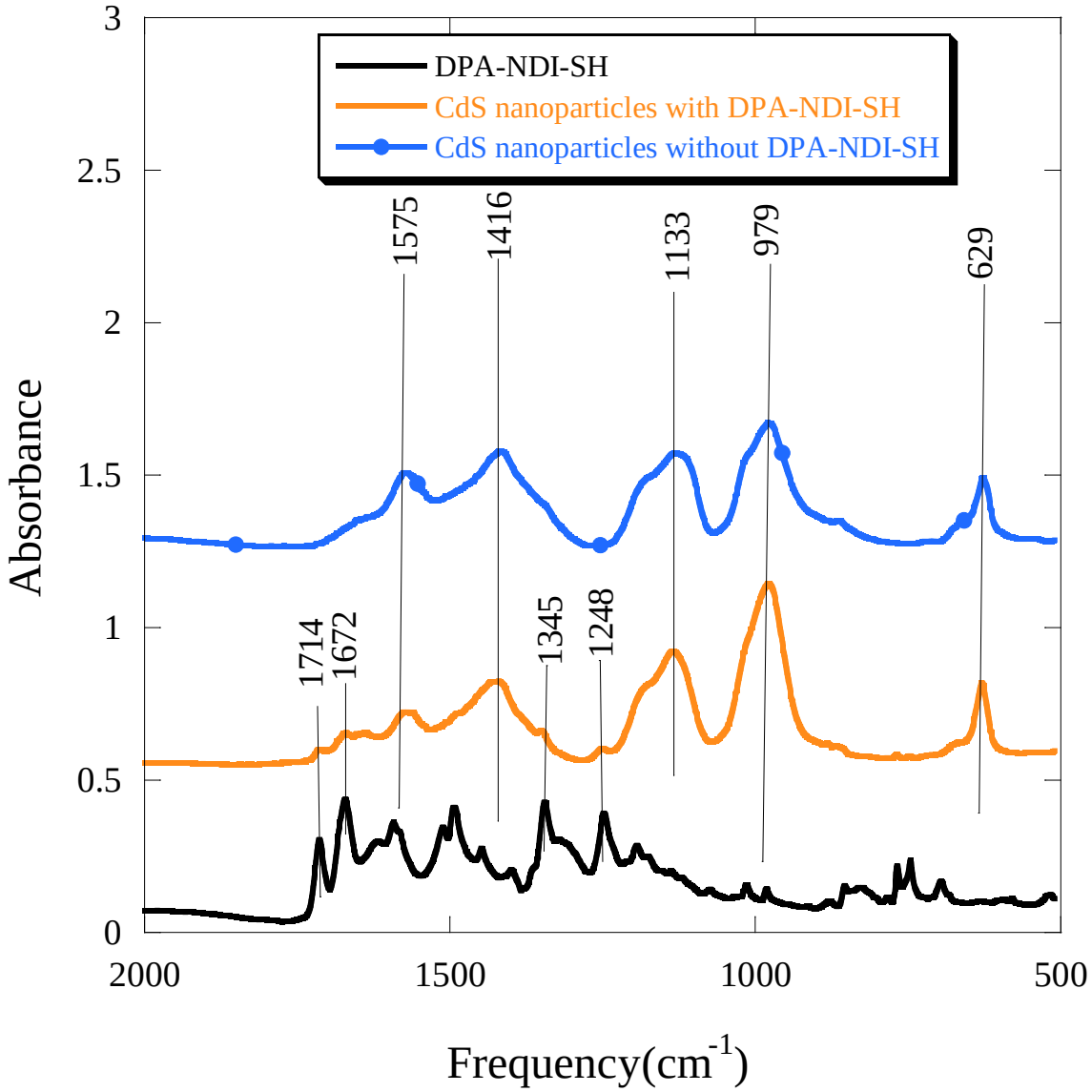

Figure 5.6: FT-IR spectrum of DPA-NDI-SH (bottom) and CdS nanoparticles with DPA-NDI-SH (middle) and without DPA-NDI-SH (top).

similar result has been reported in the case of DPA-NDI-SH functionalized Au and Ag nanoparticles which were discussed in Chapter Two. This might be due to the position of the imide group in the compound DPA-NDI-SH being far away from the surface of the particles.

5.4 Conclusion

In this chapter, we have incorporated naphthalene diimide materials onto the surface of CdS nanocrystals. Particle preparation from the $Cd(OAc)_2$ and Na_2S at room temperature was monitored using the characteristic yellow color, the UV-visible spectra and the emission band. CdS formation was further confirmed bydiffraction data corresponding to hexagonal CdS, both XRD and TEM provided results on the size distribution of the particles although the outcome of these methods is not in agreement. Incorporation of naphthalene diimide on the surface of the particles was characterized by FT-IR. The emission of CdS nanoparticle is quenched when the naphthalene diimide is positioned on the surface of the particles. This quenching effect needs to be confirmed using a standard fluorophore. Time resolved spectroscopy experiments are also needed to explore the electron transfer mechanism. In this way we could build a donor-acceptor system with the naphthalene diimide functionalized CdS nanoparticles.

5.5 References

1. Hines, M. A.; Scholes, G. D. Colloidal PbS Nanocrystals with Size-Tunable Near-Infrared Emission: Observation of Post-Synthesis Self-Narrowing of the Particle Size Distribution. *Adv. Mater*. **2003**, *15*, 1844–1849.

2. Gur, I.; Fromer, N. A; Geier, M. L.; Alivisatos, P.A. Air-Stable All-Inorganic Nanocrystal Solar Cells Processed from Solution. *Science* **2005**, *310*, 462–466.

3. Smyder, J. A.; Krauss, T. D. Coming Attractions for Semiconductor Quantum Dots. *Mater. Today* **2011**, *14*, 382–387.

4. Semonin, O. E.; Luther, J. M.; Beard, M. C. Quantum Dots for next-Generation Photovoltaics. *Mater. Today* **2012**, *15*, 508–515.

5. Aldeek, F.; Balan, L.; Medjahdi, G.; Roques-carmes, T.; Malval, J.; Mustin, C.; Ghanbaja, J. Enhanced Optical Properties of Core / Shell / Shell CdTe / CdS / ZnO Quantum Dots Prepared in Aqueous Solution. *J. Phy. Chem C* **2009**, 113, 19458–19467.

6. Jamieson, T.; Bakhshi, R.; Petrova, D.; Pocock, R.; Imani, M.; Seifalian, A. M. Biological Applications of Quantum Dots. *Biomaterials* **2007**, *28*, 4717–4732.

7. Chatterjee, A.; Priyam, A.; Das, S. K.; Saha, A. Size Tunable Synthesis of Cysteine-Capped CdS Nanoparticles by γ-Irradiation. *J. Colloid Interface Sci.* **2006**, *294*, 334–342.

8. Chan, W. C. W.; Nie, S. Quantum Dot Bioconjugates for Ultrasensitive Nonisotopic Detection. *Science* **1998**, *281*, 2016–2018.

9. Mo, Y. M.; Tang, Y.; Gao, F.; Yang, J.; Zhang, Y. M. Synthesis of Fluorescent CdS Quantum Dots of Tunable Light Emission with a New in Situ Produced Capping Agent. *Ind. Eng. Chem. Res.* **2012**, *51*, 5995–6000.

10. Onwudiwe, D. C.; Krüger, T. P. J.; Oluwatobi, O. S.; Strydom, C. A. Nanosecond Laser Irradiation Synthesis of CdS Nanoparticles in a PVA System. *Appl. Surf. Sci.* **2014**, *290*, 18–26.

11. Onwudiwe, D. C.; Krüger, T. P. J.; Strydom, C. A. Laser Assisted Solid State Reaction for the Synthesis of ZnS and CdS Nanoparticles from Metal Xanthate. *Mater. Lett.* **2014**, *116*, 154–159.

12. Young, A. G.; Green, D. P.; McQuillan, A. J. Infrared Spectroscopic Studies of Monothiol Ligand Adsorption on CdS Nanocrystal Films in Aqueous Solutions. *Langmuir* **2006**, *22*, 11106–11112.

13. Qi, L.; Co, H.; Antonietti, M. Synthesis and Characterization of CdS Nanoparticles Stabilized by Double-Hydrophilic Block Copolymers. *Nano lett.* **2001**, 2, 61-65.

14. Wankhede, M. E.; Haram, S. K. Synthesis and Characterization of CD-DMSO Complex Capped CdS Nanoparticles. *Chem. Mater.* **2003**, *15*, 1296–1301.

15. Bai, H. J.; Zhang, Z. M.; Guo, Y.; Yang, G. E. Biosynthesis of Cadmium Sulfide Nanoparticles by Photosynthetic Bacteria Rhodopseudomonas Palustris. *Colloids Surfaces B Biointerfaces* **2009**, *70*, 142–146.

16. Shenton, W.; Douglas, T.; Young, M.; Stubbs, G.; Mann, S. Inorganic-Organic Nanotube Composites from Template Mineralization of Tobacco Mosaic Virus. *Adv. Mater.* **1999**, *11*, 253–256.

17. Fischer, C.-H.; Henglein, A. Photochemistry of Colloidal Semiconductors. 31. Preparation and Photolysis of CdS Sols in Organic Solvents. *J. Phys. Chem.* **1989**, *93*, 5578–5581.

18. Steigerwald, M. L.; Alivisatos, A. P.; Gibson, J. M.; Harris, T. D.; Kortan, R.; Muller, A. J.; Thayer, A. M.; Duncan, T. M.; Douglass, D. C.; Brus, L. E. Surface Derivatization and Isolation of Semiconductor Cluster Molecules. *J. Am. Chem. Soc.* **1988**, *110*, 3046–3050.

19. He, R.; Qian, X. F.; Yin, J.; Xi, H. A.; Bian, L. J.; Zhu, Z. K. Formation of Monodispersed PVP-Capped ZnS and CdS Nanocrystals under Microwave Irradiation. *Colloids Surfaces A Physicochem. Eng. Asp.* **2003**, *220*, 151–157.

20. Majumder, M.; Karan, S.; Chakraborty, A. K.; Mallik, B. Synthesis of Thiol Capped CdS Nanocrystallites Using Microwave Irradiation and Studies on Their Steady State and Time Resolved Photoluminescence. *Spectrochim. Acta - Part A Mol. Biomol. Spectrosc.* **2010**, *76*, 115–121.

21. Aldana, J.; Lavelle, N.; Wang, Y.; Peng, X. Size-Dependent Dissociation pH of Thiolate Ligands from Cadmium Chalcogenide Nanocrystals. *J. Am. Chem. Soc.* **2005**, *127*, 2496–2504.

22. Zhou, J.; Yang, Y.; Zhang, C. Y. Toward Biocompatible Semiconductor Quantum Dots: From Biosynthesis and Bioconjugation to Biomedical Application. *Chem. Rev.* **2015**, *115*, 11669–11717.

23. Mi, C.; Wang, Y.; Zhang, J.; Huang, H.; Xu, L.; Wang, S.; Fang, X.; Fang, J.; Mao, C.; Xu, S. Biosynthesis and Characterization of CdS Quantum Dots in Genetically Engineered Escherichia Coli. *J. Biotechnol.* **2011**, *153*, 125–132.

24. Shibu, E. S.; Sonoda, A.; Tao, Z.; Feng, Q.; Furube, A.; Masuo, S.; Wang, L.; Tamai, N.; Ishikawa, M.; Biju, V. Photofabrication of Fullerene-Shelled Quantum Dots Supramolecular Nanoparticles for Solar Energy Harvesting. *ACS Nano* **2012**, *6*, 1601–1608.

25. Brown, P.; Kamat, P. V. Quantum Dot Solar Cells. Electrophoretic Deposition of CdSe-C_{60} Composite Films and Capture of Photogenerated Electrons with *n*C_{60} Cluster Shell. *J. Am. Chem. Soc.* **2008**, *130*, 8890–8891.

26. Bang, J. H.; Kamat, P. V. CdSe Quantum Dot-Fullerene Hybrid Nanocomposite for Solar Energy Conversion: Electron Transfer and Photoelectrochemistry. *ACS Nano* **2011**, *5*, 9421–9427.

27. Song, N.; Zhu, H.; Jin, S.; Zhan, W.; Lian, T. Poisson-Distributed Electron-Transfer Dynamics from Single Quantum Dots to C60 Molecules. *ACS Nano* **2011**, *5*, 613–621.

28. Gocalińska, A.; Saba, M.; Quochi, F.; Marceddu, M.; Szendrei, K.; Gao, J.; Loi, M. A.; Yarema, M.; Seyrkammer, R.; Heiss, W.; *et al.* Size-Dependent Electron Transfer from Colloidal PbS Nanocrystals to Fullerene. *J. Phys. Chem. Lett.* **2010**, *1*, 1149–1154.

29. Guldi, D. M.; Zilbermann, I.; Anderson, G.; Kotov, N. A.; Tagmatarchis, N.; Prato, M. Versatile Organic (Fullerene)-Inorganic (CdTe Nanoparticle) Nanoensembles. *J. Am. Chem. Soc.* **2004**, *126*, 14340–14341.

30. Xu, Z.; Cotlet, M. Quantum Dot-Bridge-Fullerene Heterodimers with Controlled Photoinduced Electron Transfer. *Angew. Chemie - Int. Ed.* **2011**, *50*, 6079–6083.

31. Guo, X.; Watson, M. D. Conjugated Polymers from Naphthalene Bisimide. *Org. Lett.* **2008**, *10*, 5333–5336.

32. Wang, L.; Goodloe, G. W.; Stallman, B. J.; Cammarata, V. Synthesis, Electrooxidation, and Characterization of Bis(diphenylamine)naphthalene Diimide. *Chem. Mater.* **1996**, *8*, 1175–1181.

33. Wang, L.; Wang, Q.; Cammarata, V. Electro-Oxidative Polymerization and Spectroscopic Characterization of Novel Amide Polymers Using Diphenylamine Coupling. *J. Electrochem. Soc.* **1998**, *145*, 2648–2654 .

34. Wang, L.; Cammarata, V. Electropolymers Based on Diphenylamine Π-Stacking in Cationic Benzidine Units. *Thin Solid Films* **1996**, *284-285*, 297–300.

35. Cammarata, V.; Hao, N.; Metz, J.; Liang, J. Electrochemical Quartz Crystal Microbalance Studies of the Growth of Perylene-Containing Films *ACS Symposium Series 832. Conducting Polymers and Polymer Electrolytes* **2009**, *5*, 59–74.

36. Wang, Q. Copolymerization and Characterization of Novel Bis(Diphenylamine) Monomers, Auburn University, **1999**.

37. Diaz, D.; Rivera, M.; Ni, T.; Rodriguez, J.-C.; Castillo-Blum, S.-E.; Nagesha, D.; Robles, J.; Alvarez-Fregoso, O.-J.; Kotov, N. A. Conformation of Ethylhexanoate Stabilizer on the Surface of Cds Nanoparticles. *J. Phys. Chem. B* **1999**, *103*, 9854–9858.

38. Voggu, R.; Shireen, A.; Rao, C. N. R. One-Step Synthesis of High-Purity Fluorous-Capped Inorganic Nanoparticles. *Dalt. Trans.* **2010**, *39*, 6021–6023.

39. Elbaum, R.; Vega, S.; Hodes, G. Preparation and Surface Structure of Nanocrystalline Cadmium Sulfide (Sulfoselenide) Precipitated from Dimethyl Sulfoxide Solutions. *Chem. Mater.* **2001**, *13*, 2272–2280.

40. Cotton, F. A.; Francis, R.; Horrocks, W. D. Sulfoxides As Ligands. II. The Infrared Spectra of Some Dimethyl Sulfoxide Complexes. *J. Phys. Chem.* **1960**, *64*, 1534–1536.

Appendix One: Copyright Permissions

Scheme 1.1: Adapted from Neouze, M.-A.; Schubert, U. Surface Modification and Functionalization of Metal and Metal Oxide Nanoparticles by Organic Ligands. *Monatshefte für Chemie - Chem. Mon.* **2008**, *139*, 183–195. with permission Copyright 2008. Springer.

Figure 1.1 Reprinted from Zin, M. T.; Yip, H-L.; Ma, W. H.; Jen, A. K.-Y. Arrays of Covalently Bonded Single Gold Nanoparticles on Thiolated Molecular Assemblies. *Langmuir* **2006**, *22*, 6346-6351. with permission Copyright 2006. American Chemical Society.

Figure 1.2 Reprinted from Labande, A.; Ruiz, Astruc, D. Supramolecular Gold Nanoparticles for the Redox Recognition of Oxoanions: Syntheses, Titrations, Stereoelectronic Effects, and Selectivity. *J. Am. Chem. Soc.* **2002**, *124*, 1782–1789. with permission Copyright 2002. American Chemical Society.

Figure 1.3 Reprinted from Woehrle, G. H.; Brown, L. O.; Hutchison, J. E. Thiol-Functionalized, 1.5-nm Gold Nanoparticles through Ligand Exchange Reactions: Scope and Mechanism of Ligand Exchange. *J. Am. Chem. Soc.* **2005**, *127*, 2172–2183. with permission Copyright 2006. American Chemical Society.

Figure 1.4 Reprinted from Quinn, B. M.; Liljeroth, P.; Ruiz, V.; Laaksonen, T.; Kontturi, K. Electrochemical Resolution of 15 Oxidation States for Monolayer Protected Gold Nanoparticles. *J. Am. Chem. Soc.* **2003**, *125*, 6644-6645. with permission Copyright 2003. American Chemical Society.

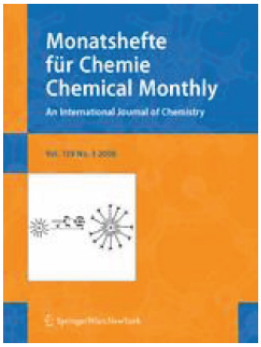

Title: Surface Modification and Functionalization of Metal and Metal Oxide Nanoparticles by Organic Ligands
Author: Marie-Alexandra Neouze
Publication: Monatshefte fü Chemie/chemical Monthly
Publisher: Springer
Date: Jan 1, 2008

Quick Price Estimate

I would like to... use in a thesis/dissertation

Portion Figures/tables/illustrations

Number of figures/tables/illustrations 1

Are you the author of this Springer article? Yes

You are ... make a selection

Select your currency USD - $

Quick Price Click Quick Price

The material can only be used for the purpose of defending your thesis limited to university-use only. If the thesis is going to be published, permission needs to be re-obtained (selecting "book/textbook" as the type of use).

No content delivery. This service provides permission for reuse only. Once licensed, you may use the content according to the terms of your license.

Price quoted is an estimate based on this request for this title only. Final price will depend on the total amount of requested Springer material.

QUICK PRICE CONTINUE

Title: Arrays of Covalently Bonded Single Gold Nanoparticles on Thiolated Molecular Assemblies
Author: Melvin T. Zin, Hin-Lap Yip, Ngo-Yin Wong, et al
Publication: Langmuir
Publisher: American Chemical Society
Date: Jul 1, 2006

Quick Price Estimate

I would like to... reuse in a Thesis/Dissertation

Requestor Type make a selection

Portion Table/Figure/Micrograph

Number of Table/Figure/Micrographs

Format Print

Select your currency USD - $

Quick Price Click Quick Price

QUICK PRICE CONTINUE

This service provides permission for reuse only. If you do not have a copy of the article you are using, you may copy and paste the content and reuse according to the terms of your agreement. Please be advised that obtaining the content you license is a separate transaction not involving Rightslink.

Note: Individual Scheme and Structure reuse is free of charge and does not require a license. If the scheme or structure is identified as a Figure in the article, permission is required.

To request permission for a type of use not listed, please contact the publisher directly.

Title: Supramolecular Gold Nanoparticles for the Redox Recognition of Oxoanions: Syntheses, Titrations, Stereoelectronic Effects, and Selectivity

Author: Agnès Labande, Jaime Ruiz, Didier Astruc

Publication: Journal of the American Chemical Society

Publisher: American Chemical Society

Date: Feb 1, 2002

Quick Price Estimate

I would like to... reuse in a Thesis/Dissertation

Requestor Type make a selection

Portion Table/Figure/Micrograph

Number of Table/Figure/Micrographs

Format Print

Select your currency USD - $

Quick Price Click Quick Price

QUICK PRICE CONTINUE

This service provides permission for reuse only. If you do not have a copy of the article you are using, you may copy and paste the content and reuse according to the terms of your agreement. Please be advised that obtaining the content you license is a separate transaction not involving Rightslink.

Note: Individual Scheme and Structure reuse is free of charge and does not require a license. If the scheme or structure is identified as a Figure in the article, permission is required.

To request permission for a type of use not listed, please contact the publisher directly.

Title: Thiol-Functionalized, 1.5-nm Gold Nanoparticles through Ligand Exchange Reactions: Scope and Mechanism of Ligand Exchange

Author: Gerd H. Woehrle, Leif O. Brown, James E. Hutchison

Publication: Journal of the American Chemical Society

Publisher: American Chemical Society

Date: Feb 1, 2005

Quick Price Estimate

I would like to...	reuse in a Thesis/Dissertation
Requestor Type	make a selection
Portion	Table/Figure/Micrograph
Number of Table/Figure/Micrographs	
Format	Print
Select your currency	USD - $
Quick Price	Click Quick Price

QUICK PRICE CONTINUE

This service provides permission for reuse only. If you do not have a copy of the article you are using, you may copy and paste the content and reuse according to the terms of your agreement. Please be advised that obtaining the content you license is a separate transaction not involving Rightslink.

Note: Individual Scheme and Structure reuse is free of charge and does not require a license. If the scheme or structure is identified as a Figure in the article, permission is required.

To request permission for a type of use not listed, please contact the publisher directly.

Title: Electrochemical Resolution of 15 Oxidation States for Monolayer Protected Gold Nanoparticles

Author: Bernadette M. Quinn, Peter Liljeroth, Virginia Ruiz, et al

Publication: Journal of the American Chemical Society

Publisher: American Chemical Society

Date: Jun 1, 2003

Quick Price Estimate

I would like to... reuse in a Thesis/Dissertation

Requestor Type make a selection

Portion Table/Figure/Micrograph

Number of Table/Figure/Micrographs

Format Print

Select your currency USD - $

Quick Price Click Quick Price

QUICK PRICE CONTINUE

This service provides permission for reuse only. If you do not have a copy of the article you are using, you may copy and paste the content and reuse according to the terms of your agreement. Please be advised that obtaining the content you license is a separate transaction not involving Rightslink.

Note: Individual Scheme and Structure reuse is free of charge and does not require a license. If the scheme or structure is identified as a Figure in the article, permission is required.

To request permission for a type of use not listed, please contact the publisher directly.